MECHANICAL PROPERTIES OF LASER WELDED SEMI-SOLID METAL CAST A356 ALLOY

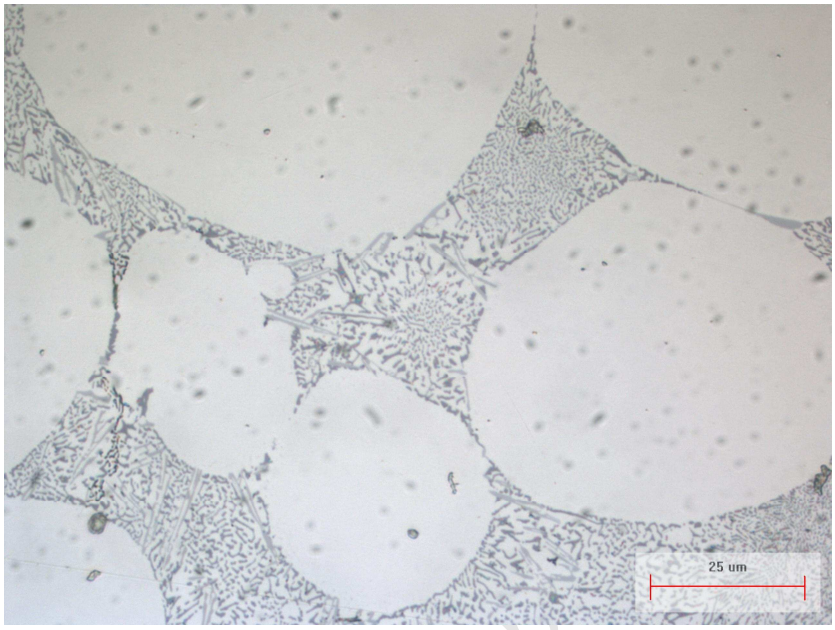

University of Cape Town

By

Gordon Nhlanhla Kunene

A thesis submitted to the faculty of Engineering and the Built Environment of the University of Cape Town in fulfilment of the requirements for the degree of MSc (Applied Sciences) in Materials Engineering

Centre for Materials Engineering
Department of Mechanical Engineering
University of Cape Town
October 2008

DECLARATIONS:

(i) I hereby grant the University of Cape Town free licence to reproduce for the purpose of research either the whole or any portion of the contents in any manner whatsoever of the above dissertation. I am presenting this dissertation in **COMPLETE** fulfilment of the requirements for my degree.

(ii) I know the meaning of plagiarism and declare that all of the work in the document, save for that which is properly acknowledged, is my own.

Signature: Signed by candidate

Date: 20 October 2008

University of Cape Town

Acknowledgements

I would like to express my deepest gratitude to my supervisor, Professor R D Knutsen for his enthusiasm, his inspiration, and his great efforts to explain things clearly and simply. I would have been lost without him. Secondly it is difficult to overemphasize my gratitude to my mentor, Dr Gonasagren Govender. Throughout my thesis preparation, he provided encouragement, sound advice, excellent teaching and very helpful ideas.

I would also like to thank and appreciate the following people for their assistance in various ways during the tough times of the project

- The CSIR for the financial support and assisting in my personal growth.
- Dr Lilian Ivanchev – for constantly being there throughout the project and always willing to assist.
- Dr Herman Burger – for helping with the production of excellent quality welds.
- Danie Wilkins – for your assistance in casting good quality plates.
- Mrs Christelle Stearn – for all the administrative assistance.
- The MSM team for your constant words of encouragement.

I wish to thank the entire Kunene family for providing a loving environment for me. My brothers, sisters and daughters, uncles and aunt thank you all for your much appreciated support. To my fiancé, thank you for your constant support and encouragement.

Lastly, and most importantly, I wish to thank my late mother, Tholakele Kunene. I would have been lost without you mother and I always appreciate that even in your final sleep you are still with me. To you I dedicate this thesis and all the credit that comes with it.

The greatest thank of all goes to the Almighty God for the strength and the blessing throughout the project.

University of Cape Town

Abstract

The high usage of Al and its alloys in both the automotive and aerospace industries is attributed to its excellent specific strength and corrosion resistance. High demand of Al usage has led to the improvement of both the casting techniques and joining processes, in order to improve on the quality of the final product. The selection of the manufacturing process for Al and its alloys is based on the capabilities of the specified requirements for components and the alloy used. High pressure die casting (HPDC) is the most widely used casting process in the automotive industry due to its high production rate, and ability to produce complex shaped components. However, HPDC is prone to porosity making it difficult to heat treat and weld. Semi solid metal (SSM) forming has the potential to produce near-net-shape components with high integrity. Due to laminar filling characteristics of SSM HPDC, low porosity or porosity free castings can be produced. This offers the opportunity to apply heat treatment as well as weld the SSM HPDC components.

A high continuous wave Nd: YAG laser has been used to investigate the weldability of SSM cast A356 alloy. The CSIR rheo-process was used to prepare the aluminium A356 SSM slurries and thereafter plates (4X80X100 mm^3) were cast using a 50 Ton Edgewick HPDC machine. Plates in the as cast, T4 and T6 heat treatment conditions which had passed radiography inspection were then laser welded. Some of the initial as-cast plates that were welded were subjected to pre or post weld T4 or T6 heat treatment and are referred to as pre-weld T4 or pre-weld T6 and post-weld T4 or post-weld T6 specimens.

The results revealed that semi-solid metal A356 castings are weldable by solid state laser welding. Particularly, the high powered Nd: YAG laser provides high welding speeds, narrow and deep welds, excellent mechanical properties resulting from a small heat-affected zone and low distortion due to low heat input. It was also found that the application of both the pre and post weld heat treatments greatly alters the microstructure and substructure. Thirdly found was that the laser welding process caused a substantial decrease in the mechanical properties of pre-weld heat treated samples however, the application of post-weld heat treatments regenerates the mechanical properties which were initially lost.

From tensile measurements it was found that welded as-cast, pre-weld T4, post-weld T4 and post-weld T6 tensile specimens fractured in the base metal. However, the pre-weld T6

University of Cape Town

specimens were found to have fractured in the heat affected zone (HAZ). Furthermore a number of findings are noted and discussed in chapter four.

University of Cape Town

Table of contents

University of Cape Town

University of Cape Town

Glossary

HPDC	High pressure die casting
SSM	Semi-solid metal
Nd : *YAG*	Neodymium-doped yttrium aluminium garnet
ζ	Fraction transformed
k	Constant related to transformation fraction
τ	Quench factor
C_t	Critical time of temperature to transform
GP zones	Guinier Preston zones
β	Equilibrium Mg_2Si
β' and β"	Metastable precursors of β
ΔS_f	Entropy of fusion
R	Universal gas constant
YS_T	Total yield strength
YS_O	Yield strength of pure aluminium
ΔYS_{Si}	Yield strength due to eutectic silicon particles
ΔYS_{Fe}	Yield strength due to eutectic iron-phase particles
$\Delta YS_{SS,Si}$	Yield strength due to Si in solid solution
$\Delta YS_{SS,Mg}$	Yield strength due to magnesium in solid solution
$\Delta YS_{ppt,Si}$	Yield strength due to Si precipitates
$\Delta YS_{ppt,Mg-Si}$	Yield strength due to Mg-Si precipitates
FEA	Finite elemental analysis
BPP	Beam parameter product
I	Incident laser intensity
η	Power transfer coefficient
ε	Melting efficiency
T	Top of the plate (near the gate)
B	Bottom of the plate (opposite the gate)
BM	Base metal
HAZ	Heat-affected zone

University of Cape Town

FZ	Fusion zone
SDAS	Secondary dendritic arm spacing
SIMS	Secondary ion mass spectroscopy
CT	Computer tomography
LAT	Linear attenuation coefficient
SCC	Stress corrosion cracking
OES	Optical emission spectrometer
SEM	Scanning electron microscope
HV	Vickers hardness

University of Cape Town

Chapter One

Introduction

1.1 Background

Since the discovery of aluminium (Al) by Charles Hall and Paul Héroult, its usage has grown rapidly. The high usage of Al and its alloys is attributed to its strength light weight and excellent corrosion resistance. This led to the replacement of conventional steel components with Al components by both the automobile and aerospace industries. Also due to stringent environmental regulations both the automobile and aerospace industries have been pressing hard for weight reduction. The first commercial applications of Al were mirror frames and cooking utensils. However, today the excellent mechanical properties of Al, give it a huge range of possible applications, from transport, medicine, electrical application, packaging, and construction of homes and furniture. Figure 1.1 shows that the major consumers of Al in the western world are the building and construction industry (18%) and transportation industry (30%).

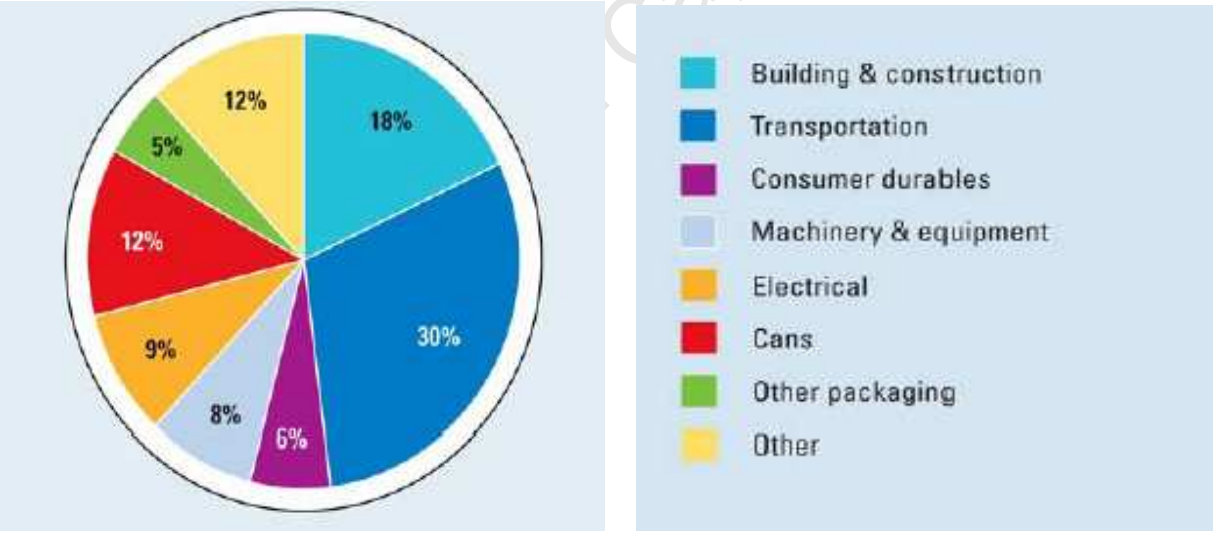

Figure 1.1: Total Al consumption by products from the western world[1].

There are several casting techniques which have been developed to improve on the quality of the castings, such as high-pressure die casting (HPDC), squeeze casting, Cosworth process, indirect squeeze casting, metal compression forming and semi-solid metal (SSM) processing[2]. The selection of the manufacturing process for Al and its alloys is based on the capabilities of each process and specified requirements for each component and alloy type. The shape

University of Cape Town

complexity of the component and cost are the two factors of paramount importance when selecting a manufacturing process. Generally semi-solid metal (SSM) forming process offers several advantages over conventional processes such as forging, HPDC, and conventional casting. Other advantages of SSM forming processes are that components of different wall thicknesses can be designed and furthermore joining by laser welding is possible. The most commonly used cast alloys are A356 and A319 because they are important for many automotive components such as suspension, driveline, and engine parts, where increased durability and reliability are always desirable[3, 4].

1.2 Objectives

Extensive research has been conducted on laser welding of wrought aluminium alloys. However, very little research has been conducted on the feasibility of laser welding of casting alloys especially semi-solid cast A356 alloy. Generally laser welding of aluminium and its alloys posses challenges such as porosity formation during welding. The control of porosity formation is often achievable only if there is the balance between the pressure in the keyhole and out of the keyhole. For all the laser welding experiments constant welding parameters will be used on semi-solid metal cast A356 alloy. Due to limited research on laser welding of semi-solid metal cast A356 alloy, the aims of this research are to:

- Establish the laser welding process parameters for stable and repeatable welding to produce quality welds. (e.g. reduction of defects; such as porosity and inclusions)
- Investigate the effects of the pre and post laser welding heat treatments on the microstructure.
- Establish the mechanical properties of the laser welded joints under different heat treatment conditions.

1.3 Research approach

The CSIR Rheo-process will be used for casting the A356 alloy plates. This will be followed by X-ray radiography analysis on the castings to check the quality of the castings. Thereafter the pre and post weld heat treatments will be conducted on quality castings. Semi-solid metal

University of Cape Town

cast A356 plates which have passed X-ray radiography will then be welded. Some of the initial as-cast plates will be given post-weld T4 and T6 heat treatments; these will be called post-weld T4 and post-weld T6 specimens. Resulting microstructural changes due to heat treatments will then be evaluated under light microscope, scanning electron microscope (SEM), microhardness tester and tensile tester.

1.4 Thesis Layout

The researched work is presented in six chapters, where chapter one introduces the research work. Chapter two will then review the relevant work to this research. The followed experimental procedures during research are summarised in chapter three. Thereafter results are presented and discussed in chapter four. The conclusions which were drawn from the results are declared in chapter five. Suggestions for future work are presented under recommendations in chapter six.

University of Cape Town

Chapter Two

Literature Review

2.1 Introduction

Aluminium and its alloys are much admired in the industrial world mainly due to their versatility. As a result, aluminium alloys are widely used in the automobile and aerospace industries, owing to their lightweight, excellent formability, machinability, corrosion resistance, forgeability and physical properties. Aluminium and aluminium alloys can also be joined by various joining methods, such as fusion and resistance welding, soldering, brazing, adhesive bonding and mechanical joining. The ability to manipulate both the mechanical and physical properties of aluminium by alloying and heat treatments is remarkable. The most widely used cast alloys are the A356 and A319[3, 4], however, for the scope of this project only A356 alloy will be discussed in detail. The section presents the review of pure aluminium and overview of casting alloys. A more detailed review is presented specifically on the hypoeutectic casting alloy, A356 alloy. Also reviewed in this section is the effect of major alloying elements on the microstructure of the A356 alloy. The effect of the different heat treatment conditions on the microstructure and hence mechanical properties of A356 alloy are also reviewed. An overview of laser welding process and also laser welding of aluminium alloys are also reviewed

University of Cape Town

2.2 Aluminium and aluminium alloys

Aluminium displays a face-centred cubic (fcc) lattice at room temperature which is stable to the melting point[5, 6]. Aluminium in its purity form has limited application due to low melting point and low strength. Aluminium is a good thermal and electrical conductor which by weight is better than copper. In its purity form aluminium has excellent corrosion resistance due to the inherent oxide layer that forms on the surface when the metal is exposed to air, effectively preventing further oxidation. However, pure aluminium cannot be used in strength demanding structural applications. Although addition of alloying elements improves on mechanical properties to some extent, the application of relevant heat treatments leads to

optimum mechanical properties. Illustrated in table 2.1 are the physical properties of pure aluminium.

Table 2.1: Physical properties of aluminium[5, 7]

Physical Property	Value
Atomic Number	13
Atomic weight	$26.9815 g/mol$
Density	$2.685 gcm^3$
Modulus of elasticity	$71 GPa$
Melting range	$550 - 660°C$
Coefficient of linear expansion (20 – 100 ºC)	$22x10^{-6} K^{-1}$
Specific heat (100ºC)	$963\ Jkg^{-1}$
Latent heat of fusion	$389\ kJkg^{-1}$
Thermal conductivity (25 ºC)	$151 Wm^{-1}K^{-1}$
Electrical conductivity	$39\ \%IACS$
Resistivity (20 ºC)	$0.0442x10^{-6}\Omega m$
Pouring range	$700 - 710°C$

Aluminium is capable of being a superconductor, with a superconducting critical temperature of 1.2 Kelvin and a critical magnetic field of about 100 gauss[5, 7, 8]. The yield strength of pure aluminium is 7–11 MPa, while aluminium alloys have yield strengths ranging from 200 MPa to 600 MPa. As indicated by the mechanical properties of pure aluminium in table 2.2, pure aluminium has low strength which is the reason aluminium has limited applications in its pure form.

Table 2.2: Mechanical properties of the different purity forms of aluminium at room temperature[5].

% Purity	YS at 0.2% offset (MPa)	UTS (MPa)	% Elongation (in 50 mm)
99.9	10	45	50
99.8	20	60	45
99.6	30	70	43

University of Cape Town

However, the presence of impurity elements and the addition of alloying elements improve the mechanical properties. Ideally aluminium alloys are classified into two main categories: cast and wrought alloys. The two categories are also subdivided into heat treatable and non-heat treatable alloys. The heat treatable alloys also called precipitation hardening aluminium alloys are those in which mechanical properties may be enhanced by either heat treatment or heat treatment in combination with cold working[5, 7]. Generally heat treatable aluminium alloys for wrought and cast products contain alloying elements that decrease in solubility with decreasing temperature. Unless the major criteria for strengthening by age hardening is met, addition of major alloying elements alone in binary systems show little effect on strength from thermal treatment, regardless of the solubility effect of the solute in solid solution. Therefore, the major criteria for strengthening by age hardening involve formation of coherent clusters of solute atoms. The mismatch in size caused between the solute and solvent generates large coherency strains in the lattice. The coherent clusters of solute hinder dislocation movement hence the alloy is considerable strengthened and hardened.

University of Cape Town

2.2.1 Effects of alloying elements[5]

Addition of alloying elements to pure aluminium greatly improves the mechanical properties. The different alloying elements which are added to aluminium and its alloys have different effects. For the purpose of this study the effects of major alloying elements found in A356 alloy are discussed.

Copper (Cu) substantially improves strength and hardness in the as-cast and heat treated conditions. Additions of copper also reduce hot tear resistance and decrease castability. Generally copper reduces resistance to general corrosion and in certain condition also stress-corrosion susceptibility.

Iron (Fe) improves hot tear resistance and decreases the tendency of die soldering in die casting. However, high iron content leads to decreased ductility. Insoluble phases (e.g. $FeAl_3$, $FeMnAl_6$ and αAlFe) formed when iron reacts with molten aluminium, are responsible for improvements in strength especially at elevated temperatures. As the iron content increases so

does the fraction of insoluble phases, casting considerations such as flowability and feeding characteristics are adversely affected.

Magnesium (Mg) is the basis of strength and hardness improvement in heat-treated Al-Si alloys and is generally used in more complex Al-Si alloys containing copper, nickel, and other elements for the same purpose. The hardening phase Mg_2Si displays a useful solubility limit corresponding to approximately 0.70% Mg. In A356 alloy the composition of magnesium is in the range of 0.25 to 0.45 wt. %.

Manganese (Mn) is normally considered an impurity in casting compositions. In the absence of work hardening, manganese offers no major benefits in cast aluminium alloys. Manganese can be added to alter response in chemical finishing and anodising.

Silicon (Si) improves the casting characteristics. Sole additions of silicon to pure aluminium severely improve fluidity, hot tear resistance, and feeding characteristics. Silicon additions are also accompanied by reduction in specific gravity and coefficient of thermal expansion.

Strontium (Sr) is normally used to modify the aluminium-silicon eutectic. High strontium levels are associated with casting porosity, especially in processes or thick-section parts in which solidification occurs more slowly.

Titanium (Ti) in combination with boron is widely used to refine the grain structure of aluminium casting alloys. Titanium is often employed at concentrations greater than those required for grain refinement to reduce cracking tendencies in hot-short compositions.

University of Cape Town

2.2.2 Major contaminant of aluminium and its alloys

Hydrogen is highly soluble in aluminium and its alloys. The solubility increases from solid to liquid aluminium with 0.034 mL/100g in the former and 0.65 mL/100g in the latter[1]. During cooling and solidification of molten aluminium, dissolved hydrogen in excess of the low solid solubility may precipitate in molecular form, resulting in the formation of primary and/or secondary voids[5, 9]. The hydrogen bubble formation is strongly resisted by surface tension

forces, by liquid cooling and solidification rates, and by absence of nucleation sites for hydrogen precipitation, such as entrapped oxides. Oxide layer in its hydrated form is known to be an important source of hydrogen. In the absence of nucleating oxides, relatively high concentrations are required for hydrogen precipitation (i.e. approximately 0.30 mL/100g).

There are two types of hydrogen porosities which occur in cast aluminium alloys, namely intermediate and secondary porosity.

Intermediate porosity occurs when hydrogen contents are sufficiently high that hydrogen rejected at the solidification front results in solution pressures above atmospheric. On the other hand, secondary porosity occurs when dissolved hydrogen content is low and void formation is usually subcritical. Because the presence of hydrogen porosity is a result of diffusion controlled nucleation and growth, increasing the solidification rate acts to suppress void formation and growth. Owing to this reason castings prepared in expandable mould processes are more susceptible to hydrogen-related defects than parts produced by permanent mould or pressure die casting[5].

The hydrogen dissolved in molten aluminium can be reduced or eliminated in the following ways:

- Gas purging or gas flushing
- Tableted flux degassing
- Mechanical mixer degassing

The most widely used and simplest method of degassing molten aluminium is by injecting a purging gas under pressure through a flux tube or pipe. This method functions by using the difference in partial pressures between hydrogen and the surrounding melt which allows hydrogen to diffuse into the purge gas bubble. The purge gas bubble then rises to the surface of the melt and is expelled into the atmosphere. Purge gases are either inert (i.e. argon or nitrogen) or reactive (chlorine or Freon 12). Generally chlorine gas or mixtures with chlorine are more beneficial than inert gases or Freon alone.

There are many major sources of hydrogen in aluminium, including:

- The furnace atmosphere,
- Charge materials,
- Fluxes,
- External components,
- Oxide layer in its hydrate form,

University of Cape Town

and

- Reaction between the molten metal and the mould.

Even under optimum melting and melt-holding conditions, molten aluminium is susceptible tot three types of degradation[5]:

- With time at temperature, adsorption of hydrogen (H_2) results in increased dissolved H_2 content up to an equilibrium value for the specific composition and temperature.
- With time at temperature, oxidation of the melt occurs; in alloys containing magnesium, oxidation losses and the formation of complex oxides may not be self-limiting.
- Transient elements characterised by low vapour pressure and high reactivity are reduced as a function of time at temperature; Mg, Na, Ca and Sr.

Turbulence or agitation of the melt and increased holding temperature significantly increase the rate of hydrogen solution, oxidation, and transient element loss. The mechanical properties of Al alloys depend on casting soundness, which is strongly influenced by H_2 porosity and entrained non-metallic inclusions. Normally the melt is treated to reduce dissolved H_2.

There is a direct relation between the pore volume fraction, cooling rate and hydrogen content. Below are the effects of cooling rate, hydrogen content and Sr modification on the pore volume fraction. The following effects apply for both Sr-modified and unmodified alloys[10, 11].

- At constant hydrogen content, the pore volume fraction decreases as the cooling rate increases.
- At constant cooling rate, the pore volume fraction increases with increasing hydrogen content.
- At constant hydrogen content and cooling rate, the pore volume fraction increases with increasing Sr modification.
-

However, the exact mechanism by which Sr modification increases the amount of porosity is not yet clearly documented. The average pore size decreases as the cooling rate increases and as the hydrogen content decreases. At high cooling rate, the hydrogen diffusion process is limited. It is believed that Sr treatment does not introduce hydrogen into molten aluminium and also does not affect the rate of hydrogen pick-up by the melt. Silicon content decreases the density of solid Al-Si alloys whilst Sr modification increases the solid density.

University of Cape Town

There are several aluminium alloys which are divided into two major categories: cast and wrought alloys. The major categories are further subdivided into heat treatable and non-heat treatable alloys. Table 2.3 illustrates the alloy designation system for cast products. A three-digit system is used for cast alloys. The aluminium alloy designation system for cast alloys is as follows[5, 8, 12, 13]:

Table 2.3: Alloy designation system for cast alloys

Alloy description	Alloy system	Major alloying elements
1xx.x	- Pure Al	(Normally ≤ 99%)
2xx.x	- Al/Cu Alloys	(Copper is the major alloying element)
3xx.x	- Al/Si/Cu/Mg Alloys	(Silicon is the major alloying element however copper and magnesium elements are also significant)
4xx.x	- Al/Si Alloys	(Silicon is the major alloying element)
5xx.x	- Al/Mg Alloys	(Magnesium is the major alloying element)
6xx.x	- Unused Alloys	
7xx.x	- A/Zn Alloys	(Zinc is the major alloying element however copper and magnesium elements are also significant)
8xx.x	- Al/Tn Alloys	(Tin is the major alloying element)
9xx.x	- Unused Alloys	

The mechanical properties are greatly improved by the combination of addition of alloying elements and by applying the relevant heat treatments. One of the major alloying elements in the Al-Si system which contributes to the strength is magnesium. It is well documented that the strength of the A356 alloy (table 2.4) is proportional to the magnesium content. The

University of Cape Town

strontium on the other hand is an excellent eutectic modifier in hypoeutectic aluminium alloys. The role of strontium in hypoeutectic aluminium alloy A356 is discussed in detail in the proceeding section.

Table 2.4: Specified chemical composition of A356 casting alloy[5].

Elemental chemical composition in wt%								
Si	Fe	Cu	Mn	Mg	Ti	Zn	Sr	Al
6.50 - 7.5	0.20 Max.	0.20 Max.	0.10 Max.	0.25 – 0.45	0.20 Max.	0.10 Max.	0.03 Max.	Bal.

The different heat treatment conditions are discussed in detail in section 2.3. However, for the scope of the study only heat treatments which were applied throughout the study will be discussed. Discussed in section 2.3 under heat treatment of aluminium alloys are:

- Solution heat treatment
- Quenching
- Natural and Artificial ageing.

University of Cape Town

2.3 Heat treatment of Al alloys

Heat treatment is any heating and cooling operation that is performed with the aim of changing the mechanical properties, the microstructure, or residual stress of a metallic material[5]. Table 2.5 illustrates the heat treatment and temper designation system which was developed by the American Aluminium Association to describe the processing of wrought and cast aluminium alloys[5]. Heat treatable alloys can be subjected into any of the heat treatment system listed in table 2.5 depending on the requirements of the aluminium alloy. However, for the purpose of this research only the F, T4 and T6 heat treatment systems will be explained in detail and extensively used.

Table 2.5: Temper designation and heat treatment system for aluminium and its alloys[5, 7].

Suffix	Treatment
F	As-fabricated.
O	Annealed.
H	Strain-hardened.
W	Solution heat-treated (unstable temper).
T	Solution heat-treated (stable temper).
T1	Cooled from an elevated temperature shaping process and naturally aged to substantially stable condition.
T2	Cooled from an elevated temperature shaping process, cold worked and naturally aged to substantially stable condition.
T3	Solution heat-treated, cold worked, then naturally aged to a substantially stable condition.
T4	Solution heat-treated, quenched and naturally aged to a substantially stable condition.
T5	Controlled cooling from elevated temperature shaping process, then artificially aged.
T6	Solution heat-treated, quenched, and then artificially aged.
T7	Solution heat-treated, quenched and artificially overaged.
T8	Solution heat-treated, quenched cold worked, and then artificially aged.
T9	Solution heat-treated, quenched, artificially aged and then cold worked.
T10	Cooled from elevated temperature shaping process, cold worked and then artificially aged.

For the purpose of this study, the heat treatment procedures that are discussed are solution heat treatment, quenching and aging.

University of Cape Town

2.3.1 Solution heat treatment

This is a process where an alloy is soaked at relatively high temperatures for long time to produce an almost homogeneous solid solution. The main objective of solution heat treatment is to achieve the maximum concentration of solute in solid solution. The solutionising temperature is determined from the phase diagram based on the composition and maximum solid solubility of the solute. For the Al-Si system there is limited solubility of silicon in aluminium and also of aluminium in silicon. Figure 2.1 shows limited solubility of silicon in aluminium which reaches a maximum of 1.65 at. % at 577ºC[5]. However, the percentage of solubility decreases with an increase in temperature. To avoid local melting during heating and at the solution heat treatment temperature, slow heating is advisable to re-dissolve non-equilibrium precipitates. Normally under heating leads to incomplete solid solution and consequently poor mechanical properties are achieved by an alloy. The most widely used solution heat treatment temperature is 540ºC for A356 alloy[4, 5, 14, 15]. Solution heat treatment times on the other hand vary from one minute to several hours depending on the alloy type, whilst the common solution heat treatment time is 6 hours for A356 alloy[4, 5, 14, 15, 16].

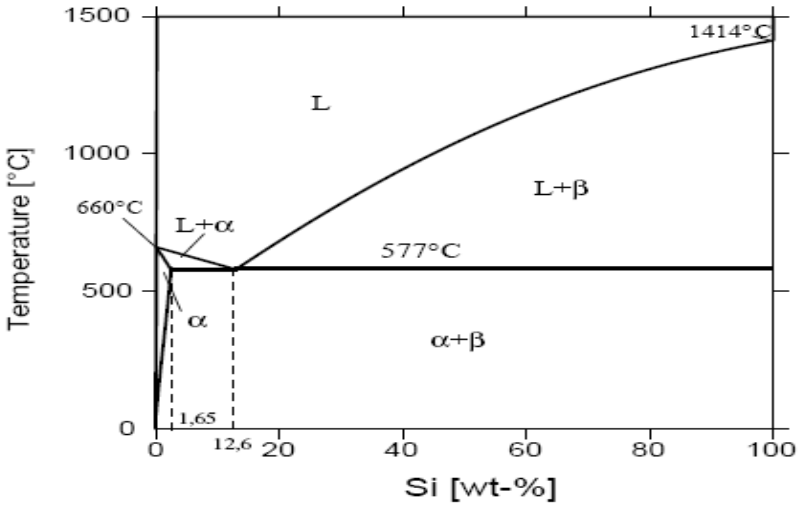

Figure 2.1: The binary phase diagram of Al-Si[17].

2.3.2 Quenching

Subsequent to solution heat treatment, quenching is the most critical in the sequence of heat treatment processes. Quenching is rapid cooling from the solution heat treatment temperature to near room temperature. In most cases water is used as the quenching agent. The main aim

University of Cape Town

of quenching is to retain the solute in solid solution, formed at the solution heat-treating temperature and also to preserve a high number of vacancies at room temperature. Normally the rapidly quenched structure shows no precipitation, however, the structure is not stable. Generally the solute that precipitates on grain boundaries or vacancies that migrate to disordered regions are detrimental to mechanical properties and corrosion properties. In order to avoid such types of precipitation, the solid solution must be rapidly quenched enough to produce a supersaturated solid solution at room temperature. Generally the highest strength levels, improved corrosion resistance, and improved stress corrosion resistance are achieved by rapid quenching rates. However, it is reported that critical range for quenching is alloy-dependent. For example the quenching range for 7075 is reported to be 400-290 ºC[5]. As a result of the sensitivity of alloys to quench rate is determined from the quench factor analysis. Quench factor analysis (table 2.5) is useful in planning appropriate limits for quench delays, or when it is not adequate to ensure that the cooling curve misses the nose of the C-curve (figure 2.2). The nose of the C-curve identifies the critical temperature range (i.e. the region of high precipitation rates).

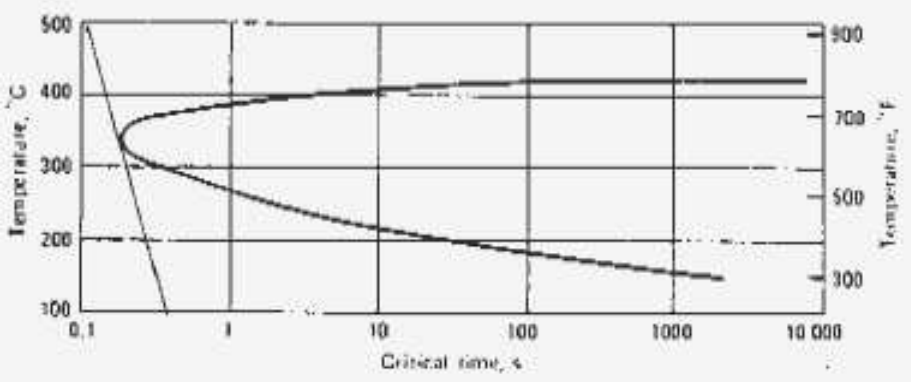

Figure 2.2: C-Curve for 99.5% maximum yield strength of 7075-T6 sheet[5].

As illustrated in table 2.6 the yield strengths predicted from quench factor agree very well with measured yield strengths. It is for this reason that predicting yield strength from quench factor instead of average quench rate is advantageous. In addition cooling curves that have long holding times either above or below the critical temperature range from 400 to 290ºC cannot be used to predict yield strength from average quenching rate.

Table 2.6: Yield strength values for 7075-T6 sheet predicted from cooling curves using average quench rate and quench factor[5]

Quench	Average quench rate from 400 to 290ºC (ºC/s)	Quench factor	Measured YS (MPa)	YS predicted from average quench rate (MPa)	YS predicted from quench rate (MPa)
Cold water	935	0.464	506	499	498
Denatured Alcohol to 290ºC, then cold water	50	8.539	476	463	478
Boiling water to 315ºC, then cold water	30	15.327	458	443	463
Still air to 370ºC, then cold water	5	21.334	468	242	449

Below is the equation for precipitation kinetics during continuous cooling[5]:

$$\zeta = 1 - \exp(k\tau) \quad (2.1)$$

where ζ is the fraction transformed and k is a constant related to the transformation fraction of a given C-curve. The quench factor (τ) is defined as:

$$\tau = \int \frac{dt}{C_t} \quad (2.2)$$

where t is time and C_t is critical time as function of temperature to transform a given fraction (x). In general the quench sensitivity is higher for higher solute concentrations and also in alloys containing dispersoids which act as nucleation sites for coarser precipitates. Subsequent to quenching, the material can either be naturally or artificially aged.

University of Cape Town

2.3.3 Aging

Aging process is the decomposition of a metastable supersaturated solid solution to form finely dispersed intermetallic compounds. The strengthening mechanism during age hardening is based on the formation of the secondary phase (intermetallic compounds) during decomposition of a metastable supersaturated solid solution[5, 7, 18, 19]. The far most important change in the mechanical properties during aging of Al alloys is attributed to the coherency strain field created by the GP (Guinier-Preston) zones. Illustrated in figure 2.3 is the classical age hardening diagram for binary aluminium alloy systems.

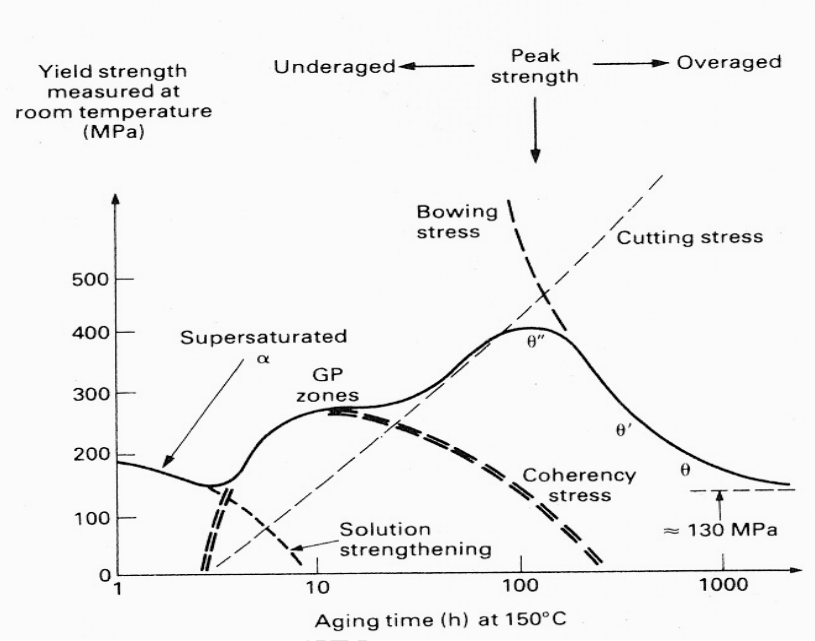

Figure 2.3: The yield strength of quenched Al-4wt. %Cu as a function of ageing time at 150ºC[13].

In Al-Mg-Si alloys containing an excess of silicon, the ageing process occurs in several stages and is believed to occur as follows[15, 16, 18, 19]:

$SSS \rightarrow (Mg + Si)_{clusters}/GP(I)_{spherical} \rightarrow \beta''/GP\ (II)_{needles} \rightarrow \beta'_{rods} + Si + others \rightarrow \beta_{plates} + Si$

where GP = Guinier-Preston zones

β = equilibrium Mg_2Si

β' and β'' = metastable precursors of β

The 3xx aluminium alloys are strengthened by precipitation of metastable β" precipitates. The metastable phases formed at the intermediate stage of ageing and positioned semi-coherent with the matrix are resistant to the movement of dislocations. It has been reported that the

metastable phase, β', nucleate and grow on dislocation at the expense of fine and uniformly dispersed GP zones. Gupta et. al[16] have reported that as the amount of Mg_2Si precipitates is increased the Al-Mg-Si alloy begins to strengthen slightly earlier and higher peak strength is achieved at a shorter time (figure 2.4). Figure 2.4 displays the relationship between ageing time, concentration of Mg_2Si precipitates and yield strength of Al-Ng-Si alloys.

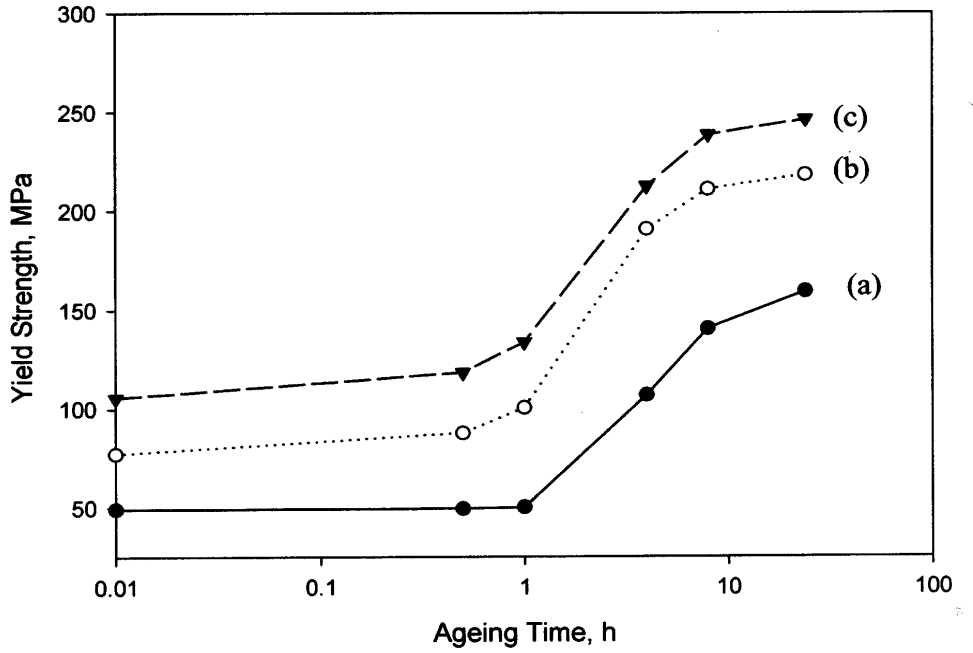

Figure 2.4: The effect of ageing time and Mg_2Si concentration on ageing behaviour of Al-Mg-Si alloys[20]. (a) 0.63 wt. % Mg_2Si; (b) 0.95 wt.% Mg_2Si; (c) 1.26 wt.% Mg_2Si.

Depending on the difference in sizes between the solvent and solute atoms, GP zones could either form as spherical zones or disk like planar aggregates. For example, if there is a large difference in atoms sizes, the GP zones usually form as disks[13]. In most cases the solute rich clusters, GP zones, are coherent with the matrix (i.e. form on the fcc lattice of the matrix).

According to the Orowan's theory, for strength to be increased or improved the following requirements need to be satisfied[19];

- a two-phase microstructure of the dispersed type which impedes slipping of dislocation in the matrix,
- particle diameter and spacing need not to be larger than atomic size b: Sp <<100b,

particles must be strong enough to promote looping of dislocations without being sheared: $d_c < d_p$.

University of

There are two types of aging processes that can be applied to alloys depending on the required properties, namely natural aging or artificial aging.

2.3.3.1 Natural ageing

Natural aging involves the decomposition of a metastable supersaturated solid solution at room temperatures to form finely dispersed Guinier-Preston (GP) zones. The two useful tempers that are associated natural aging are the T3 and T4-type tempers. These tempers produce moderate tensile and yield strength, high fracture toughness and high fatigue resistance. The initial increase in strength during natural aging is attributed to GP zone formation and the more stable precipitates are achievable after four or six days. In some alloys where cold work needs to be applied prior to aging, aging may be avoided by refrigerating.

2.3.3.2 Artificial ageing

This type of ageing process refers to the decomposition of a metastable supersaturated solid solution at elevated temperatures to form finely dispersed intermetallic compounds. The process is normally carried out in the temperature range of 100-200 ºC and ageing times vary from 2 to 48h. The aim of artificial ageing treatment is to produce the optimum precipitate size and distribution pattern[5]. During the ageing treatment process, there is always a compromise between the mechanical properties. For example, the aging conditions required to maximise tensile strength are frequently different from that required to maximise yield strength. To achieve maximum strength, both high quench rate and peak ageing are necessary however, for maximum elongation peak ageing is not necessary. Generally differences in type, size and distribution of the precipitated particles preside over mechanical properties. As illustrated in figure 2.3, hardening during artificial aging treatment is achieved by partially coherent precipitates. The mechanical properties change continuously with time and temperature. Of all the aging treatment tempers, the T6-type temper generally yields the highest strengths without compromising other properties which are useful for engineering applications. Castings of heat treatable alloys have the highest combination of strength, ductility and toughness when produced in T6 temper. Both the T5 and T7 are unique aging treatment tempers for castings. The T5 temper is normally applied to materials where high

University of Cape Town

hardness, and dimensional and strength stability are required at elevated temperatures (e.g. pistons and other engine parts). The T7 temper develops excellent ductility and toughness, and carries precipitation almost completely to prevent further precipitation during service. Although during the T7 aging temper ductility is improved however, strength is compromised.

2.4 Solidification of A356 alloy

The largely constant reactions found in figure 2.1 is the eutectic reaction,

$$L \longrightarrow \alpha + \beta$$

where L refers to liquid phase, α is mainly aluminium and β is predominantly silicon. The Al-Si eutectic can form through the following mechanisms[21]:

- directly from homogenous liquid in the case of a silicon concentration of 12.6% (i.e. for a eutectic Al-Si alloy);
- in the presence of primary aluminium in the case of silicon contents < 12.6% (i.e. for hypoeutectic Al-Si alloys);

  and
- in the presence of primary silicon crystals in the case of silicon contents > 12.6% (i.e. for hypereutectic Al-Si alloys).

During cooling of binary alloy from liquid phase, the eutectic microstructure can be lamellar or fibrous, regular or irregular, refer to figure 2.5. The criterion is that one phase must have low entropy of fusion, such that $\Delta S_{f,\alpha} < 2R$. For example in Pb-Sn binary system, at high volume fraction of both phases $(f \cong 0.5)$ there is preference for the formation of lamellar eutectic structure. However, when one phase is present in small volume fraction, there is tendency to the formation of fibrous of that phase (e.g. Cr in NiAl-Cr).

University of Cape Town

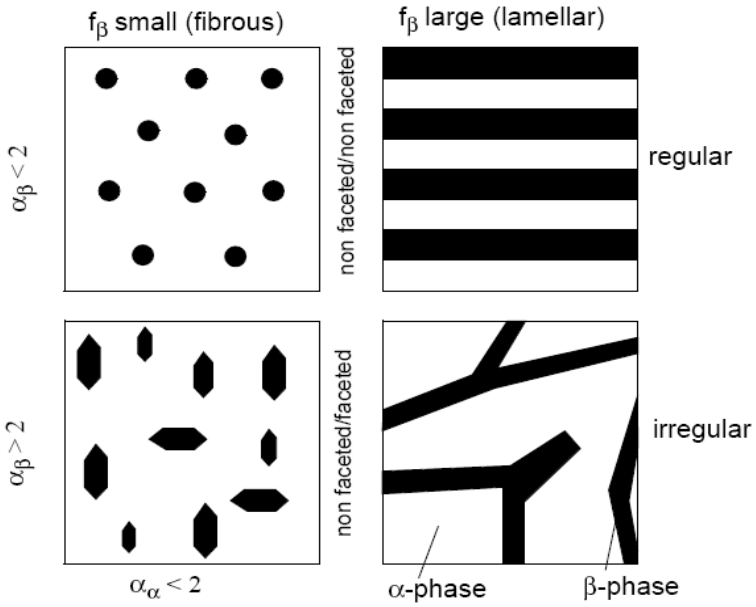

Figure 2.5: Types of binary eutectic morphology. $\alpha = \Delta S_f / R$, where ΔS_f indicates the entropy of fusion and R the universal gas constant[17].

It is reported that when the volume fraction of one phase is between 0 and 0.25, the eutectic structure will presumably be fibrous. However, if it lies between 0.25 and 0.5 the eutectic will have a tendency to be lamellar. When the low volume fraction phase possesses high entropy of melting, as in Al-Si system, the eutectic structure is of non-faceted/faceted type and irregular.

2.5 Heat treatment of cast Al-7 wt% Si-Mg alloy (A356)

The ability of an alloy to transformation to different phases at various temperatures forms the basis of the different heat treatments. Illustrated in figure 2.1 is the simple binary phase diagram of aluminium-silicon. It is reported that the solubility of silicon in aluminium reaches a maximum of 1.65 atomic percent at the eutectic temperature however, the solubility of silicon reaches 0.016 % silicon at 1190 ºC[5, 21].

During the T6 heat treatment, a high quench rate is necessary in order to achieve maximum strength[14]. Although high quench rate attains high strength, such quench rates induce problems of high internal stresses and distortion. However, low quench rate results in lower strength, ductility, and toughness and corrosion resistance due to unfavourable precipitate

University of Cape Town

characteristics. During the solution treatment of the casting alloy, Al-7wt% Si-0.4wt% Mg, an amount of 1.3-wt% Si is reported to be retained in solid solution of the matrix. In such alloy the level of Si in excess of the amount required to balance the Mg content to form the Mg_2Si compound is approximately 1-wt% [14]. In turn the high excess Si level may cause the casting alloy to develop high quench sensitivity. Additionally excess Si may also cause the formation of finer β" precipitates because of its effect on nucleation. This results in the high volume fraction of β" precipitates.

2.5.1 Age hardening model for Al-Si-Mg casting alloys

The total yield strength (YS_T) of an age hardening Al-7Si-Mg casting alloy is reported to be the sum of the yield strength of pure aluminium (YS_o) and the contributions to the yield strength due to eutectic Si particles (ΔYS_{Si}), eutectic Fe-phase particles (ΔYS_{Fe}), Si in solid solution $(\Delta YS_{ss,Si})$, Mg in solid solution $(\Delta YS_{ss,Mg})$, Si precipitates $(\Delta YS_{ppt,Si})$ and Mg-Si precipitates $(\Delta YS_{ppt,Mg-Si})$[22]:

$$YS_t = YS_o + \Delta YS_{Si} + \Delta YS_{Fe} + \Delta YS_{SS,Si} + \Delta YS_{SS,Mg} + \Delta YS_{ppt,Si} + \Delta YS_{ppt,Mg-Si} \quad \text{(2.4)}$$

where YS_o is the yield strength of pure Al, ΔYS_{Si} is the contributions to yield strength due to eutectic Si, ΔYS_{Fe} is due to eutectic Fe-phase particles, $\Delta YS_{SS,Si}$ is due to Si in solid solution, $\Delta YS_{SS,Mg}$ is due to Mg in solid solution, $\Delta YS_{ppt,Si}$ is due to Si precipitates and $\Delta YS_{ppt,Mg-Si}$ is due to Mg-Si precipitates. Since ΔYS_{Si}, ΔYS_{Fe} and $\Delta YS_{SS,Si}$ remain unchanged during aging and $\Delta YS_{ppt,Si}$ is negligibly small, then equation (2.4) is simplified to:

$$YS_t = YS_i + \Delta YS_{SS,Mg} + \Delta YS_{ppt,Mg-Si} \quad \text{(2.5)}$$

where YS_i intrinsic strength, is the sum of YS_o and those strengthening contributions which remain constant during aging.

According to Rometch and Schaffer[22], the model includes expressions for:

University of Cape Town

- the decrease in solute concentration and growth in volume fraction of precipitates during the early stages of precipitation;
- the effect of aging temperature on the equilibrium volume fraction;
- the coarsening of precipitates by Ostwald ripening;
- the strengthening contribution from solute atoms

and

- the strengthening contribution from both shearable and non-shearable precipitates

Möller et. al[15] investigated the influence of solution treatment time (at 540ºC), artificial ageing temperature and time, and prior natural ageing time on the T6 heat treatment response of rheocast A356. They performed solution heat treatment at 540ºC for times varying from 30 minutes to 6 hours, followed by water quench (25ºC). The artificial ageing times were varied from 0 to 240 hours and then samples were naturally aged for 20 hours, before artificially aged at 160, 180 and 190ºC. They concluded that the optimum solution treatment time at 540ºC to give maximum hardness after artificial ageing is 1 hour. They also found that SSM-HPDC A356 hardens significantly at room temperature after solution treatment at 540ºC, followed by water quench. They reported that the artificial aging response of the alloy can be increased by an immediate transfer from quench to artificial aging. According to Möller et. al[15] the time required to obtain maximum hardness at artificial ageing (T6 heat treatment) temperatures of 160 to 190ºC can be predicted using equations (3.4) and (3.5) respectively:

$$t_{T6} = 2.3x10^{-15}\exp(163000/8.314T) \quad \text{(3.4)}$$

$$t_{T6} = 4.9x10^{-16}\exp(163000/8.314T) \quad \text{(3.5)}$$

Equation (3.4) is used when there was prior natural ageing time while equation (3.5) is used when there was no natural ageing time.

It has been reported that the precipitates which grow during artificial ageing from the clusters are somehow coarser than those that develop in certain aluminium alloys aged immediately after quenching. This has adverse effects on the tensile properties of certain alloys (i.e. 10% reduction in tensile properties[15].

University of Cape Town

2.6 The general overview of Al-Si binary system

The addition of the alloying elements to pure aluminium improves its mechanical properties. Some of the major alloying elements in the hypoeutectic Al-Si alloys are copper (Cu), magnesium (Mg), titanium (Ti), iron (Fe), strontium (Sr) and manganese (Mn)[6, 23, 24]. All these alloying elements have different effects on the microstructure and subsequently on the mechanical properties. Both Mg (figure 2.6) and Cu are the most important hardening alloying elements in the Al-Si alloys because they form magnesium silicide (Mg_2Si) and copper aluminide ($CuAl_2$). In binary Al-Si alloys the strength depends more on the distribution and shape of the Si particles and other alloying elements rather than on the composition. Addition of Mg improves the strength of the alloy after proper heat treatment is applied. It is reported that magnesium addition to Al-Si eutectic base alloys refines the microstructure up to 0.3% and beyond that point refining action starts to fade[6]. There are several factors which need to be considered before an alloy is selected for casting applications, such as casting applications, such as casting process consideration (e.g. fluidity), casting design consideration (e.g. solidification range), mechanical-property requirements, service and economics. One of the most important requirements for an alloy to be modifiable by age hardening is that solid solubility of one or more alloying elements should decrease with decreasing temperature[5, 12, 14, 19]. Some of the casting alloys contain amounts of silicon which far exceeds the solubility limit required for strengthening purpose. In such cases with high silicon content, the silicon acts to improve castability, prevent cracking and increase wear resistance[13]. The most commonly used cast alloys are, A356 and A319 (table 2.7) because they are important for many automotive components, such as suspension, driveline, and engine parts, where increased durability and reliability are always desirable[3, 4]. The A356 alloy has low solidification cracking susceptibility, due to the narrow temperature range between the liquidus and solidus on the Al-Si binary phase diagram[25]. Due to its excellent castability characteristics, A356 is a semi-solid metal (SSM) cast alloy, precipitation hardened by β" phase, coherent with the aluminium matrix.

University of Cape Town

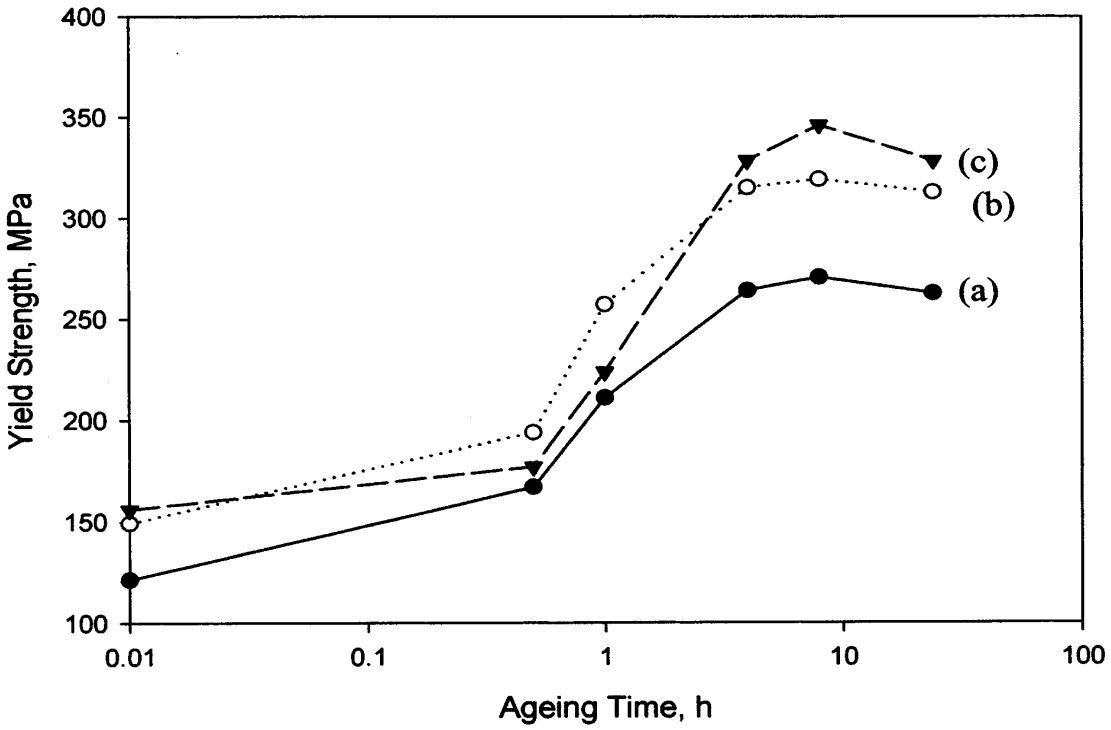

Figure 2.6: The effect of Mg addition on the ageing behaviour of Al–Mg–Si alloys[20]. (a) 0.4 wt. % Mg (b) 0.6 wt. % Mg and (c) 0.8 wt. % Mg.

Table 2.7: Specified chemical composition for A319 casting alloy[5]

Elemental chemical composition in wt%									
Si	Fe	Cu	Mn	Mg	Zn	Ti	Zn	Ni	Al
5.5 - 6.5	1.0 Max.	3.0 - 4.0	0.5 Max.	0.10 Max.	1.0 Max.	0.25 Max.	0.10 Max.	0.35 Max.	Bal.

University of Cape

2.6.1 The effects of Sr addition on A356 Alloy

The mechanical properties of hypoeutectic aluminium-silicon (Al-Si) alloy, A356, can be improved by addition of chemical modifiers to modify the eutectic silicon[26, 27]. In general, the addition of chemical modifiers such as strontium or sodium (Na) to hypoeutectic Al-Si alloys, results in a finer elongated or fibrous eutectic phase. It has been reported that individual additions of the grain refiner (e.g. TiBAl) raises the primary α-Al nucleation temperature by as much as 4–5 ºC[28]. However, additions of Sr-based modifier depress the eutectic temperature by approximately 7-8 ºC. The addition of Sr decreases the eutectic nucleation temperature and eutectic maximum temperature. Consequently this leads to a larger α-Al solidification range and hence more α-Al formation. There is a specific limit of grain refiner addition beyond which segregation and agglomeration of Sr-based intermetallic compounds are not avoidable[29]. The main disadvantage of the formation of the intermetallic compounds is on the mechanical properties of the finished product because these compounds act as crack initiation sites in the finished product[29]. The primary α-Al crystals are normally surrounded by the eutectic region. Strontium particles provide the number of nucleation sites for the eutectic Si. In turn the silicon lamellar is transformed to fibrous (elongated) morphology with extremely branched Si which grows in three dimensional structures around the existing primary α-Al crystals[29].

University of Cape Town

2.7 Microstructure and mechanical properties of Al-Si cast alloys

Usually cast aluminium alloys are susceptible to void-crack nucleation, growth and coalescence from magnesium, iron and silicon particles[23]. In some cases cast alloys contain micro-voids (porosity) due to feeding impediment through dendritic solidification fronts, trapped gases, or temperature gradient driven solidification[11, 30, 31]. The size, shape and distribution of porosity will have a strong effect on the mechanical properties. Generally a more homogenous equiaxed grain structure is preferred in aluminium casting alloys as it improves resistance to hot tearing and mass feeding[5]. Clearly, the more homogenous the grain structure is, the less is liquid segregation hence the casting responds better to heat treatment.

The mechanical properties on the other hand are greatly enhanced by achieving a smallest grain size. Grain size is greatly affected by the following factors: number of nucleation sites,

alloy composition, freezing rate, temperature gradient in the melt, and casting method[5]. The aluminium-titanium (Al-Ti) binary alloy contains a grain refiner, $TiAl_3$, which is soluble in molten aluminium. However for $TiAl_3$ to maintain its grain refinement effectively, Ti levels greater than 0.15% need to be added. Unfortunately such high levels of Ti can give rise to very coarse intermetallic particles, which are harmful to mechanical properties. The most used chemical grain refiners are based on aluminium-titanium-boron (B) master alloys. These master alloys contain 3 to 10% Ti and a Ti:B ratio ranging from approximately 3 to 50. The Al-Ti-B mater alloys also consist of the soluble $TiAl_3$ particles and insoluble boride particles in an aluminium matrix[5].

The tensile properties of A356 aluminium castings depend strongly on the porosity levels, the size of the microstructure and heat treatment conditions[3, 32]. In addition to the porosity levels, the fatigue properties of Al castings also depend on the size, shape and distribution of the second phase particles in the microstructure[3]. Although the microstructural and mechanical factors affect the fatigue resistance of cast Al alloys, problems can also arise from the presence of porosities and oxide films generated during the casting process[33, 34]. Large pores present at or near the specimen surface act as fatigue crack initiation sites. Several microstructural features such as secondary dendrite arm spacing, Si particles, Fe-rich intermetallic plates, and Al matrix play an important role in fatigue damage evolution. Finite elemental analysis (FEA) is an analytical tool used to investigate the debonding and cracking behaviour of Si particles during fatigue in cast Al-Si alloys[33, 34].

Table 2.8: Mechanical properties of A356 alloy cast under different casting conditions.

Casting condition	Heat treatment Condition	YS (MPa)	UTS (MPa)	% Elong.
SSM Cast[35]	T4 (540ºC, 6 hrs)	133	244	17
SSM Cast[36]	T4 (540ºC, 6 hrs)	144	255	13.3
Sand Cast[5]	T6 (540ºC, 6 hrs,20 hrs NA, 170ºC)	165	230	3.5
Permanent Mould[5]	T6 (540ºC, 6 hrs,20 hrs NA, 170ºC)	185	262	5
SSM Cast [35]	T6 (540ºC, 6 hrs,20 hrs NA, 180ºC)	255	317	9.3

University of Cape Town

2.8 General overview of casting methods

The casting process involves pouring of molten metal into a mould or die having a cavity of the desired shape of the casting[5, 7]. Casting processes are classified into different categories depending on the type of mould and pattern, or by force required to fill the mould with molten metal[5, 7]. Additionally, there are important factors affecting the selection of a casting methodology which include the following:

- Quantity of castings required
- Practical ability to cast the product required
- Complexity
- Design of the casting
- Tolerances required for net or near net shape
- Cost of equipment
- Metal specification
- Surface finish required
- Mechanical properties desired
- Joinability
- Minimum wall thickness
- Financial limit on capital costs
- Value of net shape or near net shape.

The most important factors for all casting processes are feasibility, cost and quality. In most cases when more than one casting methods are equality feasible for a given part, the method used very often is dictated by costs. To mention casting processes in decreasing order of amount of aluminium cast, are: die casting, permanent mould casting, sand casting (green sand and dry sand), plaster casting, and investment casting. Casting methods can be classified into four main groups, namely: conventional moulding processes, precision moulding processes, chemically bonded sand casting processes and special and innovative moulding processes[8].

University of Cape Town

2.8.1 Conventional moulding processes[5, 7]

2.8.1.1 Sand casting

Sand casting is a common form of casting aluminium and can produce complex shaped castings that may not be possible with other methods.

Advantages

- Requires low equipment cost
- Suitable for wide range of casting alloys
- Sand recovery systems enable reuse of sands.

Disadvantages

- Ideal for production of small number of castings
- Sand castings require machining since dimensions of castings are not precise
- Low strength because of slower rate of solidification.

University of Cape Town

2.8.1.2 Green sand moulding

The process uses a mould made of compressed or compacted moist sand. Compaction is achieved by either jolting or squeezing the mould and hence this type of moulding is most ideal for light to medium sized castings or for use with production moulding machines.

Advantages

- Most metals are castable by this method
- Material costs are relatively low
- Method is adaptable to large or small quantities.

Disadvantages

- Practical limits to the complexity of the design of the component
- Machining often required to achieve finished product
- Dimensional accuracy not controllable.

2.8.2 High density moulding (high squeeze pressure / impact)

Squeeze casting also known as liquid-metal forging, is a process by which molten metal solidifies under pressure within closed dies positioned between the plates of a hydraulic press. This method is easily automated to produce near-net to net-shape high-quality components.

Advantages

- Most metals can be cast by this method
- Close dimensional tolerances achievable
- Castings with good surface finish are produced
- Reduced feed material
- Improved casting soundness.

Disadvantages

- Tighter quality controls are required with this type of moulding
- High density moulding is generally accustomed to more sophisticated equipment, maintenance and operating procedures.

2.8.3 Precision casting processes

These processes produce castings with an improved surface finish, while producing excellent detail with higher degree of dimensional accuracy.

2.8.3.1 Permanent mould (gravity die) casting

Permanent mould method also known as gravity die casting, is suited to high-volume production. Permanent mould castings are larger than die castings with a maximum weight of usually 10 kg. Surface finish of permanent mould castings depend on whether or not a mould wash is used.

Advantages

- Castings with excellent mechanical properties can be produced
- Good casting soundness
- Castings are heat treatable

University of Cape Town

- Consistent quality of finish on castings.

Disadvantages

- High tooling cost
- Limited to the production of small castings of simple exterior design.

2.8.3.2 High pressure die casting (HPDC)

The essential feature of HPDC is the use of permanent metal dies into which molten metal is injected under pressure and at high speed. The production of a casting requires three stages:

- Pre-filling (moving metal to the front of the gate)
- Filling in a short time at high speed
- Solidification under high pressure.

Generally the speed of metal introduction and rapid cooling rate encourages turbulent flow and shrinkage porosity.

Advantages

- Cost of castings is relatively low with high volumes
- Die castings can be produced with a high degree of complexity and good surface finish
- Considerable design flexibility with high degree of accuracy offered
- Die castings are heat treatable.

Disadvantages

- Size of castings that can be produced is limited
- Equipment and die costs are very high
- Process is prone to porosity
- Good die design is essential.

University of Cape Town

2.8.3.3 Investment casing (Lost wax)

The principal feature of the investment mould is that a fluid mixture flows around a prepared wax pattern providing excellent detail. Wax (plastic) patterns are assembled on a "tree" and invested with ceramic slurry. The tree is then immersed into a fluidised bed of refractory particles to form the first layer of the ceramic shell. The mould is allowed to dry and the process is repeated with coarser materials until sufficient thickness has been built up to withstand the impact of hot metal. The wax is then melted out for sufficient recovery and then moulds are fired prior to casting.

Advantages

- Extreme accuracy and flexibility of design offered by the process
- Ideal for casting alloys that are difficult to machine
- Castings with excellent surface finish produced
- Suitable for large and small quantities.

Disadvantages

- Limitation on the size that can be produced
- Low scale production
- High casting costs.

Even though there are few casting processes (e.g. squeeze casting) that are equality feasible with semi-solid high pressure die casting for a given part, overall semi-solid high pressure die casting dominates by costs.

University of Cape Town

2.9 Semi-solid metal high pressure die casting (SSM-HPDC)

Conventional casting technologies such as HPDC have turbulent filling characteristics and as a result components with high porosity and poor integrity are produced. Although HPDC is the most efficient casting process to reduce porosity, it is limited by blistering and heat treatment and possesses poor weldability. Convectional HPDC possess poor weldability because of the blistering phenomena which is caused by gas entrapment during casting. Such phenomena limit the feasibility of thermal treatment of high-pressure die cast components. Another important reason why high pressure castings are not heat treatable is because of the residual stresses in the casting after it is ejected from the die[7]. The residual stresses are caused by the

rapid injection of metal into the die, the high intensification pressure applied during solidification and the rapid cooling rates during solidification. Such stresses also cause excessive distortion.

Unlike conventional metal forming processes which uses either solid metals or molten metals as feedstock material, SSM forming uses semi-solid slurries as starting material[31, 37, 38, 39]. An ideal microstructure for semi-solid slurry before the forming process will be finely dispersed solid particles in a liquid matrix. Such microstructure can be achieved via two SSM forming routes, thixocasting and rheocasting.

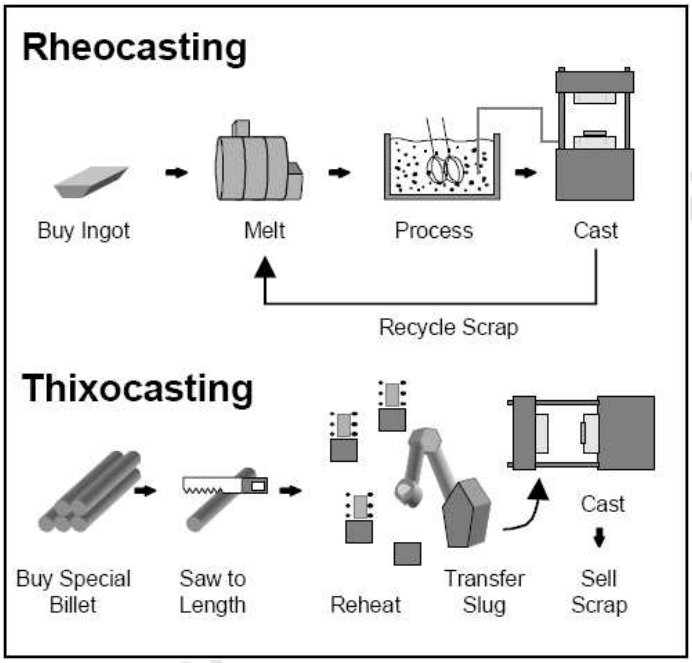

Figure 2.7: Schematic of the Rheocasting and Thixocasting processes[38].

Thixocasting uses feedstock material with the desired fine round grain structure which was previously formed from the liquid state and allowed to solidify (figure 2.7). The fine round grained feedstock material is reheated into semi solid and formed[37, 39]. The main advantage of thixocasting over rheocasting is that the material composition and quality is consistent throughout the material. The main disadvantage of thixocasting over other casting processes such as HPDC or rheocasting is high capital investment. The high capital investment arises because of high cost special feedstock material needed and reheating stations.

The second route, rheocasting, begins with molten material which is cooled to a semi solid state with the desired fine round grained microstructure under controlled conditions

(figure 2.7). Rheocasting offers the advantage of eliminating the need for specially prepared feedstock and reheating stations hence reduction of cost.

The advantage of both SSM forming processes, thixocasting and rheocasting, is that gas entrapment is reduced, due to laminar characteristics as the material flows into the die cavity. Therefore, because gas entrapment is reduced, almost all heat treatments conditions are possible. Since the discovery of semi solid metal (SSM) processing by Spencer, the process continues to find its place in the manufacturing of complex components because of its ability to provide near-net-shape components with high integrity[37]. Other advantages of SSM forming processes are that components of different wall thicknesses can be designed and joining by Laser, MIG or WIG welding is possible. Laser welding provides superior advantages to convectional welding processes based on the facts discussed in section 2.8 below.

University of Cape Town

2.10 Overview of laser welding

Generally laser welding represents the balance between heating and cooling within a localised volume overlapping two or more solids such that liquid pool is formed and remains stable until solidification. The main aim of laser welding is to create the liquid melt pool by absorption of incident radiation, allow it to grow to the required size, and then to spread this melt pool through the solid interface eliminating the original seam between the components to be joined. Laser welding is superior to most conventional welding techniques owing to the advantages such as low heat input, high welding speed, and high production rate[4, 8, 9, 40, 41, 42, 43]. The increase in absorption of laser beam with temperature has resulted in the usage of laser beam as a heat source for welding[9]. For all laser welding irrespective of the types of laser used, energy is absorbed at the surface of the metal by a process known as Fresnel Absorption[8]. At relatively high intensities, vaporisation occurs thereby exciting some of the metal electrons hence becoming free electrons (ionisation) [9]. The free electrons then absorb energy directly from the laser beam by a process known as inverse Bremsstrahlung. Laser welding is superior to most conventional welding techniques however; laser is comparable to electron beam welding. The main difference between the laser and electron beam welding is

that lasers heat with photons of approximately 0.l eV energy whilst electron beams use particles of 100 000 eV energy. The beam of laser light interacts easily with free electrons found in the plasma which then defocuses part of the incident beam[40]. Due to relatively high energy offered by an electron beam, electrons are hardly deflected by plasma which makes it easier to couple the energy much more efficiently using electron beam welding compared to laser welding. However laser beam welding has an added advantage of being able to be conducted at ambient conditions[41]. Another important advantage in weld design is that joints that might require access from different directions such as, resistant spot welding of lap seams, can be laser welded from one direction only[42, 43]. Although laser welding is superior to most conventional welding techniques because of the combination of its low heat input, low welding distortion and high speed which reduces defects that are normally evident during welding of aluminium alloys, its effectiveness depends highly on the thermophysical properties (e. g conductivity and diffusivity) of the material to be welded[42].

There are two main types of industrial lasers, carbon dioxide (CO_2) and neodymium doped yttrium aluminium garnet (Nd: YAG), however for this project (Nd: YAG) laser will be used. The CO_2 laser consists of the mixture of nitrogen (N_2) and helium (He) gas in addition to CO_2 and gases flow in a closed system. This closed system allows the gas mixture to be recycled through the discharge hence lowers the operating costs[42]. Although the CO_2 laser has proven reliability, high power output, high efficiency and safety, an Nd: YAG laser has greater penetration depth relative to the CO_2 laser[42, 43]. Nd: YAG laser has fewer tendencies to form plasma compared to CO_2 laser[42]. Another added advantage of Nd: YAG laser compared to CO_2 laser is the flexibility offered by fibre-optic delivery[43]. For the same laser beam, spot diameter and welding speed, an Nd: YAG laser has greater penetration depth compared to CO_2 laser. Commercial Nd: YAG lasers for welding application may be operated in three modes; continuous output, pulsed pumping and Q-switched mode.

There are two modes of laser welding which are heat conduction and deep penetration welding[43, 44]. Illustrated in figure 2.8 is the schematic representation of the deep penetration laser welding.

University of Cape Town

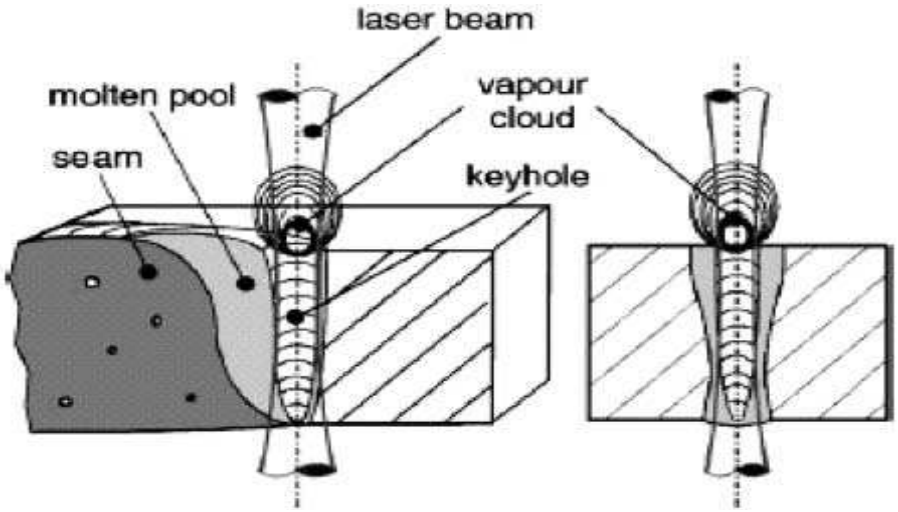

Figure 2.8: Deep penetration (keyhole) mode laser welding[45].

The heat conduction welding occurs when the laser beam light changes to heat energy. Additionally part of the heat energy must melt the metal whilst the other part conducts into the metal. Cladding is an example of the heat conduction welding process[44]. The main advantage of conduction welding is that the surface of the weld pool remains unbroken. This result in fewer disturbances to the system because laser radiation does not penetrate into the material being welded. There are three possible energy losses that can occur in the plume (figure 2.9): defocusing, absorption, and scattering[44]. Therefore the loss of energy in the laser beam welding results in seam imperfections like porosity or holes in the seam which reduces the mechanical properties. Such seam imperfections (e.g. surface holed and porosity) are normally caused by process instabilities. In general conduction welds are less affected by gas entrapment during conduction welding because fusion occurs without any melting of material. Depending on the on the peak laser intensity and duration of the laser pulse applied to the workpiece, the mode of laser welding can change from conduction mode to that in which a keyhole (deep penetration welding) is formed. Therefore, the keyhole is formed at the region in which the laser intensity is high enough to melt and vaporise some of the workpiece material[46]. The position and size of the laser keyhole are kept changing when workpieces are joined during the deep penetration welding[47].

University of Cape Town

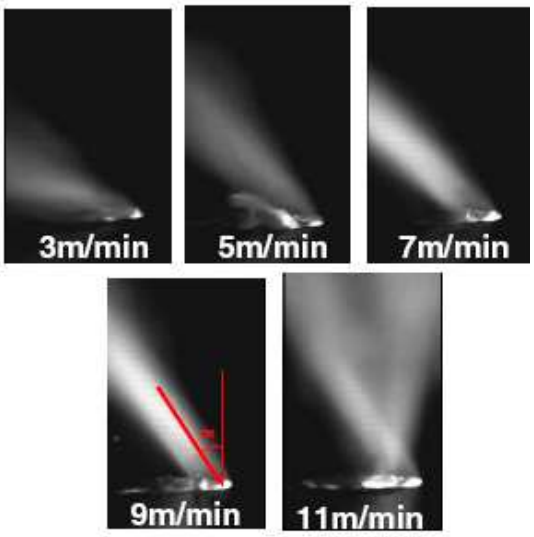

Figure 2.9: Visualisation of maximum plume deviation as the function of welding speed[48].

This is due to the changing of the laser incidence angle at keyhole front, keyhole shifting caused by change of vapour-flow vectors, such as recoil force, dynamic pressure and shear stress and the change in the effective laser power by plasma absorption induce keyhole fluctuation. Jin et al.[46] did some pioneering work on keyhole shapes in laser deep penetration welding, which proved that when the focal plane is located near the surface of the workpiece, the laser intensity increases and the keyhole diameter is near or larger than the Gaussian beam diameter at that position.

The selection of the welding process for Al and its alloys is based on the following considerations, such as[49]:

- the amount of power required for the application and that available from the laser.
- the complexity of the component and flexibility of the light delivery system.
- the wavelength of the laser light affecting both it's transmission to, and interaction with, the processing medium.
- capital cost and proven reliability against proposed production benefits.
- beam quality. A measure of the capability of a laser system to produce a minimum focused spot size.

University of Cape Town

The most important properties of the laser beam are both its wavelength and beam parameter product (BPP). For example, the clean undisrupted surface of aluminium and its alloys is highly reflecting at both CO_2 and Nd: YAG laser wavelengths. However, the reflectivity decreases with an increase in temperature[43]. However, the absorption of laser light depend strongly on the product of incident laser intensity, I, and dwell time, t, at a particular point on the metal surface. Where large values of It lead to vaporisation, surface disruption and formation of a keyhole. The welding efficiency which is also defined as power transfer coefficient, η, is small below the threshold for keyhole formation but can approach unity once a keyhole has been formed[43]. The rate of melting to incident power is related by the melting efficiency or melting ratio (ε). It has been reported that the maximum value for ε is 0.48 for penetration welds and 0.37 for conduction welds. Laser welding offers a combination of low heat input, low welding distortion and high speed compared with other welding processes. During the welding process some of the volatile alloying elements evaporate, therefore the addition of the filler wire with enough alloying elements improves the morphology of the weld[50]. One of the most important parameters in laser welding of aluminium and its alloys is the shielding gas. Section 2.8.1 below provides a detailed discussion on the shielding gas.

University of Cape Town

2.10.1 Shielding gas

Shielding gas is of paramount importance in welding of aluminium alloys as it serves several purposes. One of the most important roles of the shielding gas is to prevent oxidation of the weld pool and to create a slag near the fusion zone. However, the most critical role of the shielding gas is to suppress the formation of plasma over the weld zone[43, 51, 52]. Additionally to the usage of the shielding gas to suppress the formation of plasma, plasma can also be charged and forced away from the keyhole by electric and magnetic fields with the proper magnitudes and directions[44]. During laser welding, plasma formation is initiated above the workpiece and the laser-induced plasma tends to absorb the laser energy entering the workpiece. Therefore the absorption of laser energy by plasma reduces the penetration capability of the laser beam, resulting in changes from the weld beam shape and to producing instabilities due to fluctuation of laser energy reaching the workpiece[51]. The formation of weld instabilities such as porosity becomes easier in the presence of plasma because, plasma covers the weld pool and prevents the release of metal vapour or gases[51]. However the proper

functionality of the shielding gas also depends on the gas chemical composition and flow rate. Helium gas is used for both shielding and plasma control purposes because it suppresses the formation of plasma due its high ionisation potential and good thermal conductivity[42, 51]. An increase in the shielding gas flow rate suppresses the formation of undesirable plasma until a critical flow rate is reached. Above the critical flow rate, the gas not only removes the plasma but also destroys the weld pool and keyhole stability, which leads to a decrease in penetration depth[51].

In addition to the process parameters influencing the shape and properties of the molten pool, there are relative factors[43, 50]. The relative factors are as follows:

- The position of the laser beam relative to the welded materials and to the flow of the shielding gas.
- The movement between the laser beam and welded material.

University of Cape Town

2.10.2 The weld and its thermal cycle

In 1935 Rosenthal gave the solutions to the heat flow equations of a moving point source[53]. The assumption made was that the energy of the heat source moves with a constant speed, v, along the x-axis of a fixed rectangular system.

The geometry and penetration of the pool are greatly influenced by the heat flow and fluid flow in the molten weld pool. Consequently, this affects the temperature gradient in the weld pool and the solidification behaviour of the weld. There are some dynamic mechanisms of fluid flow in laser weld pool, such as forces resulting from temperature-dependent surface tension, the friction force of the metal vapour escaping from the keyhole, density variations and movement of the keyhole relative to the workpiece[47]. It is known that liquid turbulence within the pool does affect pool geometry. Liquid turbulence is greatly affected by the surface tension of the melt. This surface tension-influence convection is known as Marangoni convection[47, 53]. In addition aerodynamic drag forces of the plasma jet may contribute to the convection in the weld pool. Wang et. al[47] investigated the effect of pressure gradient driven convection in the molten pool during the deep penetration laser welding. They concluded that the pressures on the keyhole front wall and on the rear wall are larger that the atmospheric

pressure. The pressure difference between the front wall and rear wall (former is larger than the latter) makes molten metal flow from the front part in the weld pool to its rear part. Consequently this might cause the laser keyhole to close. They also concluded that the dynamic pressure of the keyhole walls is one of the important driving forces of fluid flow in the weld pool. The composition of the melt (i.e. presence of oxygen and sulphur) is the primary factor which is reported to greatly influence surface tension. Apart from surface tension effects, there are additional factors which need to be considered such as: electromagnetic forces and bouncy within the melt.

2.10.3 Advantages of laser welding

Due to narrow heat affected zone (HAZ) of laser welds, thermal distortion is limited. Consequently the mechanical properties are improved because of narrow HAZ and deep penetration. Evaporation of alloying elements can be reduced and contamination from electrode material is limited with laser welding. The high heat intensity at the beam focus introduces the concept of keyhole or penetration welding and the possibility of laser welds with a high aspect ratio, narrow HAZ, and high processing speed.

The option of using filler metal during deep penetration laser welding serves many advantages such as to[42, 43]:

- compensate for metal loss due to vaporisation of volatile alloying elements
- reduce porosity
- control seam compositions to reduce susceptibility to the fusion zone brittleness or stress corrosion cracking or to avoid weld cracks.
- lower the sensitivity to joint gaps and lead to a wider fusion zone.

2.10.4 Disadvantages of laser welding[42, 43]

High capital cost

Laser welding of high reflective materials often results in the problem of reflection of laser radiation back into the laser where damage to optical components can occur.

University of Cape Town

2.11 Laser welding of aluminium alloys

Aluminium and aluminium alloys can also be joined by various joining methods, such as fusion and resistance welding, soldering, brazing, adhesive bonding and mechanical joining. Inherently, welding of aluminium alloys poses some defects such as a lack of penetration, porosity and blowholes, liquidation and solidification cracking, loss of alloying elements and reduced mechanical properties. When dealing with laser beam welding of aluminium alloys, thermal properties of aluminium alloys are of paramount consideration[54]. Some of the reasons for laser beam welding instabilities are; resonant reaction in the system laser, vapour cloud and keyhole[41]. Alloying elements such as Silicon (Si) or Magnesium (Mg) decrease the viscosity which puts the system into resonance and thus, low damping effect of the liquid material around the keyhole[55]. However, elements like copper (Cu), titanium (Ti) or iron (Fe) increases the viscosity and in their presence the welding process becomes stable. In aluminium alloys high temperature oxidation occurs rapidly at temperatures reached during laser welding. Even though the absorbing thin oxide layer film enhances the laser coupling which is essential in the initial heating phase, however it has no effect during welding. The oxide layer can greatly influence the threshold intensity for surface melting and vaporisation.

It has been proven that both the penetration depth and weld width decrease linearly with increasing the welding speed. However, relatively high welding speeds are reported to increase brittleness in the fusion zone[42]. The treatment of molten metal during casting processes by using magnetic stirring to achieve a more homogenous globular grain structure is well established. However, Thomy and Vollertsen[56] have conducted a study on the influence of magnetic fields on dilution during laser welding of aluminium. It is most common to introduce silicon-containing filler metal into the weld metal during laser welding of hot cracking sensitive aluminium alloy sheets. The filler wire has an added advantage of minimising the occurrence of hot cracking. However, to achieve the most favourable result a more homogenous distribution of more than 2 % of silicon throughout the weld metal is recommended[56]. Thomy and Vollertsen used the welding head prototype for magnetic stirring during CO_2 laser welding. They prepared overlap welds by applying magnetic flux densities in the focal point of B = 0 mT to 60 mT and frequencies in the range of f = 0 s^{-1} to 20 s^{-1} at a CO_2 laser power of P_L = 5 kW at the workpiece and a welding speed of 7.8 m/min with helium shielding gas (20l/min). They concluded that the alternating magnetic field has an important and reproducible influence on both the size and the homogeneity of the dilution area. In

University of Cape Town

addition, it was also concluded that the application of alternating magnetic fields does not have an adverse effect on the weld bead. Rapp et. al[57] did a study on the problems, solutions and readiness for application of laser welding of aluminium lightweight materials. They used the welding head of a 2.3 kW continuous welding Nd:YAG laser with flexible glass fibre to weld AA6009 alloy. The aluminium 6XXX alloys are prone to hot cracking hence the use of filler wire is necessary for such alloys. A 2 mm thick Al-Mg-Si sheet with a 2.3 kW continuous welding Nd:YAG laser with filler wire at a welding speed of 2 m/min. Rapp et al concluded that by use of filler wire, welding defects such as hot cracking, gab bringing and undercuts can be eliminated.

Kern et. Al[58] reported the initial work on the usage of magnetofluid-dynamic effects to stabilise the welding process.

Xiao et. Al[59] investigated further modification of magnetofluid-dynamic model by applying an electrical current through an external power source during laser welding. The applied electrical current flows in the weld pool thereby inducing a magnetic field. Therefore magnetic forces will be generated which will certainly influence the fluid flow in the weld pool and welding process. Xiao et. al made bead-on-plate welds on 5 mm thick plates of 1050 wrought aluminium alloy. The focus position used was set 1 mm above the surface of the workpiece using helium shielding gas (25l/min). They found that electromagnetic forces per unit volume are much higher at the surface in front of the keyhole. Therefore, the molten metal in front of the keyhole is accelerated towards the bottom hence increasing the heat in this region. This results in an increase in the weld depth. They then concluded that an external current can greatly influence the fluid flow of the weld pool and shape the seam cross section in laser welding of aluminium.

University of Cape Town

2.11.1 Surface preparation prior to welding

In general all commercial aluminium alloys possess a thin hard oxide layer. This oxide layer becomes thicker and under humid environment and at elevated temperatures. The thicker the oxide layer, the greater its undesirable effects on weld metal flow and solidification hence fusion becomes difficult. Inherently the hard oxide layer is porous and as a result traps grease, oils, dirt and moisture from the surrounding environment. Additionally, the inherent oxide layer of aluminium alloys may greatly influence the energy absorption of incident laser beams

and the power density for deep penetration welding. Therefore, abrading the surface with the aid of stainless steel brush breaks up the oxide layer[25, 45, 60, 61]. Haboudou et. al[25] investigated the importance of surface preparation prior to laser welding for A356 and AA5083 alloys. Prior to welding, they subjected samples to different surface preparations such as: acetone degreasing, 220 and 800 grit SiC grinding paper, sand blasting and pulsed YAG laser cleaning. They used the secondary ion mass spectroscopy (SIMS) technique to analyse the first 2 µm metallic layers of specimens. SIMS analysis confirmed a decrease of the oxide and hydride layer after surface preparation. It was concluded that laser cleaning is the superior surface preparation method because it reduces the hydrogen sources responsible for microporosity generation, and reduces a nearly total suppression of pores in A356.

2.11.2 Defects accompanied with welding of aluminium alloys

2.11.2.1 Porosity

There are two main groups of porosity generated during yttrium aluminium garnet (YAG) laser welding, these are; microporosity and macroporosiy[25]. Microporosity is usually 50-200µm in size, and normally occurs due to hydrogen solubility in molten aluminium. Whilst macroporosity is usually less circular than microporosity and its size ranges from 300µm to 600µm. At low welding speed the keyhole collapses more easily and is at risk of creating more macroporosities[25]. In the laser welding of aluminium alloys, four types of porosity are evident such as hydrogen porosity, porosity caused by the collapse of unstable keyholes, porosity due to entrapment of gases by surface turbulence and shrinkage porosity[5, 42, 60]. One of the factors affecting porosity is the turbulence flow of the molten pool during the welding process[41, 62]. Porosity formation is also caused by the resultant fluctuation of the keyhole during penetration laser welding[62]. The restriction of porosity formation is often achievable only if there is the balance between the pressure in the keyhole and out of the keyhole[62]. High cooling rate suppresses the formation of hydrogen porosity because of the decreased time available for the diffusion of hydrogen[60]. As a result of high cooling rates experienced in laser welding, small bubbles are formed and lowers the pore density number and volume fraction[60]. Horstemeyer et. al[30] used X-ray computed tomography (CT) to determine the three dimensional porosity distribution. The X-ray CT is a non-destructive testing machine that uses X-rays to precisely determine the local density changes. Generally the CT produces both

University of Cape Town

the two- and three dimensional spatial data twisted together with a forth dimension that is the X-ray linear attenuation coefficient (LAT). The LAT is a function of material density, elemental composition, and X-ray energy. Therefore, for specimens which have homogenous elemental composition, changes in the LAT represent changes in material density. Whilst for inhomogeneous specimens, changes in the LAT represent either density changes or segregation of elements, or both. However, voids (porosity) in material result in LAT values of zero or near zero depending on the spatial resolution.

2.11.2.2 Hot Cracking

Hot cracking is a defect which manifests itself as a surface crack during the solidification process of metal alloys. The cracks that appear during welding of aluminium alloys are formed due to several interlinked factors, such as: solidification shrinkage and thermal tensions (i.e. generates tensions and deformations), wide range of deformations, temperature and time-cycle of solidification speed, chemical composition of the alloy and fastening system of the welding components (i.e. can limit contraction). The method which is most often used to prevent hot cracking is to chemically modify the molten pool by using the filler wire which has enough alloying elements. When the filler wire is to be used, it must reach the molten pool in a liquid state to ensure that there is a continuous heat transfer into the molten pool and less reflectivity[50].

University of Cape Town

2.11.2.3 Stress corrosion cracking (SCC)

The resultant residual stresses induced by the welding process combined with structural load in the HAZ can give rise to distortion, brittle fracture, change the fatigue strength and stress corrosion cracking[63]. The aluminium alloys that contain significant concentration of soluble alloying elements, mainly copper, magnesium, silicon and zinc are prone to SCC[5]. In aluminium alloys stress-corrosion cracking is typically intergranular. Any condition along the grain boundaries that makes them anodic to the rest of the microstructure is required so that corrosion propagates selectively along the grain boundaries. Is has been reported that such a condition is created by localised decomposition of solid solution, with a high degree of

continuity of decomposition products along the grain boundaries. Therefore, to prevent stress-corrosion cracking heat treatments that produce microstructures either free of precipitate along grain boundaries or with precipitate evenly distributed with grains must be applied. However, for most alloys, optimum levels of resistance to intergranular corrosion or resistance to stress-corrosion cracking require different heat treatments. Therefore resistance to intergranular corrosion is not a reliable indication of resistance to stress-corrosion cracking.

University of Cape Town

Chapter Three

Experimental Procedure

3.1 Material

The A356 Al alloy in an ingot was supplied by BHP Billiton, Richards Bay, South Africa. Refer to table 3.1 for the chemical composition of the A356 alloy used. However, alloy composition could generate significant differences in the keyhole mode if volatile alloying elements such as Mg are present.

Table 3.1: Chemical composition of the A356 alloy feedstock.

Elemental chemical composition in wt%								
Si	Fe	Cu	Mn	Mg	Zn	Ti	Cr	Sr
Al								
7.33	0.13	0.01	0.01	0.35	0.01	0.14	0.01	0.03
91.98								

University of Cape Town

3.2 Melting procedure

Initially the chemical composition for the A356 Al alloy stock material was analysed using the Quantris Optical Emission Spectrometer (OES). Exactly 12.5 Kg of A356 Al alloy with the chemical composition as mentioned in table 3.1 was melted in a tilting induction furnace. As soon as the metal began to melt, at temperatures 640-650ºC, a handful of flux was sprinkled. After 10 minutes the flux was scooped out of the molten aluminium. Thereafter the temperature of the melt was raised to 780ºC. The melt was then grain refined with TiBAl to get an overall of 0.25% Ti in the alloy and strontium (Sr) was added to modify the eutectic structure. The addition of Sr modifies the eutectic phase. After adding the grain refiners into the melt, the melt was mechanically stirred for 10 minutes. Thereafter the melt was degassed for 10 minutes with Argon (Ar 5.0). However, before the A356 Al alloy plates were semi-solid cast, the chemical composition of the melt was checked. To check the chemical

composition of the melt, the melt was poured into a 304 stainless steel casting cup and then water cooled. The then solidified melt was machined on the lathe. The machining process was the typical method used for surface preparation for the chemical composition analysis. Then the chemical composition of the melt was analysed by using the OES. The OES system was continuously purged with Ar 5.0 to avoid Al_2O_3 formation on the specimen surface during chemical analysis. The chemical composition of the melt was then adjusted accordingly, especially for the volatile elements such as magnesium and strontium.

3.3 Casting procedure

The chemical composition was checked as outlined in section 3.2 under melting procedure. CSIR Rheo-process was used for casting the A356 alloy plates. The CSIR Rheo-process involves the preparation of semi-solid metal (SSM) slurry direct from molten metal by stirring and cooling. After having confirmed the required chemical composition of the melt, the melt was then poured at 630 ± 1ºC into a pre-heated 304 stainless steel cups. During the pouring of molten aluminium into 304 cups, cups were tilted 30 - 40º to the vertical axis. The tilting of cups helps create more nucleating sites for crystallisation of primary α-phase which in turn results to finer microstructure. The poured molten metal was then transferred onto the CSIR Rheo-cast technology where it was treated to semi-solid temperature of 580ºC. Refer to table 3.2 for the rheo processing unit settings. Thereafter the semi-solid metal slurry was transferred onto the 50 Ton Edgewick HPDC machine where the A356 Al plates were cast in rectangular molds with interior dimensions of 4X80X100 mm^3. Throughout the entire casting process, the chemical composition was monitored regularly and where necessary adjustments were made. Generally the melt was adjusted for Sr and Mg which are the most volatile elements. Summarised in table 3.2 is the rheo processing unit settings which were used during the casting process of the A356 alloy plates:

University of Cape Town

Table 3.2: Rheo processing unit settings

Parameter	Value
Liquid metal pouring temperature	630ºC
Mush metal casting temperature	580ºC
Power supplied	4.4kW/2.5 seconds (s) followed by
	14kW/5 s continuous
Cooling air setting: Top coil	2
Middle coil	3
Bottom coil	0
Total treatment time	100-150 s
HPDC machine settings:	
Gauge pressure	22 MPa
Die temperature: Right die	230ºC
Left die	230ºC
Plunger speed	350 mm/s
Consolidation time	30 s

University of Cape Town

3.4 Heat treatment procedure

The HRF 7/22 furnace was used in all the heat treatment process. The as-cast plates were either subjected to pre-weld T4, and T6, post-weld T4 and T6 heat treatment conditions. The T4 heat treatment entailed solution treatment at 540 ºC for 6 hours followed by water quench at room temperature (25 ºC). The specimens were then naturally aged (25 ºC) for 6 days. The T6 heat treatment on the other hand entailed solution treatment at 540ºC for 6 hours followed by water quench at room temperature (25 ºC). However, specimens in this case were naturally aged for 20 hours, before artificially aged at 160ºC for 6 hours. Some of the initial as-cast plates that were welded were subjected to pre-weld T4 or T6 heat treatment and are referred to as pre-weld T4 or pre-weld T6 specimens. Similarly some of the initial as-cast plates that

were welded were subjected to post-weld T4 or T6 heat treatment and are referred to as post-weld T4 or post-weld T6 specimens.

3.5 Laser welding process

Prior to welding, A356 alloy plates in the as-cast, pre-weld and post-weld heat treatments were subjected to the same surface preparations such as: brushing with stainless steel brush and degreased with acetone. Huntington et. Al[40] noted that the differences in beam power absorption due to alloy composition were much less than those due to surface preparation. Prior to welding of semi solid metal cast A356 alloy, the laser welding parameters were optimized. The initial welding parameters which were used during the parameter optimization method were obtained from literature[3, 4, 25, 41, 54, 64]. The resulting welds quality which included parameters such as penetration depth, sagging, porosity count and weld profile were used as in the Taguchi set of experiments. The above mentioned parameters were then given a rating from 1 to 5, where 1 was the best ideal case and 5 was the worst case scenario. A number of experimental trials were carried out using the Taguchi method and the trial that produced the most favorable weld quality was then selected. Table 3.2 illustrates the welding parameters which were generated from the Taguchi experimental trials and hence used during the laser welding operation. These parameters are then used throughout the study.

University of Cape Town

Table 3.2: Process parameters of Nd: YAG butt laser welding

Parameter	Value/Type
Laser type	Rofin Sinar RS DY044
Laser power	4.4 kW (set value)
Feed rate	4 m/min
Beam delivery	400 micron fibre
Collimation	1.0
Focal length	200 mm
Focal position	0
Focal geometry	Twin spot: 0.4 mm separation
Angle of incidence	15°
Assist gas	He 70 Ar 30
Assist gas flow rate	20 lpm
Assist gas nozzle	Leading off axis
Root purge	Ar 5 @ 20 lpm

University of Cape Town

Butt welds were produced using a continuous welding Nd: YAG laser (figure 3.2) on 4 mm thick plates of A356 alloy. A Rofin Sinar DY 044 laser which delivers 4.4 kW maximum mean power, in a 400 µm diameter fibre was used. The weld lines were performed with a 200 mm focal lens resulting in a 0.4 mm spot size and with 4 m/min welding speeds. A 5 l/min shielding gas of composition He 70 Ar 30 was used to prevent oxidation. The nozzle was set 30 mm above the workpiece and was 15° inclined. A four points clamping of the plates were used to ensure a constant focal length. At low welding speed, the keyhole is believed to collapse easily, and is susceptible of creating more macro-porosities[25]. Haboudou et. al[25] used the dual spot Nd:YAG laser for welding of A356 and AA5083 aluminium alloys. In addition to the importance of surface preparation prior to welding, they also concluded that a dual spot laser welding stabilises weld pools and keyhole dynamics, and reduces the porosity rate.

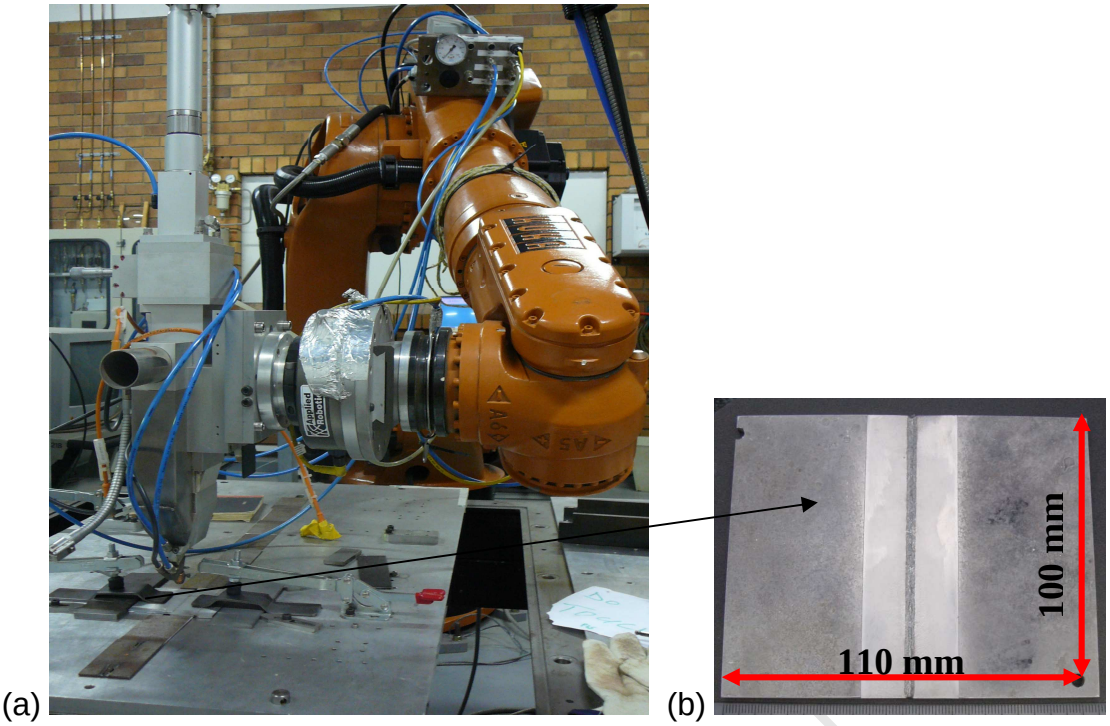

Figure 3.2: (a) High YAG ASK welding head with twin spot capability and (b) SSM cast welded plate.

3.6 Characterisation of welded specimen

The light optical microscope and scanning electron microscope (SEM) were used to study the microstructural changes under the different heat treatment conditions. Additionally microhardness measurements were conducted across the weld metal for the different heat treatment conditions.

3.6.1 Microstructural analysis

Specimens for microstructural analysis were prepared in the following manner: Firstly specimens were cross-sectioned using a Brillant 250X cut-off machine shown in figure 3.2. To prevent any further aging treatment on the specimens, the epoxy cold mounting kit was used for mounting. The third most important step in the preparation of microhardness specimens involves grinding and polishing.

The initial step was grinding the specimens with the Hermes WS Flex 220 grit SiC paper at 150 rpm whilst using water as lubricant on the Saphir 550 semi-automatic polishing machine.

University of Cape Town

A force of 20N was used for all the grinding process over two minutes. The proceeding steps was further grinding of the specimens using the 15µm pad at 250 rpm using Aka-Poly 15µm diamond paste and blue lubricant. A force of 30N was applied over 3 minutes.
The last grinding process was on the 3µm pad at 250 rpm using Aka-Poly 3µm diamond paste and blue lubricant. A force of 30N was applied over 3 minutes.

The final step was the polishing process on the Nepal pad at 250 rpm under a force of 30N for 3 minutes. The lubricant used in the polishing process was the 50 nm colloidal silica. Thereafter the metallographic samples were analysed under the optical microscope after etching with 0.5 % HF solution. Shown in figure 3.4 is the Inverted Leica DMI5000M optical microscope used for microstructural analysis.

University of Cape Town

3.6.2 Hardness measurements

The hardness of a metallic material can be defined as its resistance to plastic deformation caused by a force applied through an indenter. Microhardness measurements were done across the weld metal under the different heat treatment conditions. The different heat treatment conditions are the as-cast, pre-weld T4 and T6, post-weld T4 and T6. Some of the initial as-cast plates that were welded were subjected to pre-weld T4 or T6 heat treatment and are referred to as pre-weld T4 or pre-weld T6 specimens. Similarly some of the initial as-cast plates that were welded were subjected to post-weld T4 or T6 heat treatment and are referred to as post-weld T4 or post-weld T6 specimens.
Specimens for microhardness measurements were prepared in the following manner: Firstly specimens were cross-sectioned using a Brillant 250X cut-off machine shown in figure 3.6. To prevent any further heat treatment on the specimens, the epoxy cold mounting kit was used for mounting. The third most important step in the preparation of microhardness specimens involves grinding and polishing. The initial step was grinding the specimens with the Hermes WS Flex 220 grit SiC paper at 150 rpm whilst using water as lubricant on the Saphir 550 semi-automatic polishing machine. A force of 20N was used for all the grinding process over two minutes.

The proceeding steps was further grinding of the specimens using the 15µm pad at 250 rpm using Aka-Poly 15µm diamond paste and blue lubricant. A force of 30N was applied over 3 minutes. The last grinding process was on the 3µm pad at 250 rpm using Aka-Poly 3µm diamond paste and blue lubricant. A force of 30N was applied over 3 minutes.

The final step was the polishing process on the Nepal pad at 250 rpm under a force of 30N for 3 minutes. The lubricant used in the polishing process was the 50 nm colloidal silica. Thereafter, specimens were thoroughly rinsed in water followed by washing in ethanol then dried. The mirror-finish and scratch-free specimens were then ready for microhardness measurement.

The Future-Tech FM-700 hardness tester with a load of 300 grams (0.3 Kg) was used for the microhardness measurement. The microhardness measurements were taken in the bulk of the specimen for all the heat treated and non-heat treated specimens. Measurements were taken at the centre and across the specimen length (refer to figure 3.3a). The centre of the specimen was calculated as ½ the width and ½ the height of the weld metal. Due to the narrowness of the heat affected zone (HAZ), measurements close to this zone were taken in the zigzag trend (refer to figure 3.3b). A set of seventeen hardness measurement were taken for all the specimens in different heat treatment conditions.

University of Cape Town

(a) 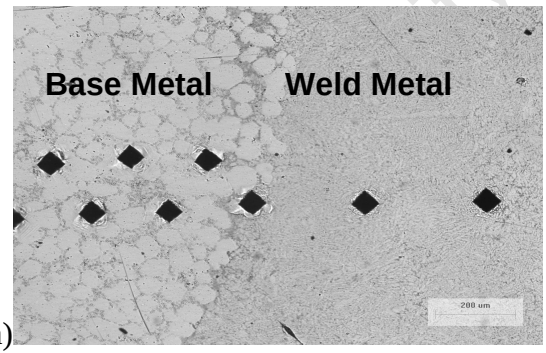

(b) 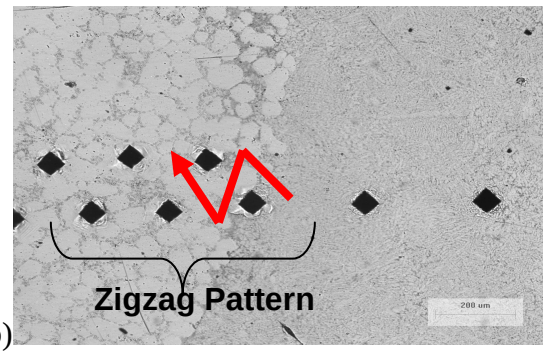

Figure 3.3: Microhardness measurements (a) across the weld metal and (b) Zigzag pattern near the HAZ.

3.7 Tensile measurements

The laser welded plates in the as-cast, pre-weld T4, and T6 and post-weld T4 and T6 heat treatment conditions were used to measure the tensile properties. Thereafter plates were X-rayed. Ideally specimens that have passed radiography should contain no voids or less than five small-sized voids through the specimen entire length. However, it must be noted that all specimens including the ones which contained more than five voids per specimen length were used for tensile properties testing. For all the welded plates, the bead and root of the weld were machined (approximately 0.2 mm of parent material was removed from both sides) to even-out the thicknesses for both the weld metal and base metal. After the machining process the plates were X-rayed again. After the second X-ray analysis some of the plates which showed porosity before machining did not show porosity after machining. This kind of observation showed that some of the observed porosity is surface-porosity rather than bulk-porosity (i.e. porosity on the entire depth of the weld). Therefore laser welded plates which have passed and failed x-ray radiography were selected for tensile test specimens.

Thereafter tensile specimens with dimensions shown in figure 3.5 were machined out (figure 3.4) of the heat treated and non-heat treated laser welded plates. The 25N Instron Tensometer was used to measure the tensile properties of both the heat treated and non-heat treated tensile specimens.

University of Cape Town

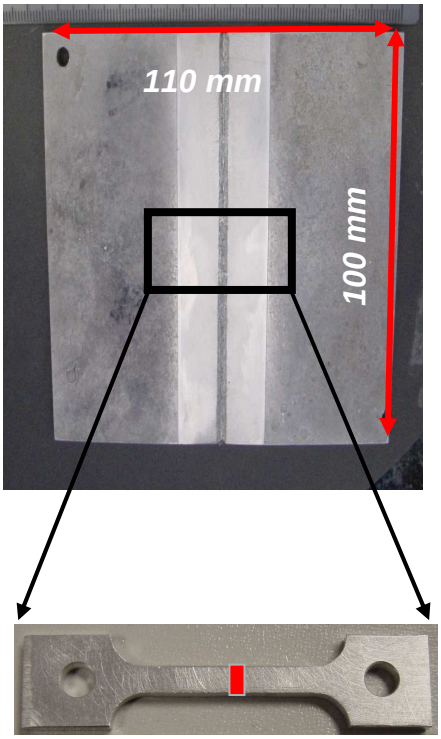

Figure 3.4: Direction in which the tensile specimens were machined from welded plates.

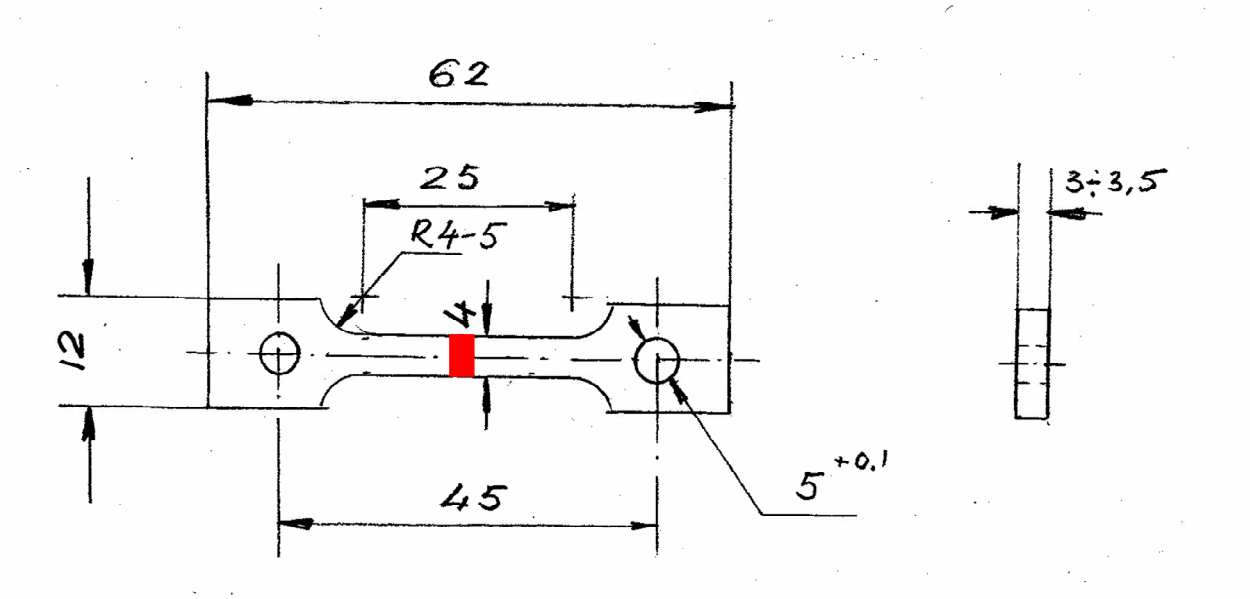

Figure 3.5: Dimensions used for the preparation of the tensile specimens.

Cape Town

Chapter Four

Experimental Results and Discussion

4.1 Introduction

The laser welded and un-welded specimens were subjected to the different heat treatment conditions such as as-cast, pre-weld T4 and T6, and post-weld T4 and T6. The optical microscope and SEM were then used to investigate the microstructural changes due to the different heat treatment conditions. Thereafter the effect of microstructural changes on the microhardness profiles and tensile properties were investigated. This chapter presents the results from the characterisation of the weld profiles and property measurement and further discusses the obtained results.

4.2 Chemical Composition

It is reported that the thermo-physical properties such as the melting temperature range, latent heat, density, coefficient of thermal expansion and electrical conductivities are affected by changes in the chemical composition of an alloy. The chemical composition analysis was conducted as specified in the previous chapter. Figure 4.1 below shows the typical specimen used to measure the chemical composition of the weld metal. Normally the weld metal was sectioned from the welded plate, pressed and annealed at 540°C for 30 minutes. The procedure of pressing and annealing was repeated until a diameter of 12 mm was reached.

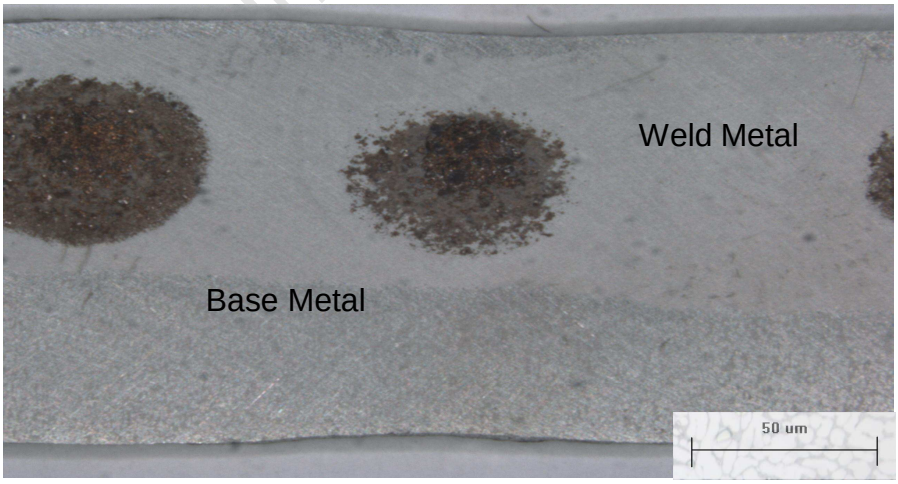

Figure 4.1: Pressed specimens used for conducting chemical composition analysis of the weld metal.

University of Cape Town

Table 4.1 indicates the chemical compositions as measured from the virgin material, cast plates and the fusion zone of the welded SSM cast plate. The values presented in table 4.1 are averages from five different plates.

Table 4.1: Chemical composition in wt% of the ingot, base metal and weld metal.

Sample	Si	Fe	Cu	Mn	Mg	Zn	Ti	Cr	Sr	Al
Nominal	6.5 - 7.5	0.2 max.	0.20 max.	0.10 max.	0.25 - 0.45	0.10 max.	0.20 max.	- -	0.30 max	Bal.
Ingot	7.33	0.13	0.01	0.01	0.35	0.01	0.14	0.01	0.03	91.98
Base Metal	7.22	0.12	0.01	0.01	0.28	0.01	0.09	0.01	0.02	92.23
Weld metal	7.19	0.11	0.01	0.01	0.24	0.001	0.07	0.01	0.01	92.35

University of Cape Town

From the chemical composition analysis, it is noticeable that there was no significant difference in composition between the base metal and the fusion zone. There was however, minor decrease in concentration of the volatile alloying elements such as strontium and magnesium. However, the decrease of these volatile alloying elements is not significant compared to the concentration of the as-received ingot. The presence of strontium serves the most important purpose in the casting which is eutectic modification. In the absence of strontium, the eutectic silicon develops into a more fibrous morphology. On the other hand, magnesium has a totally different effect than strontium. Magnesium is predominantly a strengthening alloying element in the A356 alloy, where the strength is directly proportional to the concentration of magnesium in an alloy. Therefore, for the purpose of this study the concentration of major alloying elements was able to be kept constant throughout the casting process.

4.3 Liquid segregation

The chemical composition analyses have shown that the liquid segregated zones consist of Mg-rich, Fe-rich and Si-rich particles. The morphology indicates that the segregates most likely solidify at high liquid volume fractions, f_s. At the top of the plates, the segregation is characterised by a high Mg-content as compared to the bottom of the plate. Variation in the Mg-content from the bottom of the plate to the top was revealed by measuring the Mg-content at different locations through the plate thickness. The high Mg-content at the top of the plate is due to the mould filling characteristics during SSM processing. Corresponding concentrations of Fe and Si displayed similar patterns to Mg. Forbord et. Al[65] investigated the mechanisms responsible for the formation of surface segregates. They revealed that the initial source for the formation of surface segregation was enrichment of alloying elements at the grain boundary. Observations showed that grain boundaries seem to connect and become transport paths for enriched liquid to the surface zones as concluded by Forbord et. al.

Liquid segregation is a phenomenon which leads to heterogeneous mechanical properties and to even poor surface finish[66]. There are three main factors controlling liquid segregation, such as:

- Initial solid fraction;
- Die preheating temperature

  and
- Forming speed.

It is reported[66] that segregation increases greatly for high solid fractions (f_s).

Illustrated in figure 4.2 is the typical SSM cast A356 alloy plate. Chemical analysis was performed at the two areas on the plate as indicated in figure 4.2 below.

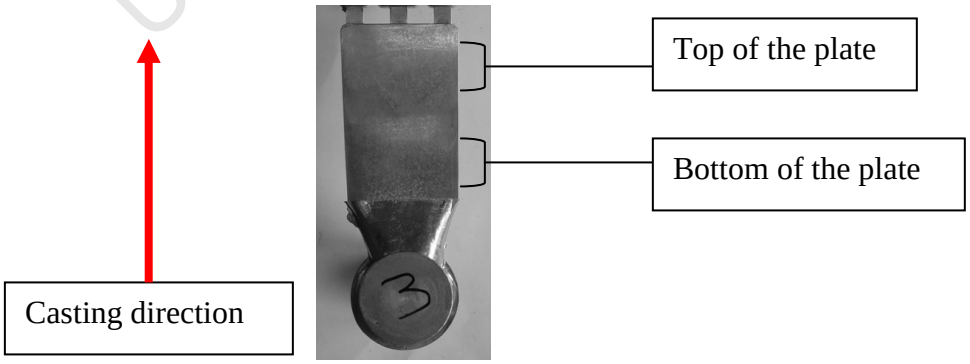

Figure 4.2: SSM cast A356 alloy plate.

University of Cape Town

Illustrated in figure 4.3 is the microstructure of the as-cast SSM A356 alloy depicting surface segregation as observed under the optical microscope. The major alloying elements such as Si, Mg, Sr, Ti and Fe were shown to have segregated to the surface. Although the weld quality is greatly affected by the welding parameters, chemical composition of an alloy has as much effect on the weld quality. It is well documented that alloying elements such as silicon have adverse effects during keyhole laser welding. Such elements decrease the viscosity which in turn puts the system into resonance and thus low damping effect of the liquid material around the keyhole occurs[55]. However, elements like copper, titanium or iron increases the viscosity and in their presence the welding process becomes stable. For the scope of this study the chemical composition is assumed unchanged throughout the welding experiments. Magnesium is the major alloying element with a major effect on strength, therefore surface segregation of this element greatly affects the mechanical properties of the alloy. Figures 4.4-4.12 depict the extent of segregation of various alloying elements in the as-cast plates. Shown in figure 4.4 is the depth profile of silicon levels both at the top and bottom of the as-cast plate.

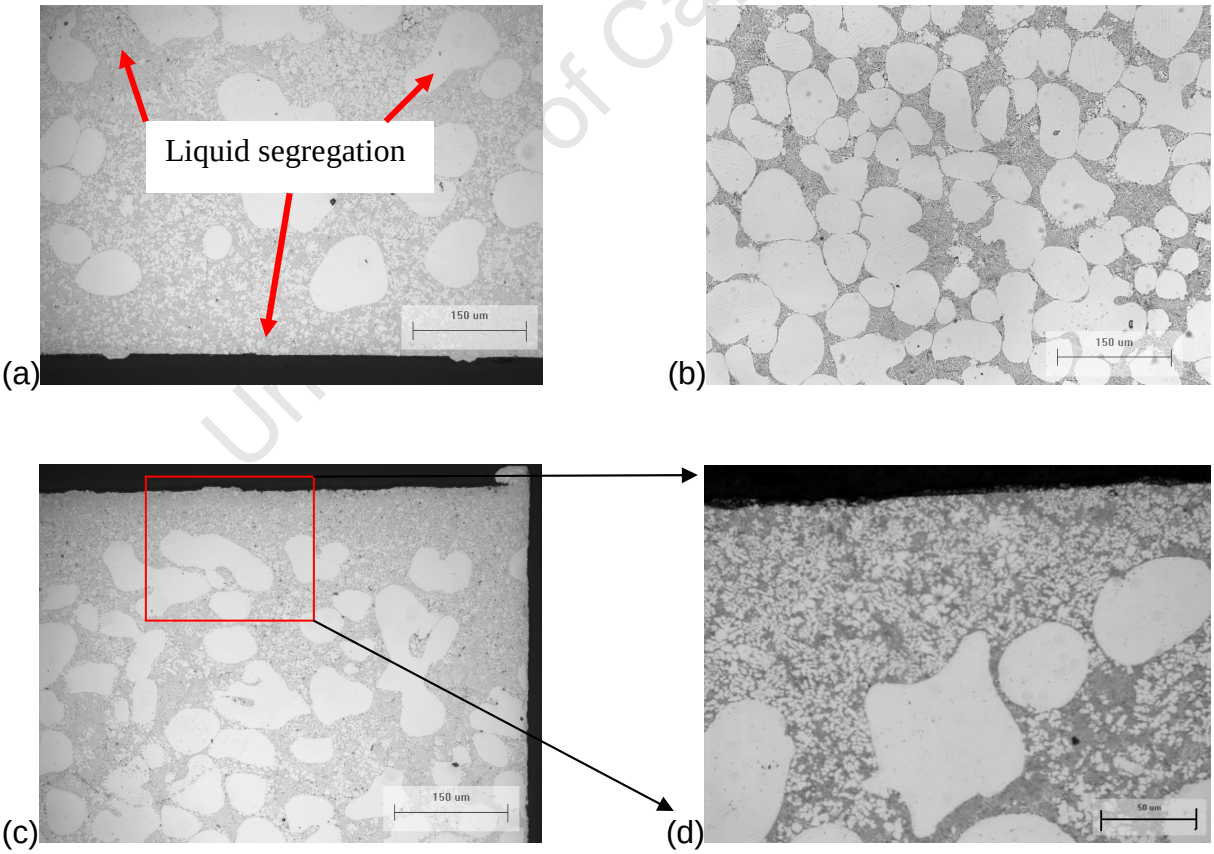

Figure 4.3: Microstructure of the as-cast SSM A356 alloy illustrating liquid segregation (a) top, (b) centre and (c-d) bottom of the plate.

University of Cape Town

As clearly indicated in figure 4.4, from the surface to approximately 1 mm below the surface, acceptable levels of silicon were observed at the bottom of the plates. The specified silicon levels for hypoeutectic alloy, A356, ranges from 6.5 to 7.5 wt%. At even greater depths than 1 mm below the surface, silicon levels dropped to less than the specified lower silicon limit of 6.5 wt%.

The opposite was observed for the top of the plates which showed an increase above the upper limit in the silicon concentration from the surface to 1 mm below the surface. However, at depths greater than 1 mm below the surface, the average silicon levels reached the specified lower silicon limit of 6.5 wt%.

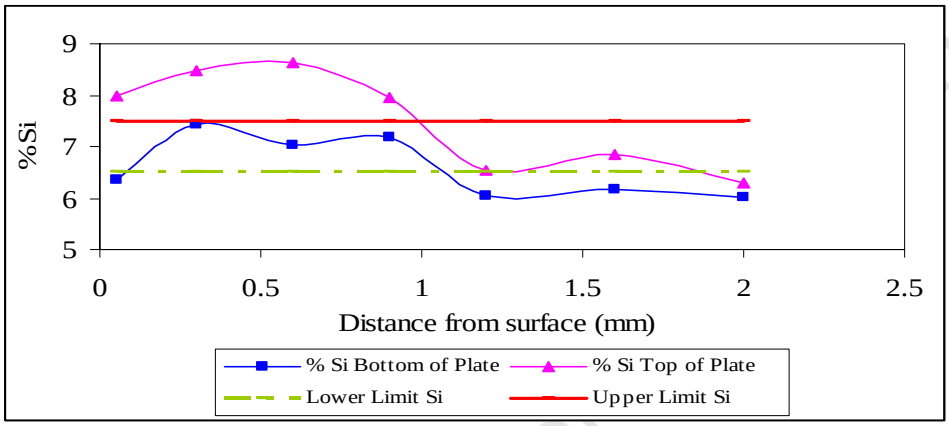

Figure 4.4: Depth profile of silicon (Si) concentration at the top and bottom of the as-cast plate.

The level of segregated silicon layer as shown in figure 4.4 is approximately 1 mm for the top part of the plates. The bottom of the plates however, showed almost no liquid segregation.

Shown in figure 4.5 is the depth profile of the magnesium concentration at the top and bottom of the plates. Magnesium is the major alloying element which contributes to a great extent to strength. The density of magnesium is 1.5 times less that of aluminium and boils at lower temperature. Differences in composition between the solid and liquid fractions are the driving force for the chemical segregation. There was however, no significant difference in magnesium concentration between both the top and bottom of the plate respectively. The bottom of the plates reached the required magnesium concentration at approximately 0.8 mm below the surface. Whilst the top of the plates reached the required magnesium level at approximately 1.1 mm below the surface. The variation in magnesium concentration will no

University of

doubt contribute to the variation in mechanical properties. For hypoeutectic aluminium alloy (A356 alloy) the specified magnesium level is 0.35 wt% as stated in table 4.1. Additionally to the effect of magnesium to the mechanical properties, high volatility of magnesium may contribute to some extent to porosity during keyhole laser welding process.

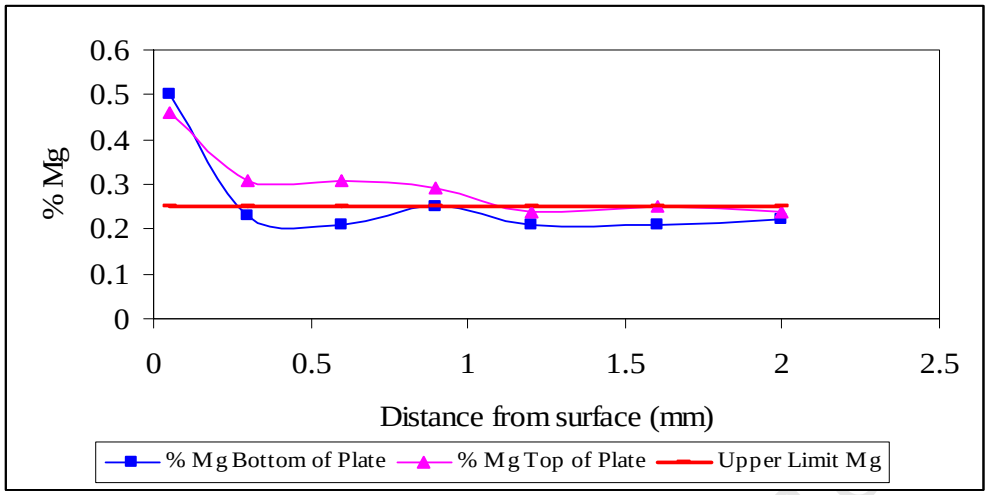

Figure 4.5: Depth profile of magnesium (Mg) concentration at the top and bottom of the as-cast plate.

Magnesium has also adverse effects during deep penetration laser welding as such an element decreases the viscosity[55]. Figure 4.6 displays the depth profile of strontium concentration both at the top and bottom of the plates respectively. Similar to magnesium depth profile in figure 4.5, the depth profile for strontium showed no significant difference between the top and bottom of the plates. Strontium is the common Al-Si eutectic phase modifier, where lower strontium levels cause the more fibrous silicon particles. The more fibrous the eutectic silicon, the more susceptible it is to brittle fracture. Whilst strontium levels between 0.02-0.03 wt% led to a more irregular lamellar Al-Si eutectic structure. Initially both the top and bottom of the plates showed the strontium level of 0.05 wt% on the surface. An upper limit strontium level was reached at 0.35 mm below the surface for both the top and bottom of the plates. Both the top and bottom of the plates reached the 0.02 wt% strontium level at approximately 0.6 mm below the surface. However, the top of the plates showed a further decrease in strontium concentration to below 0.02 wt% from 0.61 mm to 1.2 mm below the surface. A constant strontium concentration of 0.02 wt% was reached at 0.6 mm below the surface for the bottom of the plates. Whilst the top of the plates reached the 0.02 wt% strontium level at 1.2 mm below the surface. The variation in elemental chemical composition both at the top and bottom of the plates proves that casted plates were not homogenous. The weld quality is

University of Cape Town

greatly affected by the chemistry of the alloy however; the influence of chemical composition on the weld quality is not included in the current study.

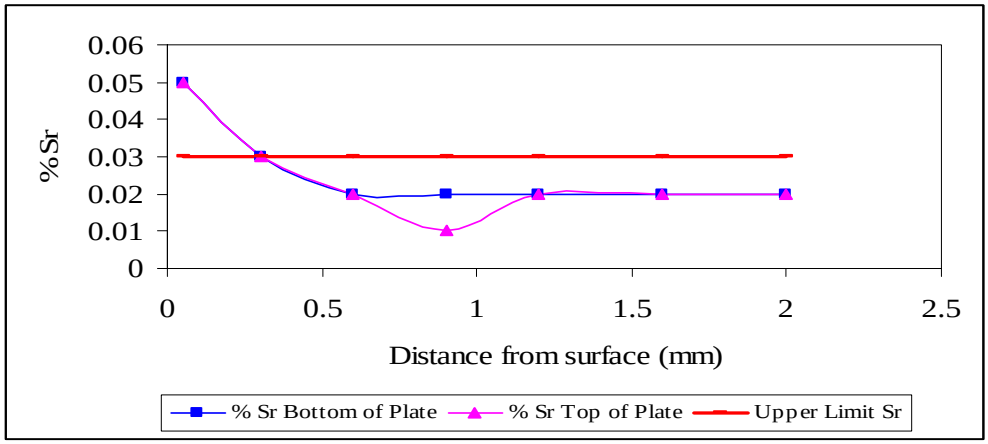

Figure 4.6: Depth profile of strontium (Sr) concentration at the top and bottom of the as-cast plate.

As illustrated in figure 4.7 the top of the plates showed the titanium concentration of 0.1 wt% on the surface. From 0.2 mm to 2 mm below the surface, titanium concentration increases from 0.11 wt% to 0.15 wt% respectively. On the other hand, the bottom of the plates displayed an initial concentration of 0.05 wt% on the surface. However, at 0.3 mm below the surface a constant concentration of 0.14 wt% Ti was reached. An element like titanium increases the viscosity and in its presence the welding process becomes stable[55]. Titanium-boron is greatly used during the casting process of A356 alloy as grain modifier. The boron concentration was found to increase considerably with every increase in titanium concentration. The immediate increase in titanium and boron concentrations was found to be more significant in the last five plates which were casted. From this effect, it was concluded that insoluble titanium boride residues formed at the bottom of the crucible as molten metal cools. The high melting temperatures for titanium boride as compared to aluminium alloys makes it difficult to re-dissolve the already formed boride residues.

University of Cape Town

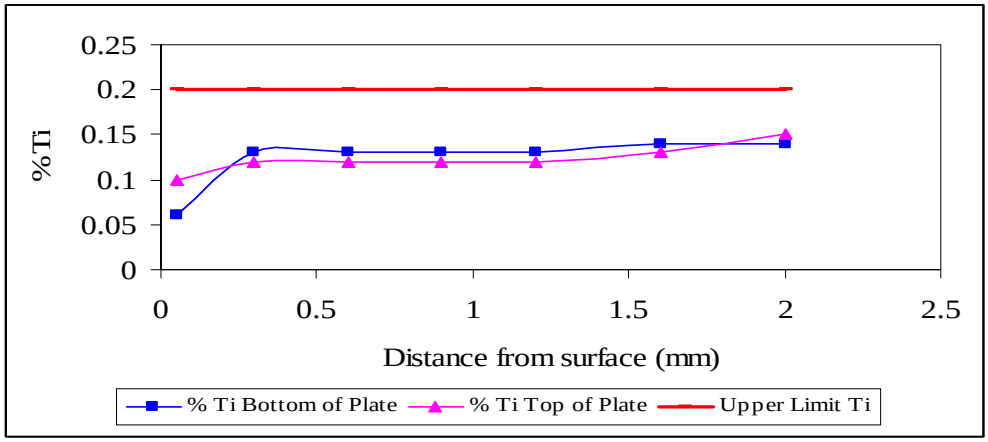

Figure 4.7: Depth profile of titanium (Ti) concentration at the top and bottom of the as-cast plate.

Shown in figure 4.8 is the depth profile of iron concentration at both the top and bottom of the plates. Initial concentrations of 0.24 wt% and 0.2 wt% Fe were observed on the surface for both the top and the bottom of the plates respectively. The iron concentration decreased to 0.1 wt% at 0.3 mm below the surface for the bottom part of the plates, whilst it decreased to 0.11 wt% Fe for the top part of the plates at the same depth (i.e. 0.3 mm below the surface). At approximately 1 mm below the surface, a constant concentration of 0.1 wt% Fe was reached for the bottom part of the plates. The top part of the plates however, reached the 0.1 wt% Fe concentration at 2 mm below the surface. In the similar manner as copper and titanium, an element like iron also increases the viscosity and in their presence the welding process becomes stable[55].

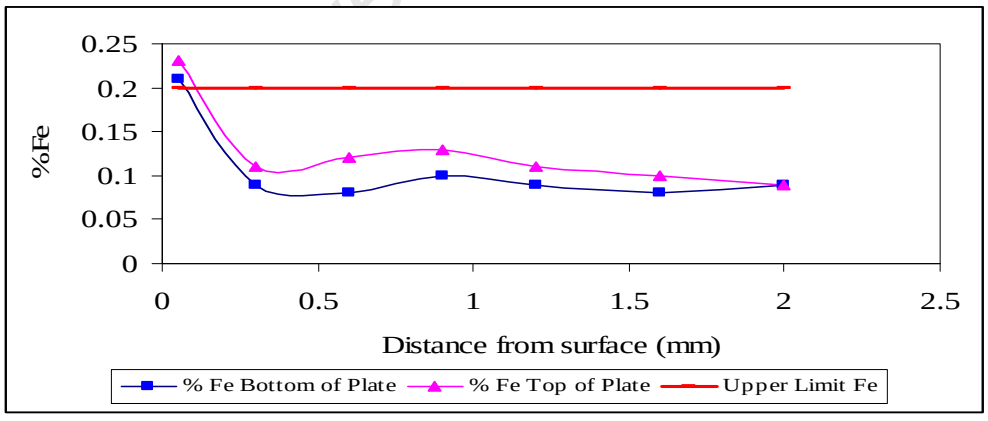

Figure 4.8: Depth profile of iron (Fe) concentration at the top and bottom of the as-cast plate.

University of Cape Town

Figures 4.9-4.13 present the depth profile for silicon, magnesium, strontium, titanium and iron after the homogenisation process of the plates. The objective of the homogenisation process was to promote even distribution of alloying elements. Homogenisation process was only applied to the top specimens of the plates since they have shown greater surface segregation. It must be emphasised that the homogenisation process did not improve liquid segregation but led to spheriodisation of the eutectic silicon particles. This means that the segregated layer remained unchanged after the homogenisation process. It is then for this reason that all the specimens used during the welding experiments were not homogenised. Therefore the results presented in figures 4.9-4.13 were extracted from the top part of the plates. After homogenisation process, the required silicon concentration of between 6.5 wt% and 7.5 wt% was reached at 0.85 mm below the surface. If no homogenisation was applied, the silicon concentration varied at even 2 mm below the surface without reaching any constant value. The homogenisation process led to a more stable required Si concentration of 7.2 wt% as opposed to the fluctuating over and under estimate in the as-cast condition.

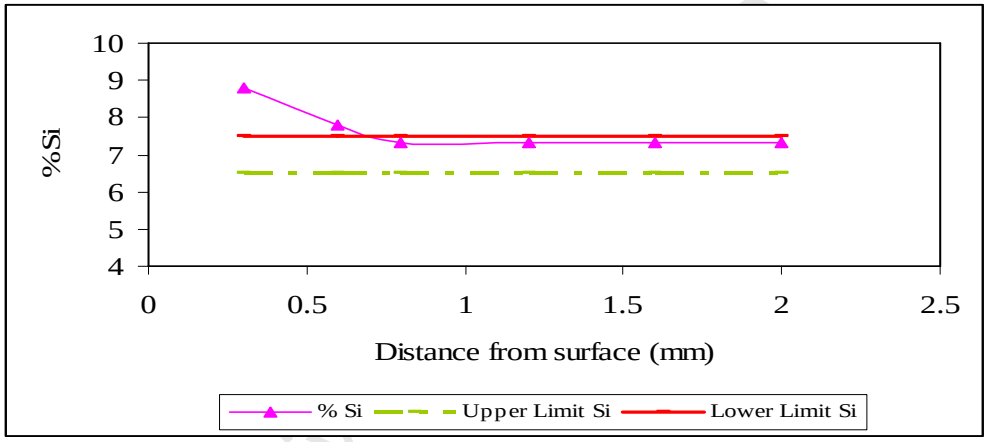

Figure 4.9: Depth profile of Si concentration at the top and bottom of the plate after homogenisation process.

Illustrated in figure 4.10 is the depth profile of magnesium concentration after homogenisation process. At 0.3 mm below the surface, the initial magnesium concentration was 0.35 wt% which is the allowed limit for hypoeutectic A356 alloy. However, at 0.6 mm below the surface, the magnesium concentration dropped to 0.26 wt% which is close to the lower limit of 0.25 wt% Mg. The effect of magnesium variation through plate thickness will be evaluated under mechanical properties in section 4.7.

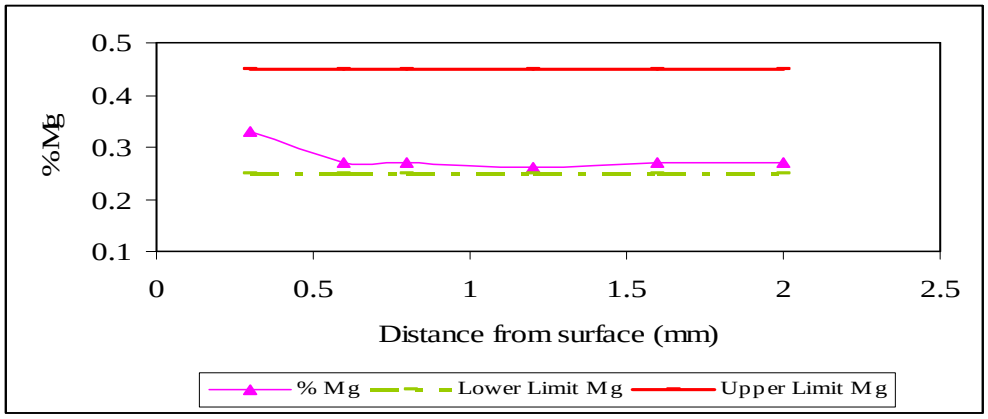

Figure 4.10: Depth profile of Mg concentration at the top and bottom of the plate after homogenisation process.

Illustrated in figure 4.11 is the depth profile of strontium concentration at the top part of the plates. The strontium concentration at 0.3 mm below the surface was measured to be 0.03 wt% Sr. It later decreased to reach a constant concentration of 0.02 wt% Sr at 0.6 mm below the surface.

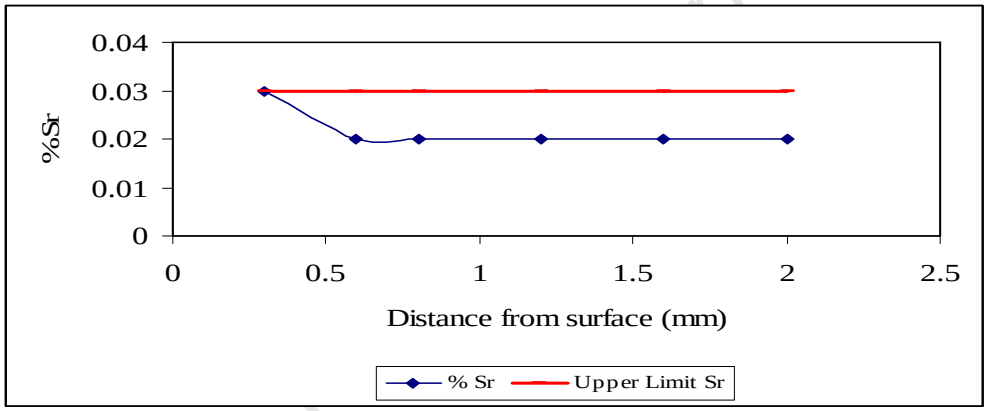

Figure 4.11: Depth profile of Sr concentration at the top and bottom of the plate after homogenisation process.

Titanium-boride plays an important role of grain refinement. Titanium-boron provides nucleation sites, which lead to fine equiaxed grain structure. Therefore the large the number of nucleation sites, the finer the grain structure. As illustrated in figure 4.12, the initial

concentration of titanium was 0.1 wt% at 0.3 mm below the surface.

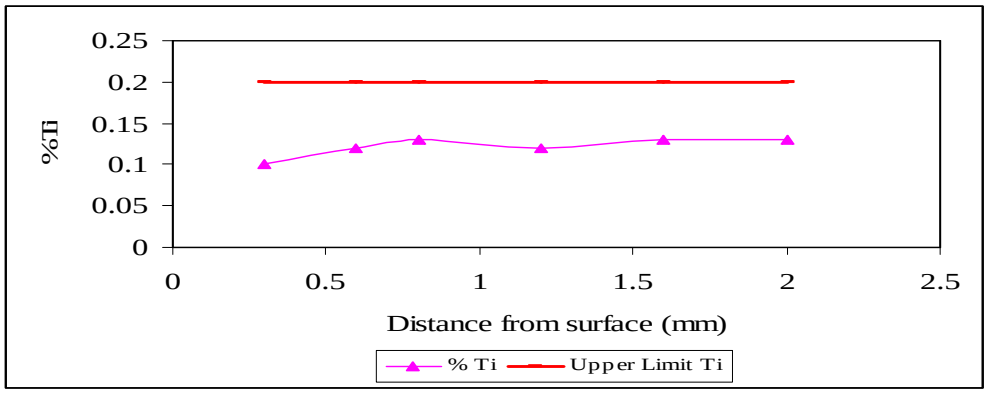

Figure 4.12: Depth profile of Ti concentration at the top and bottom of the plate after homogenisation process.

The titanium concentration fluctuated through the specimen thickness until a constant concentration, 0.15 wt% Ti, was reached from 1.5 mm below the surface. Shown in figure 4.13 is the depth profile of iron concentration from 0.3 mm to 2 mm below the surface. Iron has the ability to increase the viscosity of molten metal and also stabilises the keyhole during the laser welding process. Iron concentration fluctuates from the surface to 2 mm below the surface and never reaches a constant concentration. However, the titanium concentration fluctuates to an average of 0.145 wt% which met the specified lower limit for iron in a hypoeutectic A356 alloy.

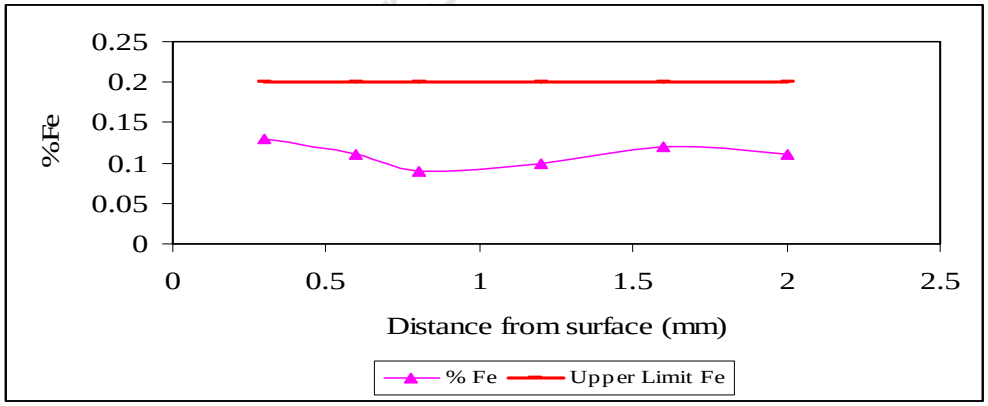

Figure 4.13: Depth profile of Fe concentration at the top and bottom of the plate after homogenisation process.

The difference in chemical composition of the alloying elements between the top and bottom of the plates was due to the feeding characteristics of the semi solid metal high pressure die

University of Cape Town

casting process. One of the parameters that might have contributed to liquid segregation was that the semi solid temperature was too high. Also the feeding rate was high. Although the homogenisation process led to spheroidisation of the eutectic silicon particles, there was substantial change in the elemental segregation profiles relative to the as-cast condition. Almost all the elemental segregation profiles in the as-cast condition showed unsteadiness at different locations through the plate thickness. However, after the homogenisation process all the elemental segregation profiles reached a constant value from 0.3 mm below the surface of the plates.

4.4 Microstructural changes under different heat treatment conditions

Heat-treatable aluminium alloys are prone to solidification cracking and hot cracking during welding resulting in the decrease of mechanical properties. The heat input offered by laser causes an annealing effect in a narrow region in the HAZ adjacent to the weld. The relatively high temperatures of welding causes dissolution of Mg_2Si precipitates thereby, destroying the effect of heat treatment for T4 and T6 heat treatment in this narrow region. However, the application of aging process at temperatures between 150 ºC and 180 ºC regenerates the strength. As discussed in the previous chapter, specimens were subjected to five different heat treatments such as; as-cast, pre-weld T4 and T6, and post-weld T4 and T6. The effect of the different heat treatment conditions on the microstructural changes and mechanical properties are discussed in the proceeding sections of this chapter.

University of Cape Town

4.4.1 Assessment of microstructural changes using light microscope

4.4.1.1 Base metal microstructure

The microstructural analysis is based on the three zones (e.g. base metal, HAZ and fusion zone) across the weld profile for all the different heat treatment conditions. Partially remelted zone is a narrow zone between the base metal and fusion zone. Figure 4.13 illustrates the microstructure of the as-cast base metal and the enlarged eutectic structure. The base metal consists of α-Al crystals surrounded by fine eutectic structure. This is due to the modification effect of strontium (Sr), creating an increased number of nucleation sites for the eutectic Si.

The eutectic structure is the dark region due to the finely distributed Si particles. Additionally high solidification rate also results in fine grain size modified Si particles[67]. Due to Sr additions the eutectic Si has a fine elongated morphology as showed in figure 4.13. Microstructural examination indicated that there was occasionally very fine shrinkage porosity in the base metal (figure 4.14). In general surface defects such as porosity and cavities create stress concentration, which make specimens prone to fracture.

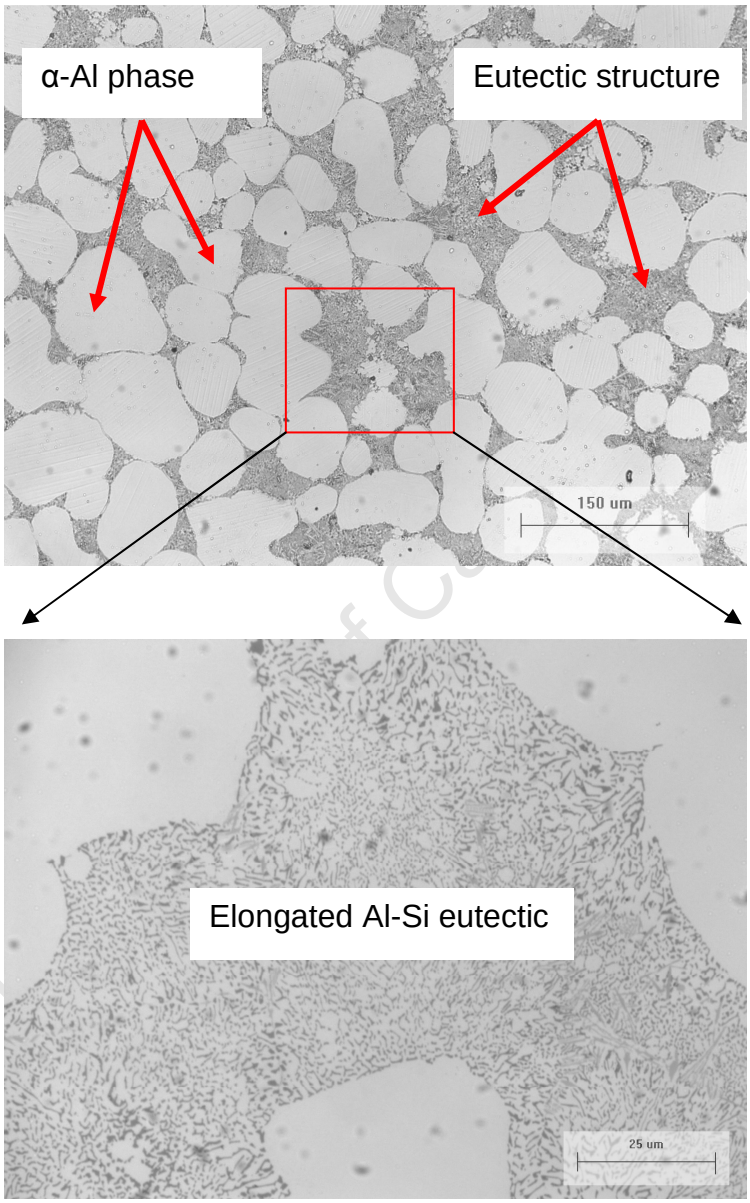

Figure 4.13: Microstructure of the as cast SSM A356 alloy (a) base metal and (b) eutectic phase.

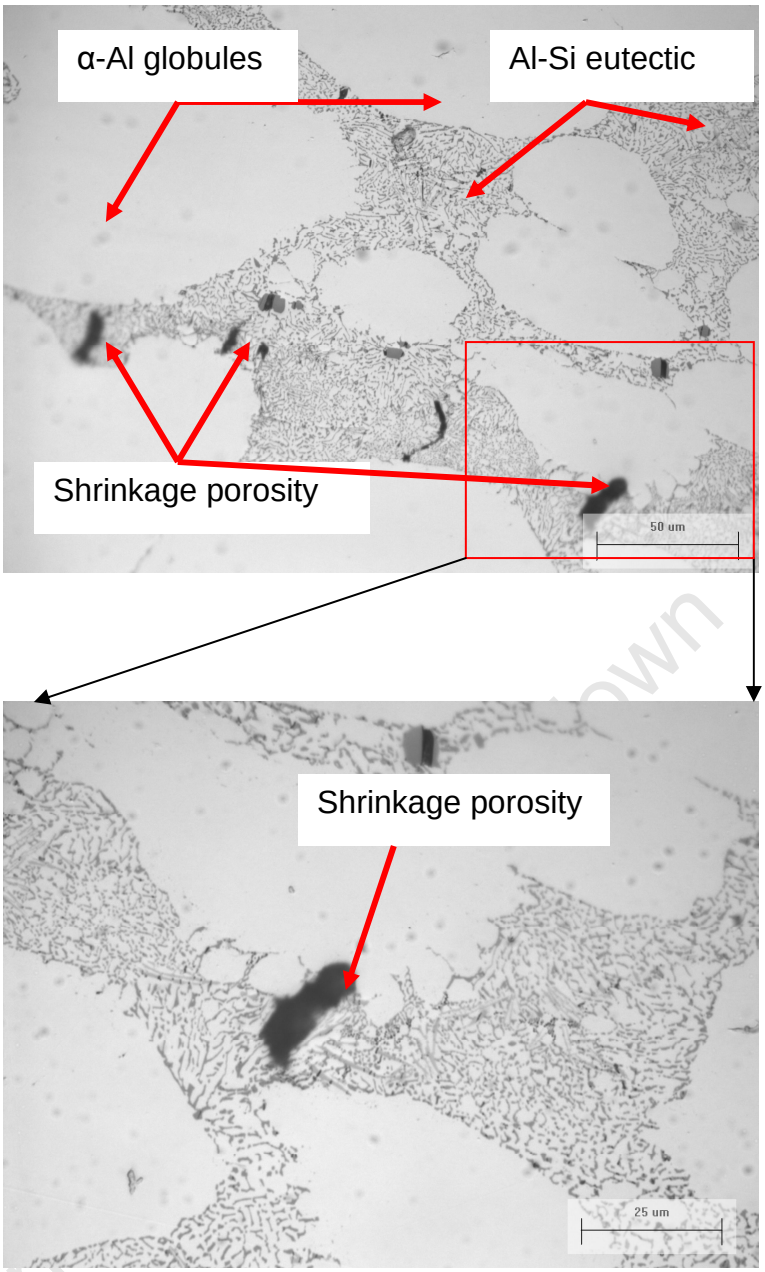

Figure 4.14: Light optical micrograph of the as-cast parent metal depicting shrinkage porosity.

The base metal microstructures of the pre-weld T4 and T6, post-weld T4 and T6 heat treated samples were found to be very similar (figures 4.15 - 4.18). These consisted of globular α-Al phase and fine spheroidal Si particles. Spheroidisation of the eutectic Si had occurred during the solution heat treatment process at 540ºC for 6 hours. Even though there were no evident final microstructural differences due to subsequent natural and artificial ageing treatments respectively, it was evident from microhardness profiles that there were significant changes in the substructure of the T6 heat treated samples. This is a result of solute clusters and GP

zones transforming to the strengthening β" phase (needles) followed by β' (rods), which are both precursors of the equilibrium β phase (plates). Further microstructural analysis of the base metal for pre-weld T4 and T6, post-weld T4 and T6 revealed shrinkage porosity. In all cases shrinkage porosity in the base was found to be not more than four pores per specimen length of 15 mm.

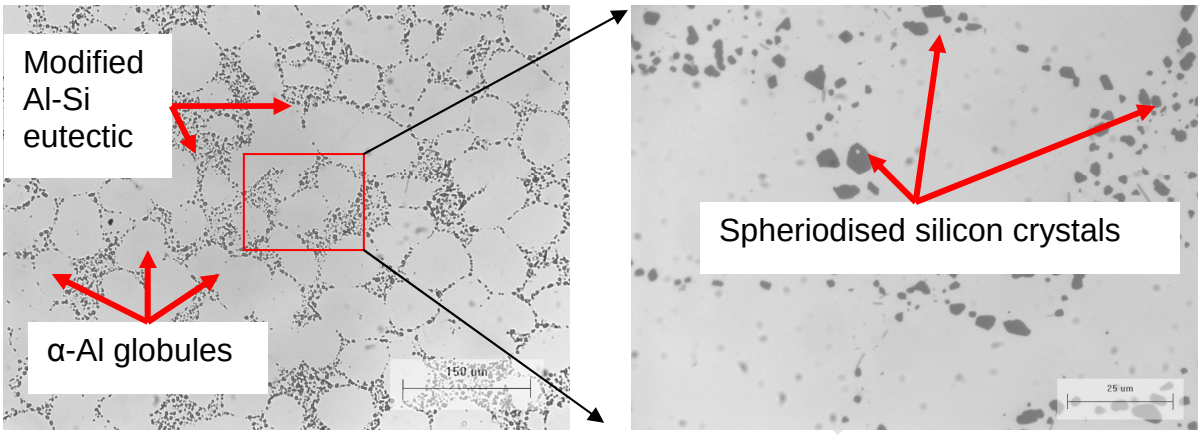

Figure 4.15: Microstructure of the pre-weld T4 heat treated SSM A356 alloy base metal with spheriodised silicon crystal.

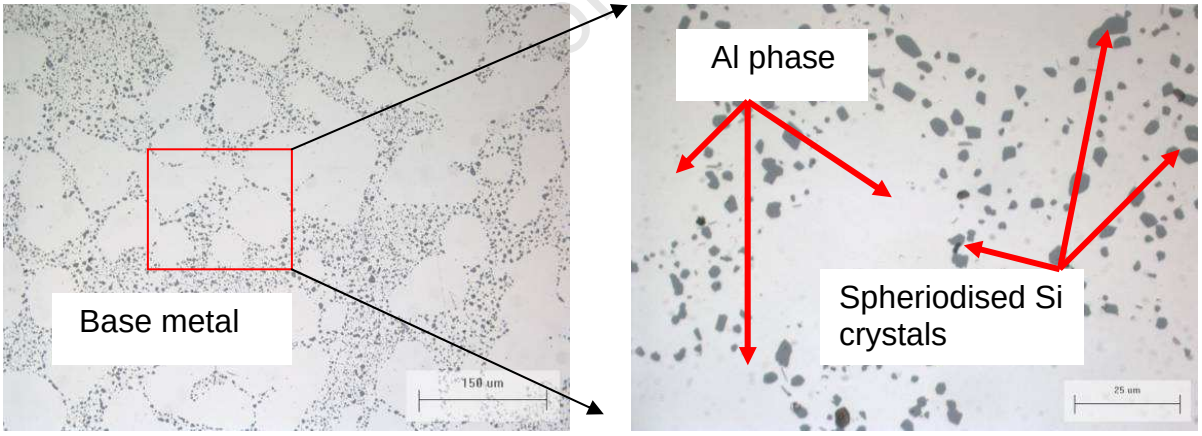

Figure 4.16: Microstructure of the post-weld T4 heat treated SSM A356 alloy base metal with spheriodised silicon crystals.

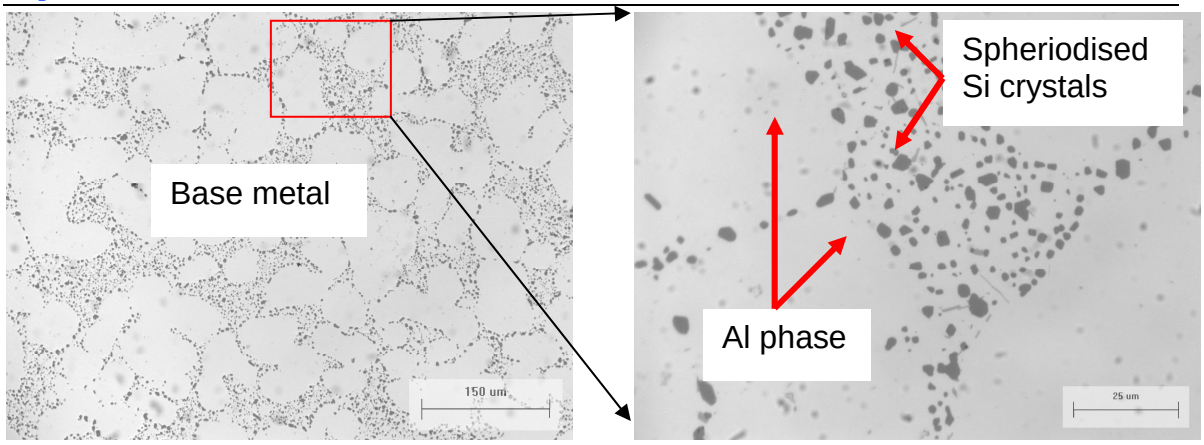

Figure 4.17: Microstructure of the pre-weld T6 heat treated SSM A356 alloy base metal with spheriodised eutectic silicon crystals.

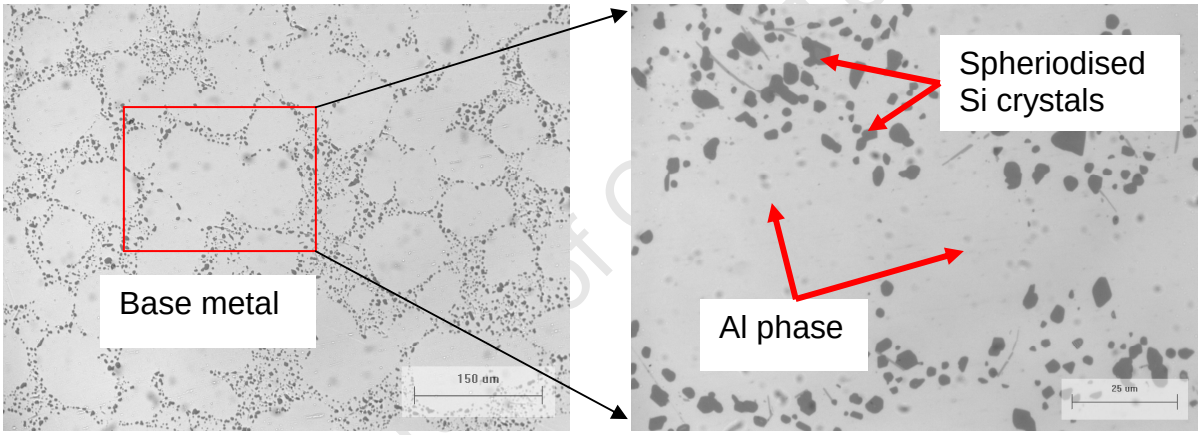

Figure 4.18: Microstructure of the post-weld T6 heat treated SSM A356 alloy base metal with spheriodised eutectic silicon crystals.

University of Cape Town

4.4.1.2 Heat-affected zone (HAZ) microstructure

The heat affected zone (HAZ) for the laser welded as-cast, pre-weld T4 and T6 heat treated samples showed minimal microstructural changes using light microscope. Illustrated in figures 4.19 – 4.21 is the typical HAZ for the as-cast, pre-weld T4 and T6 heat treated samples respectively. The partially remelted zone is narrow, only a few grains wide. However, the HAZ for both the laser welded as-cast and pre-weld T4 samples were very narrow such that it was not observable on the hardness values. The most evident feature under all three heat treated conditions was the remelting of the eutectic structure adjacent to the fusion zone (figures 4.19 – 4.21). Most importantly is that there was no new porosity formation evident resulting from the solidification of the remelted region. Although microstructural analyses of the HAZ showed no observable microstructural changes, it was evident from the microhardness profile of both the pre-weld T6 and post-weld T6 heat treated samples that substructural changes did occur (figure 4.30). Further microstructural examinations of the laser-welded as-cast sample indicated a mixture of fine to large porosity in the fusion zone and on the HAZ (figure 4.25).

University of Cape Town

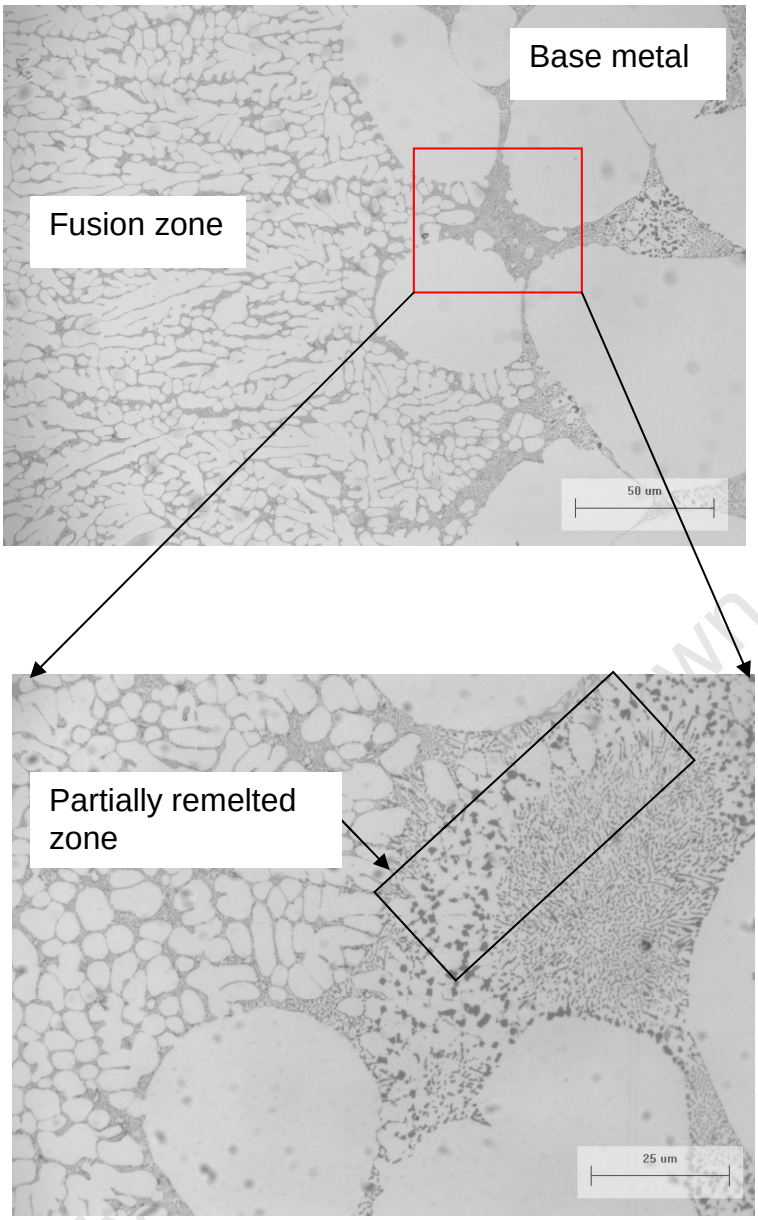

Figure 4.19: Microstructure of the as cast SSM A356 alloy base metal (right), fusion zone (left) and partially remelted zone in the middle.

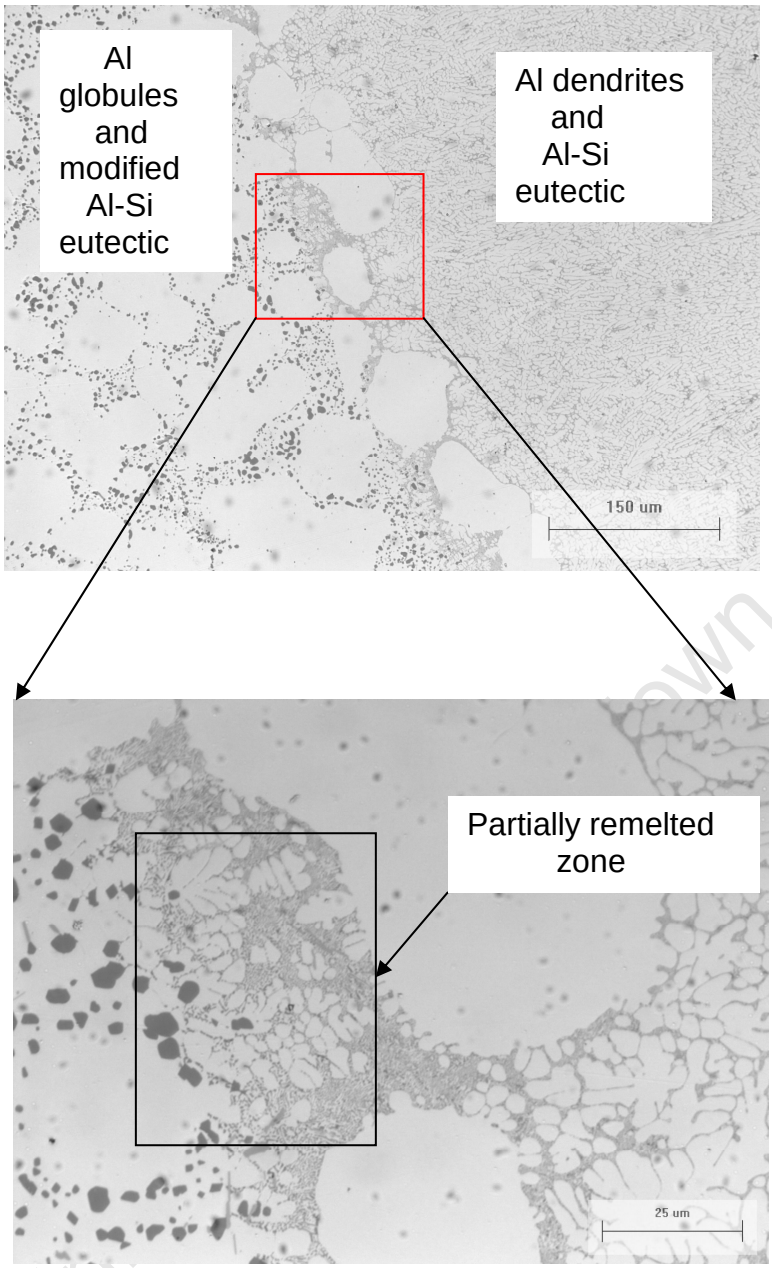

Figure 4.20: Microstructure of the pre-weld T4 heat treated SSM A356 alloy base metal (left), fusion zone (right) and partially remelted zone in the middle.

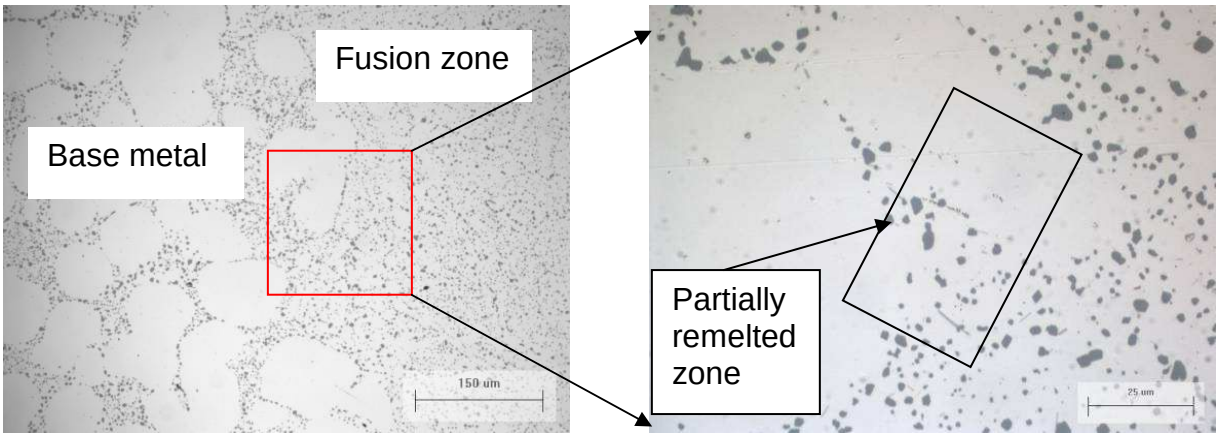

Figure 4.21: Microstructure of the post-weld T4 heat treated SSM A356 alloy base metal (left), fusion zone (right) and partially remelted zone in the middle.

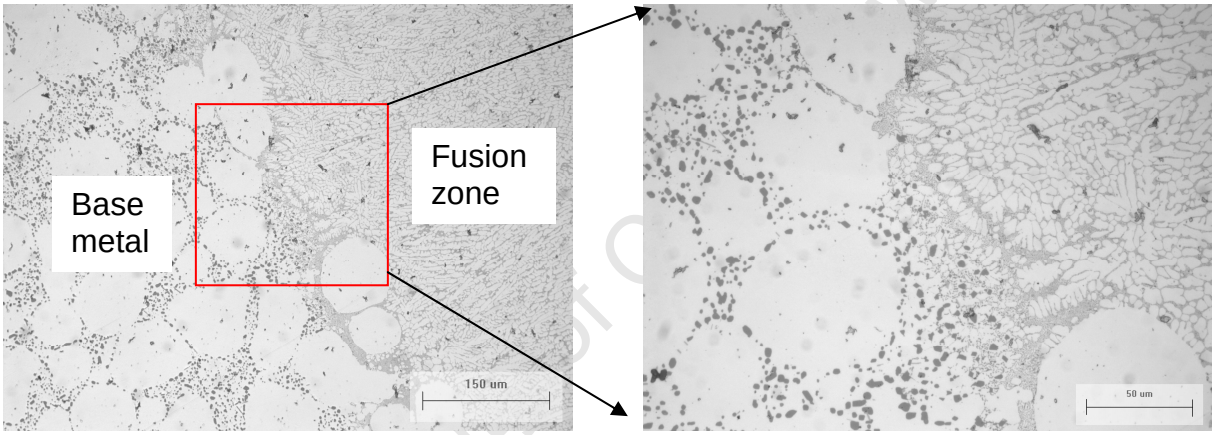

Figure 4.22: Microstructure of the pre-weld T6 heat treated SSM A356 alloy base metal (left), fusion zone (right) and partially remelted zone in the middle.

University of Cape Town

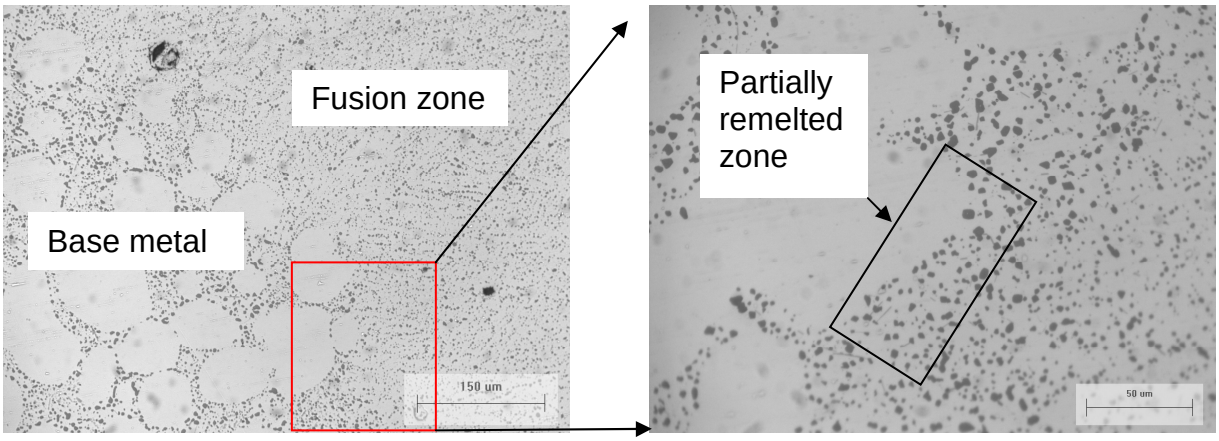

Figure 4.23: Microstructure of the post-weld T6 heat treated SSM A356 alloy base metal (left), fusion zone (right) and partially remelted zone in the middle.

University of Cape Town

4.4.1.3 Fusion zone microstructure

The fusion zone microstructures of the as-cast, pre-weld T4 and T6 heat treated samples were found to be very similar to each other (figures 4.24, 4.26 and 4.27). The fine and randomly oriented elongated dendritic structure of the laser welds in the as-cast, pre-weld T4 and pre-weld T6 heat treatment conditions is characteristic of high welding speeds in which rapid solidification of molten fusion zone occurs[68]. Generally, the total porosity count was three pores per 2 mm length of the fusion zone of all the heat treatment conditions. The average secondary dendritic arm spacing (SDAS) was 5 μm. This accounts for the higher hardness for the fusion zone as compared to its base metal under the three heat treatment conditions. On the other hand the microstructures of the fusion zone for both the post-weld T4 and T6 heat treatment conditions were also found to be similar to each other (figures 4.27 and 4.29), consisting of spheroidal silicon particles. The spheroidisation occurred during the solutionising heat treatment at 540ºC for 6 hours.

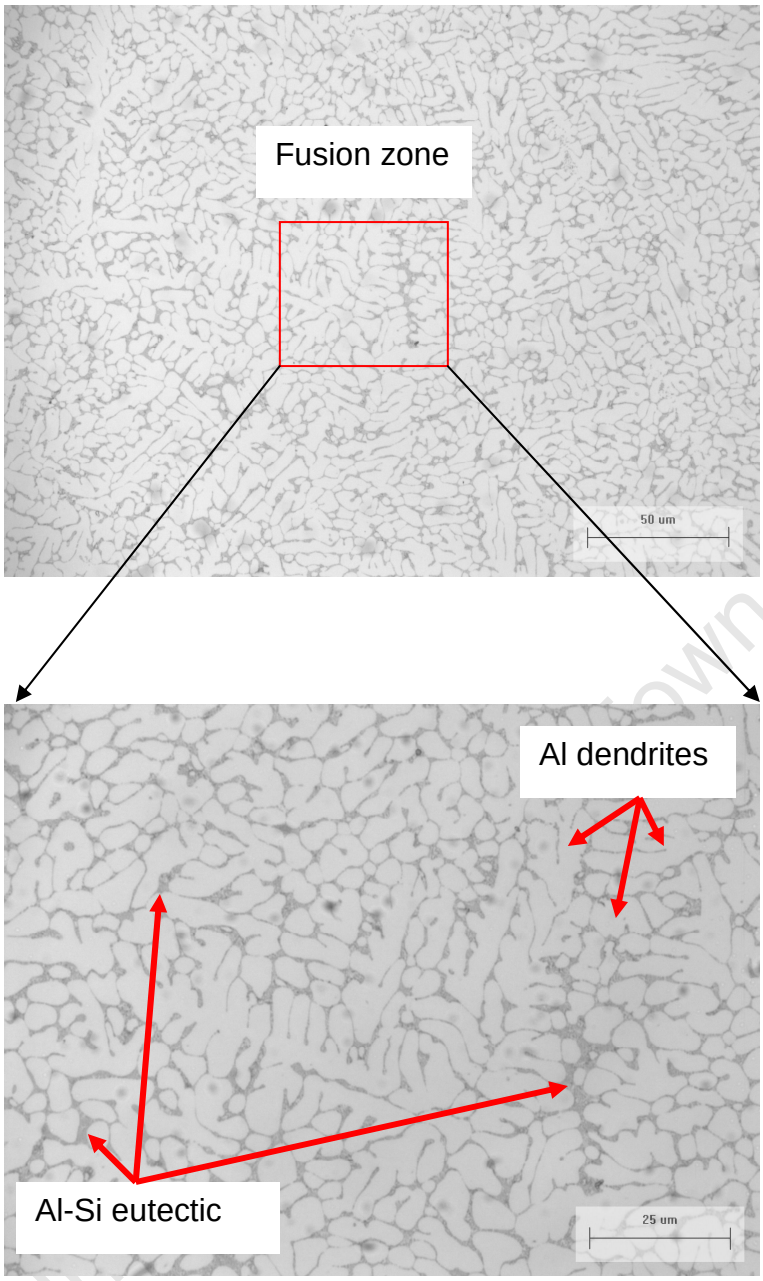

Figure 4.24: Microstructure of the as cast SSM A356 alloy fusion zone.

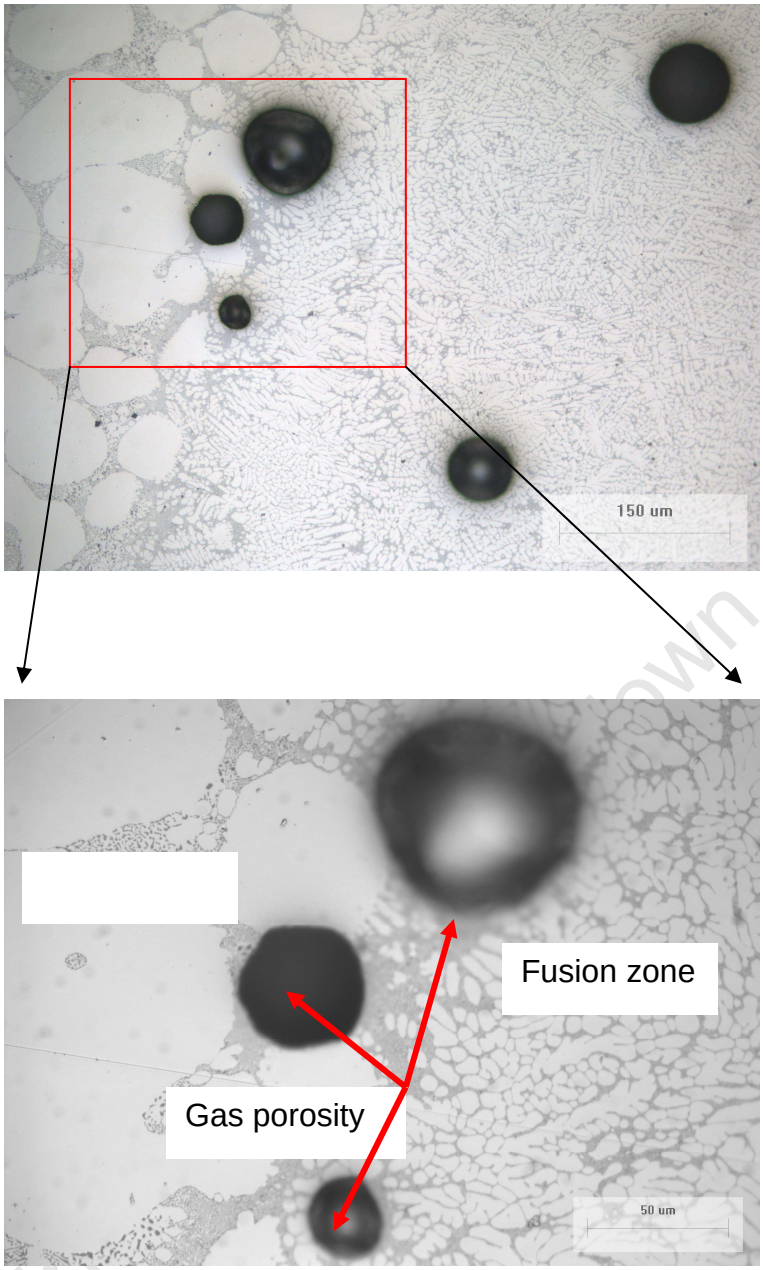

Figure 4.25: Microstructure of as-cast laser welded SSM A356 alloy depicting porosity in both the weld metal and HAZ.

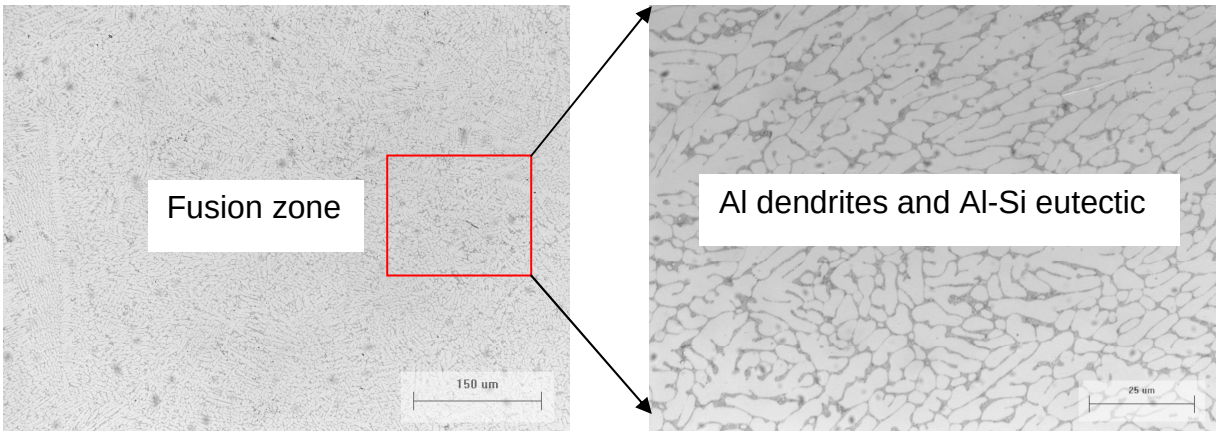

Figure 4.26: Microstructure of the pre-weld T4 heat treated SSM A356 alloy fusion zone.

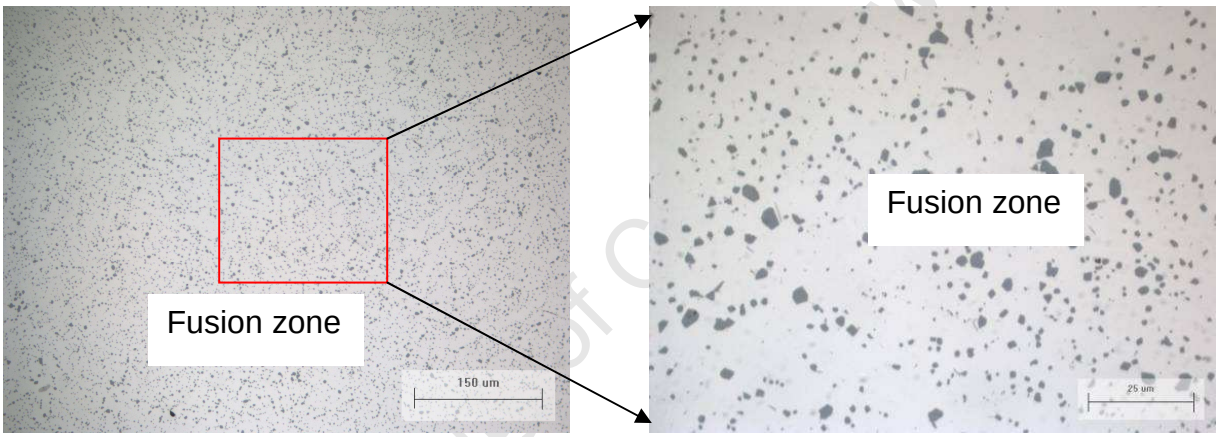

Figure 4.27: Microstructure of the post-weld T4 heat treated SSM A356 alloy fusion zone.

University of Cape Town

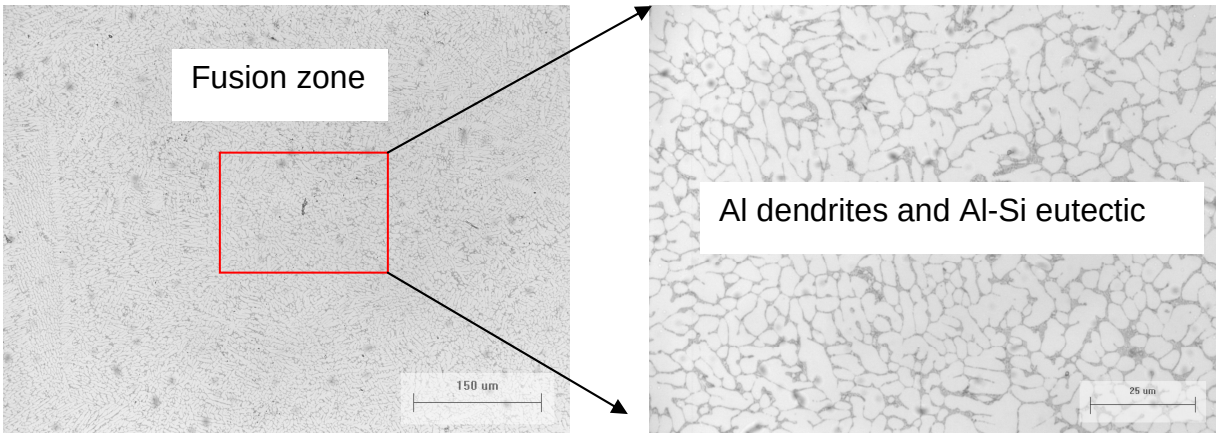

Figure 4.28: Microstructure of the pre-weld T6 heat treated SSM A356 alloy fusion zone.

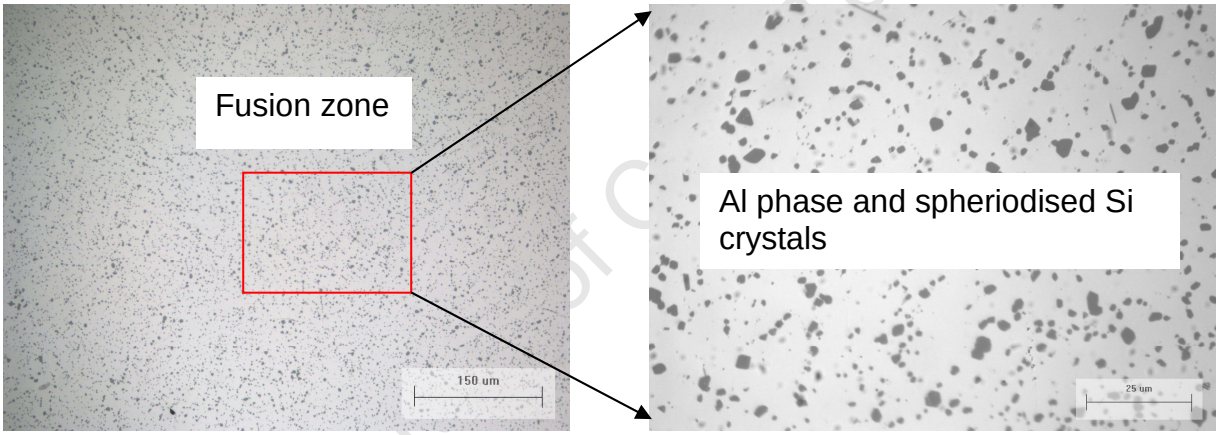

Figure 4.29: Microstructure of the post-weld T6 heat treated SSM A356 alloy fusion zone.

University of Cape Town

4.5 Micro-Vickers hardness profiles

Microhardness profiles for laser welds performed on the A356 plates for the as-cast, pre-weld and post-weld heat treatment conditions are presented in figure 4.30. As clearly indicated the hardness for the weld metal of the welded as-cast, pre-weld T4 and pre-weld T6 heat treatment conditions are very similar to each other. The average hardness at the fusion zone for welded as-cast, pre-weld T4 and pre-weld T6 plates are presented in table 4.2. The reason for the similarities in hardness in the fusion zone for the welded as-cast, pre-weld T4 and pre-weld T6 plates is attributed to the similar microstructure in this zone for the respective conditions. Solidification of liquid metal occurs in this zone and hence the pre-weld T4 and T6 heat treatment effects are eliminated. The average hardness of the fusion zone of the as-cast sample showed a substantial increase of 18.5% compared to its base metal. The increased hardness in the fusion zone as compared to the base metal is attributed to the fine dendritic structure in the fusion zone as opposed to coarser round α-Al globules in the base metal. The fine dendritic structure in the fusion zone occurred due to high welding speeds and rapid solidification rates of liquid metal. Additionally rapid solidification rates in the fusion zone most probably led to the formation of the supersaturated solid solution, which over time was naturally aged. From the microhardness profiles (figure 4.30) of the as-cast sample, there is little indication that the hardness in the HAZ has been altered. Since there was no pre-weld heat treatment in the as-cast sample, the laser energy input into the weld greatly affected the hardness at the fusion zone/HAZ interface. This effect is clearly shown in figure 4.30 by the sharp drop in hardness from the fusion zone to the base metal.

However, for pre-weld T4 sample the average hardness of the fusion zone, HAZ and base metal are similar. Similarly to the as-cast samples, the HAZ was not clearly detected by the hardness profiles most probably because it was too narrow to be detected. Also the low heat input offered by laser caused minimal effect on the ageing effects in the HAZ of the as-cast samples. Evident in the microhardness profiles is that the HAZ of the pre-weld T4 samples showed equal hardness to that of its base metal. The post-weld T4 samples showed similar hardness profile to that of the pre-weld T4 heat treated sample. Generally the application of post-weld heat treatment is to regenerate the hardness in the HAZ which was lost due to laser energy input into the weld. The hardness profiles for the pre-weld T4 and post-weld T4 heat treatment are similar, it is most probably because the pre-weld T4 solution treated condition is

University of Cape Town

not sensitive to the short thermal cycle. Therefore, the application of post-weld T4 heat treatment had little hardness to restore in the HAZ.

Shown in figure 4.30 is the significant decrease in hardness values of the fusion zone and HAZ of the pre-weld T6 heat. According to the variations of the microhardness measurements, the width of the HAZ was found to be approximately 1.3 mm for the pre-weld T6 heat treated sample. The fusion zone and the HAZ both showed similar hardness of approximately 122HV (figure 4.30 and table 4.2). Understandably so, the hardness of the fusion zone is attributed to the fine dendritic structure due to rapid solidification of liquid metal in this zone. During the solidification process of liquid metal, most probably rapid cooling rates lead to the formation of supersaturated solid solution. This would explain similar hardness of the fusion zone and HAZ. Generally the major strengthening phase in Al-Mg-Si alloys is β" and therefore, much of the softening in the HAZ is attributed to dissolution of β" during the weld thermal cycle[18]. The base metal showed high hardness due to the optimal ageing conditions of the T6 heat treatment. The average hardness of the base metal of the pre-weld T6 sample was approximately 23% higher compared to its weld metal. The post-weld T6 heat treated samples showed a substantial increase in hardness for the fusion zone, HAZ and base metal. An increase in hardness of the fusion zone is most probably due to the precipitation hardening process that is expected after the T6 heat treatment. The hardness which was lost in the HAZ of the pre-weld T6 samples is recovered during the post-weld T6 aging treatments.

University of Cape Town

Table 4.2: Average hardness measurements for base metal and weld metal. Represented in brackets are standard deviations from twenty measurements in the base metal and ten in the fusion zone.

	Heat treatment condition				
	As cast	**Pre-weld T4**	**Post-weld T4**	**Pre-weld T6**	**Post-weld T6**
Base Metal	75.2(1.1)	90.4(1.0)	92.8(1.8)	121.5(1.3)	122.4(1.6)
Weld Metal	92.3(1.0)	92.0(1.2)	95.3(1.1)	92.8(1.1)	129.4(1.6)
HAZ				122.2(2.1)	

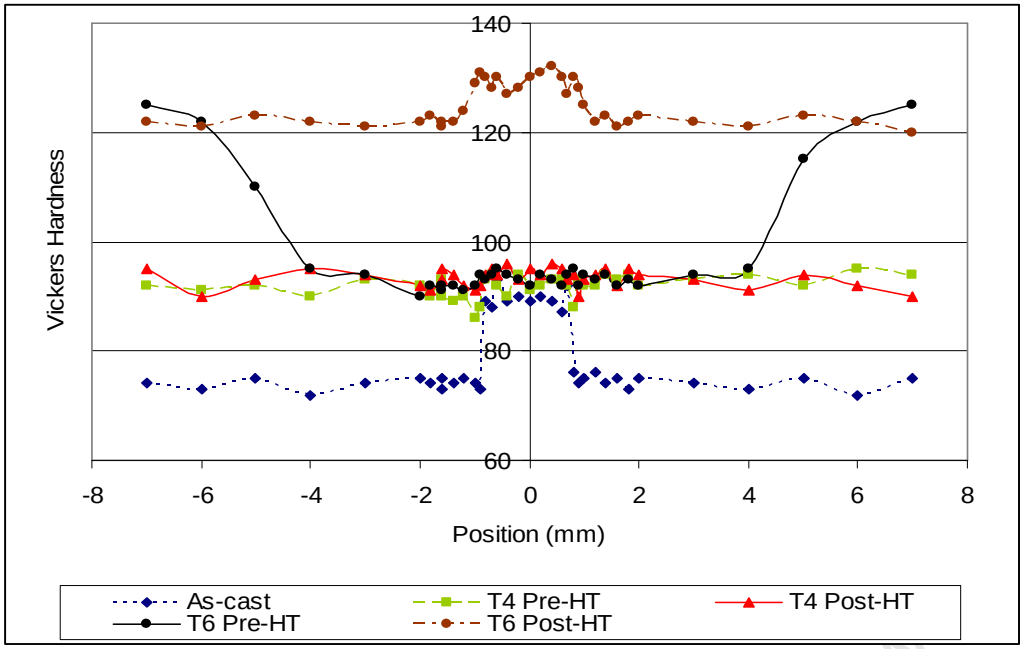

Figure 4.30: Microhardness of SSM cast A356 alloy across the weld for the different heat treatment conditions[69]. **Note:** HT- Heat treatment, Standard deviations for the different heat treatments: As-cast (7.1), T4 Pre-HT (2.0), T4 Post-HT (1.7), T6 Pre-HT (10) and T6 Post-HT (3.8).

University of Cape Town

4.6 Mechanical properties

Illustrated in table 4.3 are the mean values for mechanical properties of the SSM cast A356 in the as-cast, T4 and T6 heat treated conditions prior to welding. As expected the as-cast sample showed the lowest yield strength value because the microstructure of the as-cast condition has low level of solute supersaturation relative to the T4 condition. In addition the Mg_2Si precipitates that might have formed will be distributed heterogeneously. The application of natural and artificial ageing treatments in T4 and T6 respectively is to form finely dispersed precipitates in a more ductile matrix. The presence of these hard non-metallic precipitates hinder dislocation movement thereby strengthening the alloy. Evident in table 4.3 is the improvement in the yield strength (YS) and ultimate tensile strength (UTS) after the T4 and T6 heat treatment process relative to the as-cast condition. In most cases there is a compromise of one of the mechanical property with an increase of the other. This is evident in both the T4 and T6 heat treated samples (table 4.3) where an increase in percentage elongation of the T4 heat treated sample is accompanied by a moderate increase in strength. On the other

hand the T6 heat treated sample showed a substantial increase in strength. However, the percentage elongation remained similar to the as-cast sample.

In the as-cast condition the percentage elongation was reduced by about 14% after welding, but the un-welded base metal had highly scattered tensile strength due to shrinkage porosity (figure 4.14). On the other hand for T4 and T6 heat treated samples the tensile strength was reduced by about 46% and 60% respectively after welding (table 4.3 and 4.4). The reduction in ductility after laser welding is due to the fine dendritic structure in the fusion zone in all three heat treatment conditions. The low ductility for the laser as-cast samples is most probably due to the combination of gas porosity in the fusion and shrinkage porosity in the base metal. The effect of porosities is also noticeable in the large variation of yield strength. Overall the T4 heat treated samples showed superior ductility compared to both the as-cast and T6 heat treated samples. The excellent ductility for both the T4 and T6 heat treated samples is due to spheroidisation of eutectic Si. The mechanical properties confirm the initial conclusion attained from the hardness profiles that even though the microstructures of the T4 and T6 samples are similar when viewed using light microscopy, there is substantial substructural changes in the T6 heat treated samples.

University of Cape Town

Table 4.3: The yield strength (YS), ultimate tensile strength (UTS) and % elongation of rheocast A356 alloy. Represented in brackets are standard deviations.

Plate No	HT	% Elongation	$YS_{0.2}$ MPa	UTS MPa	Mean values			HV20	
					% Elongation	$YS_{0.2}$	UTS	T	B
1	F	11.3 (3.2)	113 (6.8)	226 (8.3)	12.5 (2.3)	111 (4.4)	223 (4.8)	72	72
2	"	13.6 (1.4)	109 (1.9)	220 (1.2)				75	73
3	T4	21.8 (1.1)	138 (8.1)	252 (5.3)	20.9 (1.4)	145 (6.2)	258 (4.3)	94	87
4	"	19.9 (1.7)	151 (4.3)	264 (3.2)				93	83
5	T6	12.1 (1.1)	252 (8.9)	325 (8.6)	12.1 (0.7)	260 (7.3)	319 (6.5)	119	121
6	"	12.1 (0.2)	267 (5.7)	312 (4.4)				116	113

Note: F- As-cast; FZ – Fusion zone; B – Bottom of the plate; (near the gate) and T – Top of the plate (opposite end of the gate)

University of Cape Town

Table 4.4 shows the individual mechanical properties of all the tested samples in the different heat treated conditions together with the mean values thereof. From each welded plate set, between 5 and 7 tensile specimens were able to be tested. There is evident variability in the tensile measurements of the laser welded as-cast samples. Most probably this is due to the combination of shrinkage porosity observed in the base metal and gas porosity in the fusion centreline and HAZ (figures 4.14 and 4.25). This is due to the fact that the mechanical properties of cast alloys such as A356 depend on the amount and size of macro-defects such as internal oxide and shrinkage macro-porosity, micro-porosity, α-Al size, and size and shape of Si particles present in the interdendritic regions[70]. Gokhale et. al[70] used quantitative fractography to analyse the variability in tensile ductility of a semi-solid metal cast A356 Al alloy. They have shown that the variability in ductility of Al-7wt% Si-0.5wt% Mg base alloy (A356) is related to the presence of processing defects such as flux and grain refiner residues. However, Zhang et. al[14] have shown that the ductility of the A356 alloy decreases with the decreasing quench rate. Such decrease in ductility is due to the fact that during low quench

rates (air cooling), the α-Al contains coarse β'-Mg_2Si rods and surrounding precipitate free zones (PFZs). However due to the brittleness of the coarse β' rods, fracture may occur at low strains during deformation. Therefore crack growth is accelerated during cracking of the brittle particles. It has been reported that early fracture of eutectic Si particles is the main factor in reducing the elongation to final failure of the casting alloys[14].

The base metal of the laser welded as-cast had highly scattered tensile strength due to shrinkage porosity. This is due to the fact that ductility of the semi-solid metal cast A356 alloy is dependent mostly on the porosity level and size. However, no evident variability was observed on the yield strength of the laser welded as-cast samples. Even though there was visible large sized porosity in the fusion zone of the laser welded as-cast samples, fracture occurred in the base metal. From the microhardness profiles, it is visible that the weld metal was harder than the base metal. This is attributed to the fine dendritic structure at the fusion zone. Secondly due to rapid solidification of the liquid metal at this zone, a supersaturated solid solution was formed. This supersaturated solid solution was naturally aged over time which most probably also accounts for the increased strength in the fusion zone. The yield strength of the T4 heat treated samples showed an increase of 10% after welding. On the other hand the yield strength and ductility for the pre-weld T6, post-weld T4 and T6 heat treated samples decreased after welding. Understandably the solidification of liquid metal occurs at the fusion zone and hence any ageing effects of the pre-weld T6 heat treatment are eliminated. However, the hardness is recovered at the HAZ during the post-weld aging treatments. The eutectic silicon is noticed to have spheriodised during the T4 or T6 solution treatment at 540 ºC for 6 hours. The spheriodisation of the eutectic silicon was primarily responsible for the excellent ductility in the T4 or T6 conditions.

University of Cape Town

Table 4.4: The yield strength (YS), ultimate tensile strength (UTS) and % elongation of laser welded rheocast A356 alloy. Represented in brackets are standard deviations.

Plate No	Pre HT	Post HT	Fracture/ Defects	% Elongation	$YS_{0.2}$ MPa	UTS MPa	Mean values			HV20	
							% Elongation	$YS_{0.2}$	UTS	T	B
1	F	-	FZ/BM/HAZ	11.7 (5.5)	121 (5.5)	229 (0.7)	10.8 (3.0)	119 (3.6)	222 (1.4)	74	73
2	"	-	BM	9.9 (0.4)	117 (1.7)	214 (2.0)				75	73
3	T4	-	BM	16.3 (0.9)	154 (1.4)	263 (2.6)	11.3 (1.8)	160 (4.8)	262 (7.4)	88	87
4	"	-	BM	10.3 (0.7)	162 (5.5)	270 (2.6)				83	83
5	"	-	BM	7.4 (4.0)	157 (4.4)	244 (24.9)				84	85
6	"	-	BM	8.2 (2.2)	170 (6.6)	269 (4.8)				84	86
7	"	-	BM	14.1 (1.3)	157 (6.3)	265 (2.3)				90	92
8		T4	BM	16.6 (2.5)	145 (1.3)	250 (4.1)	14.2 (3.3)	146 (1.8)	245 (4.6)		
9		"	BM	11.8 (4.0)	147 (2.3)	240 (5.1)					
10	T6	-	HAZ	4.7 (0.1)	171 (5.4)	267 (3.6)	4.8 (0.5)	174 (8.2)	267 (6.9)	115	116
11	"	-	HAZ	5.7 (0.4)	196 (7.0)	276 (3.9)				109	121
12	"	-	HAZ	4.8 (0.4)	158 (7.6)	262 (2.8)				121	119
13	"	-	HAZ	3.8 (1.0)	170 (12.9)	261 (17.1)					
14		T6	BM	10.9 (0.4)	242 (3.5)	303 (2.6)	9.3 (1.9)	247 (3.4)	311 (3.5)	114	111
15		"	BM	7.7 (2.8)	261 (2.0)	328 (5.0)				116	115
16		"	HAZ	9.4 (2.6)	239 (4.8)	301 (3.0)				118	116

Note: F- As-cast; FZ – Fusion zone; BM - Base metal; HAZ – Heat affected zone; B – Bottom of the plate; (near the gate) and T – Top of the plate (opposite end of the gate)

University of Cape Town

4.7 Analysis of fracture surfaces

Shown in figure 4.31(a) is the cross-section of the fracture surface of the as cast tensile sample as observed using the light optical microscope. The as cast samples fractured in the base metal. The mode of fracture for the α-Al and the eutectic Al-Si structure was ductile dimple fracture. The fracture also occurred around α-Al crystals along the grain boundaries in an intergranular form. Shown in figure 4.31(b) is the SEM image depicting the typical ductile dimple fracture surface of the as-cast base metal. Clearly visible in the microhardness profile of the laser welded as-cast sample (figure 4.30) is that the fusion was stronger than the parent base metal. The increased hardness in the fusion is attributed to the fine dendritic structure and increased solute supersaturation in this zone. The dendritic structure was formed during the rapid solidification of liquid metal in this zone. The rapid solidification of liquid metal led to the formation of the supersaturated solid solution, which was later naturally aged over time.

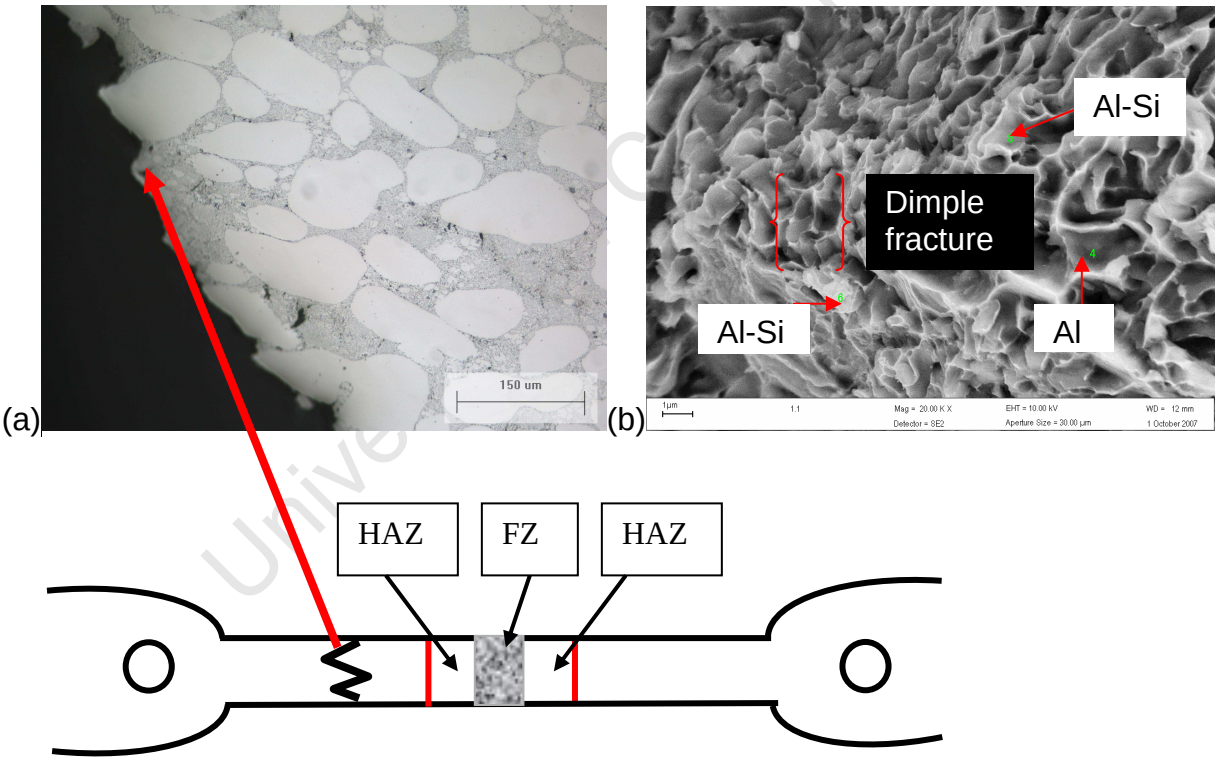

Figure 4.31: Microstructure of as-cast laser welded SSM A356 alloy: (a) cross-section of the fracture surface and (b) SEM image of fracture surface.

Most probably the laser welded as-cast samples had a very narrow HAZ which was not observed in the hardness values. Therefore the high strength, as indicated by high hardness of the fusion zone compared with the parent metal makes the parent metal more susceptible to

early fracture. Even though large sized porosities were visible in the fusion zone (figure 4.25), this did not lead to any premature fracture in the fusion zone. However, the combination of shrinkage porosity and low hardness in the base metal proved to be more dominant as fracture occurred at this zone.

Figure 4.32(a) illustrates the fracture surface of the pre-weld T4 HT tensile sample as observed using the light optical microscope. Similar to the laser welded as-cast sample, fracture of the pre-weld T4 sample occurred at the base metal. In the pre-weld T4 heat treated samples both the parent metal and fusion metal showed relatively similar hardness (figure 4.30). Therefore fracture was equally likely to occur in the fusion zone or parent metal. The relatively low heat input of laser into the weld combined with high welding speed resulted in a narrow HAZ. In addition the pre-weld T4 solution treated condition is not sensitive to the short thermal cycle. The combination of shrinkage porosity and coarsening of precipitates decreases the strength of the base metal. Even though there was no measurable difference in strength, the fusion zone was stronger than the base metal and hence the samples fractured in the base metal. Illustrated in figure 4.32(b) is the fracture surface under SEM investigation from the pre-weld T4 HT samples. Similarly to the as-cast samples, the mode of fracture is intergranular ductile dimple fracture.

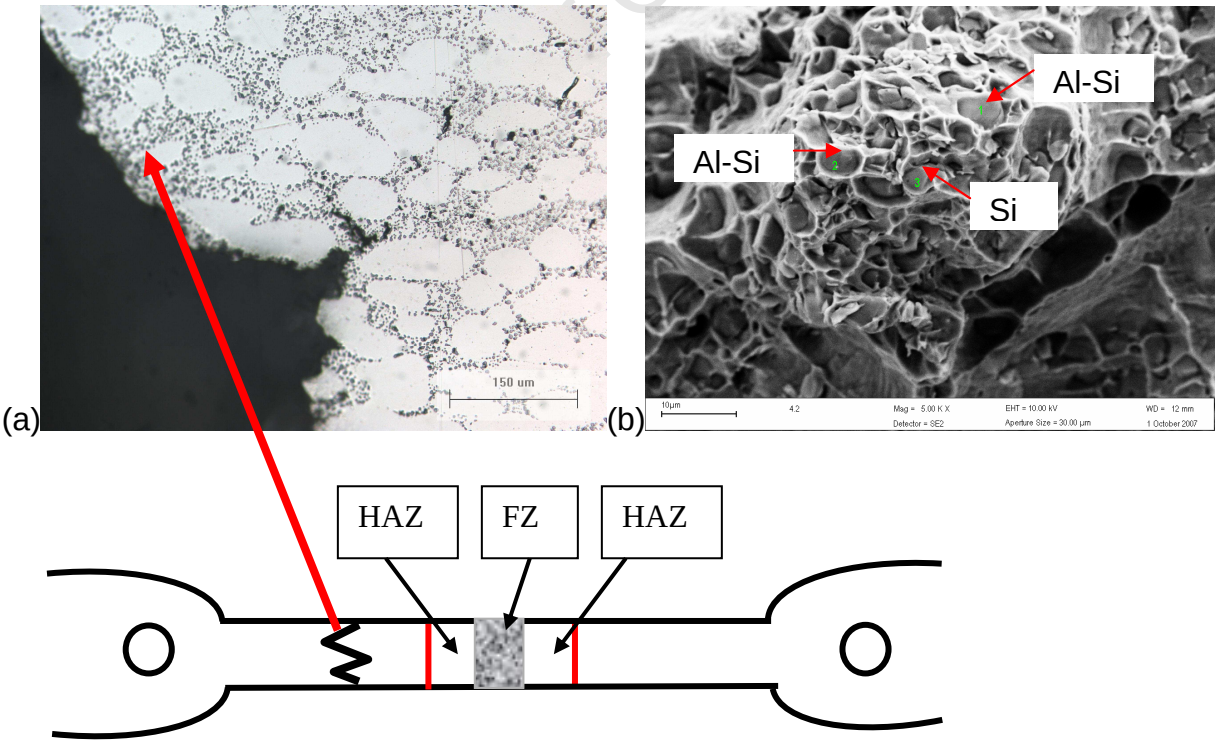

Figure 4.32: Microstructure of laser welded SSM A356 alloy after pre-T4 heat treatment: (a) cross-section of the fracture surface and (b) SEM image of fracture surface.

University of Cape Town

Figure 4.33 illustrates the cross-section of the fracture surface and the SEM image of the fracture surface for the pre-weld T6 heat treated samples. After the inspection of the grain structure in the fracture surface, it was also observed that the mode of fracture was ductile dimple fracture. However, this time the fracture occurred through both the eutectic structure and α-Al crystals. Observable in figure 4.33(b) are the striation lines in the α-Al crystals indicating cleavage fracture. The failure of the pre-weld T6 HT samples at the HAZ is due to additional artificial ageing which is caused by heat conduction from the weld zone. This effect makes the HAZ much weaker than the base metal. The pre-weld T6 HT samples exhibited ductile dimple fracture in both the eutectic Al-Si structure and α-Al phase. Shown in Fig. 4.33(b) is the fracture surface from the pre-weld T6 HT tensile samples. The pre-weld T6 HT samples fractured in the HAZ even though according to the hardness profiles the HAZ had similar hardness to the weld metal. Under all three heat treatment conditions (as cast, pre-weld T4 and T6 HT), it was observed that the fracture mode was of ductile dimple fracture. Surface defects such as pores and cavities create stress concentration, which cause samples to fracture[71], and this has been the case for the samples welded as-cast, pre-weld and post-weld T4 HT samples.

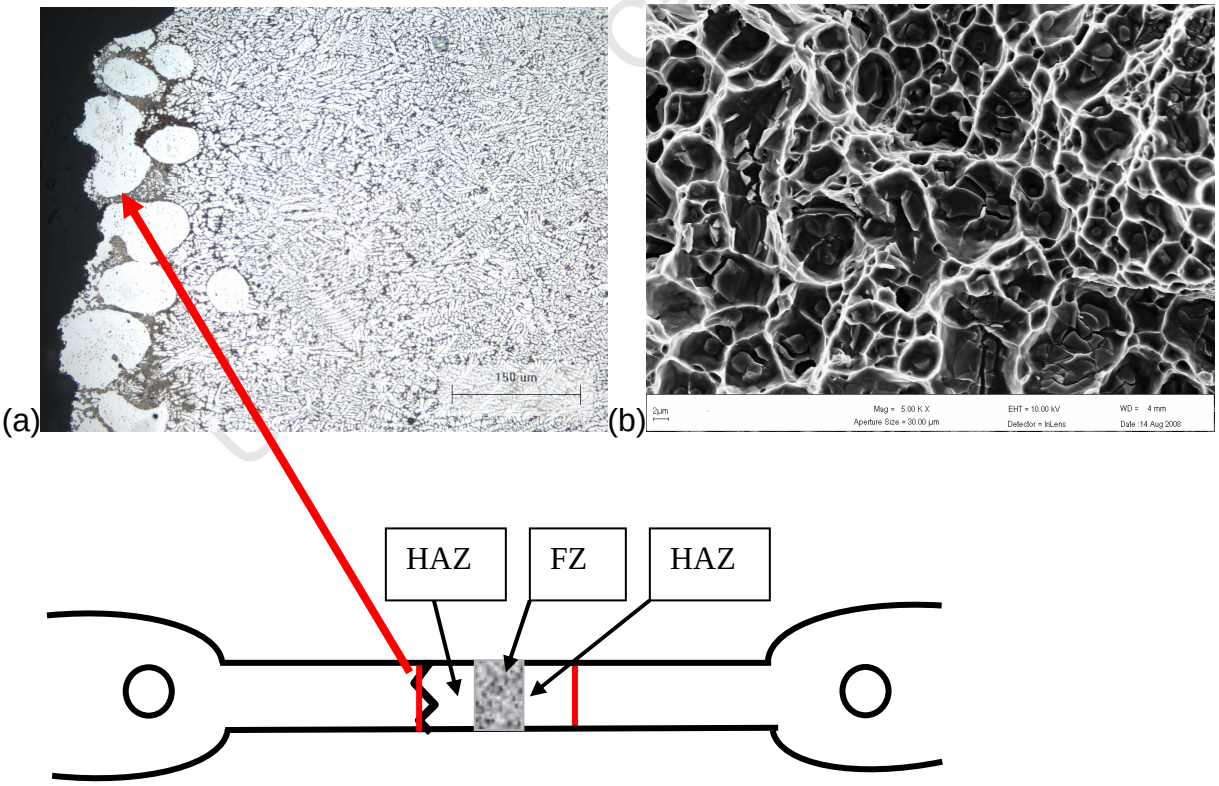

Figure 4.33: Microstructure of laser welded SSM A356 alloy after pre-weld T6 heat treatment: (a) cross-section of the fracture surface and (b) SEM image of the fracture surface.

University of Cape Town

Shown in figure 4.34(a) is the cross-section of the fracture surface for the post-weld T4 heat treated samples as observed using light optical microscope. Post-weld T4 heat treated samples fractured in the base metal. The base metal and fusion zone had equal chances of fracture as microhardness measurements showed similar hardness for both the base metal and fusion zone. The HAZ of the post-weld T4 heat treated samples was a few grains wide which were observed in the microstructure. However, the microhardness measurements did not show any variability in the hardness values which confirmed a narrow HAZ.

An SEM image of the fracture surface of the post-weld T4 heat treated samples clearly showed that the mode of fracture was ductile fracture confined to the eutectic matrix structure.

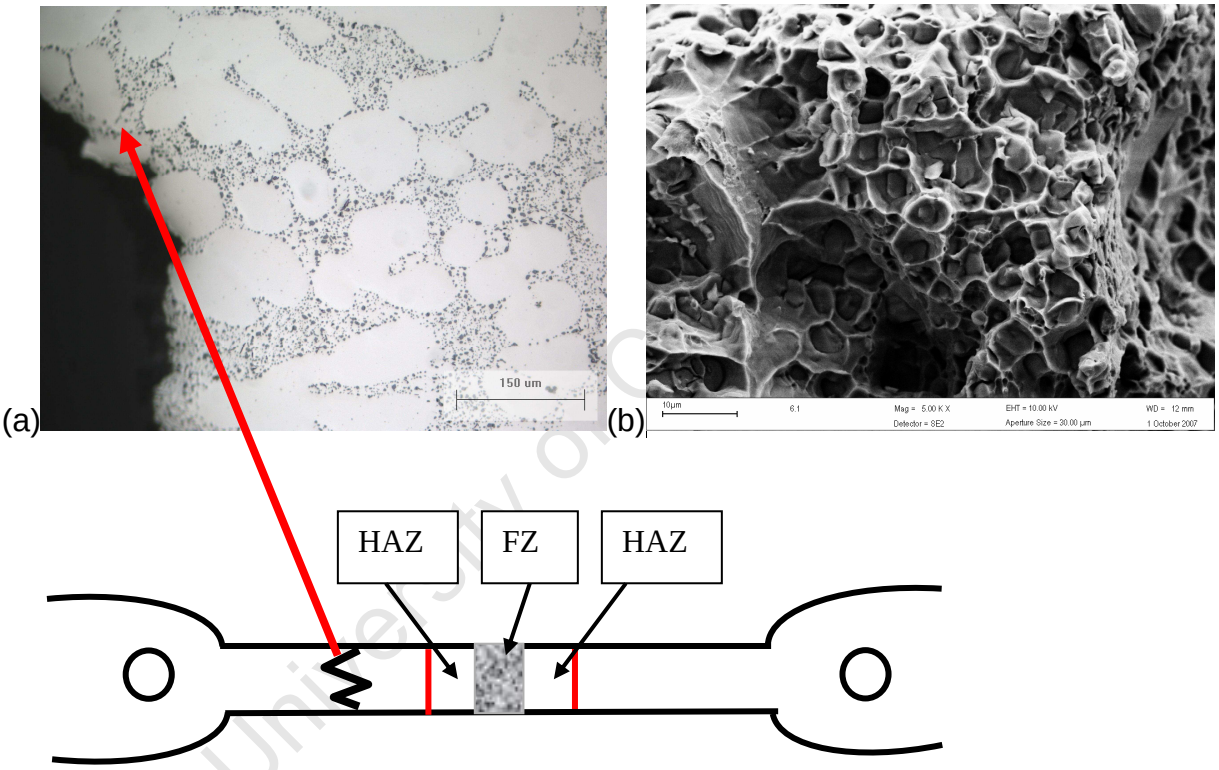

Figure 4.34: Microstructure of laser welded SSM A356 alloy after post-T4 heat treatment: (a) cross-section of the fracture surface and (b) SEM image of fracture surface.

The cross-section of the fracture surface of the post-weld T6 heat treated samples is shown in figure 4.35(a). Fracture of the post-weld T6 heat treated samples occurred in the base metal. The application of post-weld T6 heat treatment led to the recovery of hardness in the HAZ which was lost in the pre-weld T6 heat treated samples. From the microhardness profiles,

there is clear indication of the HAZ. The SEM image of the post-weld T6 heat treated samples showed a mixture of ductile fracture confined through the eutectic structure and α-Al crystals. The fracture through the eutectic structure is clearly depicted by dimples.

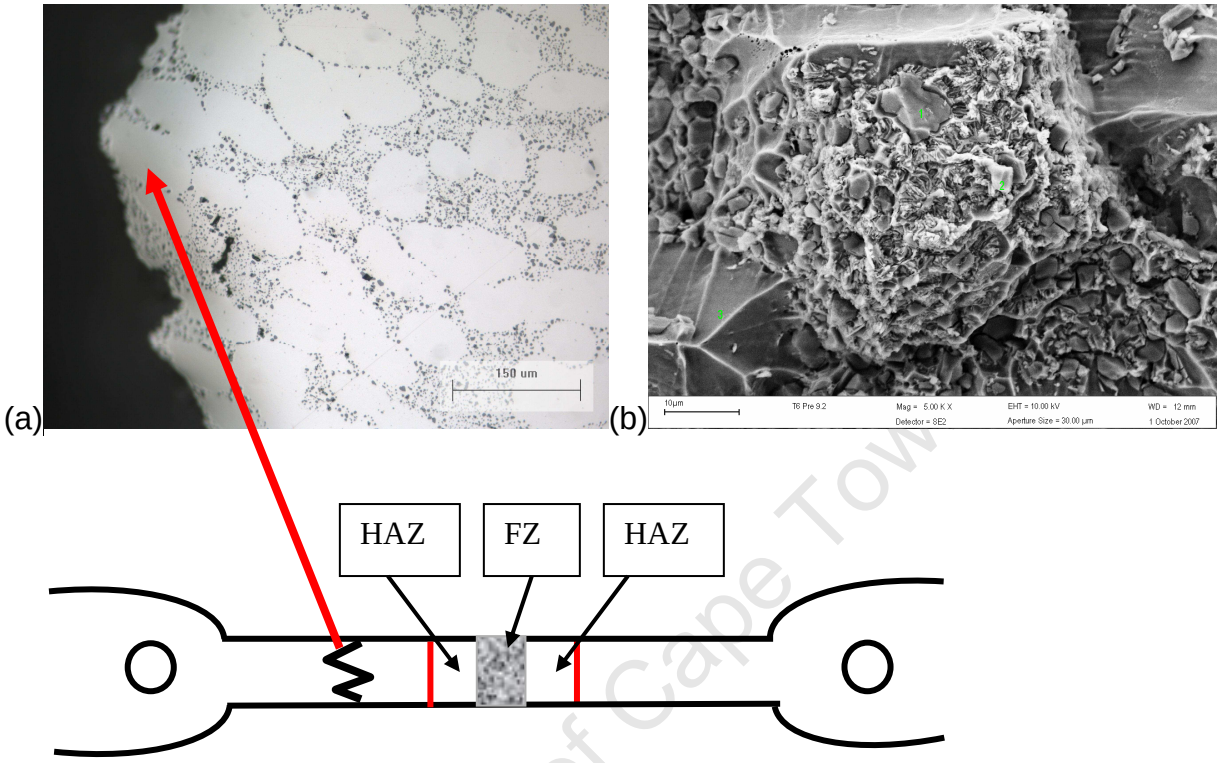

Figure 4.35: Microstructure of laser welded SSM A356 alloy after post-weld T6 heat treatment: (a) cross-section of the fracture surface and (b) SEM image of fracture surface.

University of Cape Town

Chapter Five

Conclusions

The main objectives of the research were to firstly establish the laser welding process parameters for stable and repeatable welding to produce quality welds. (e.g. reduction of defects; such as porosity and inclusions). Secondly to investigate the effects of the pre and post laser welding heat treatments on the microstructure. And finally to establish the mechanical properties of the laser welded joints under different heat treatment conditions.

From the both the objectives and findings of the study, the following main conclusions were drawn:

- Semi-solid metal A356 castings are weldable by solid state laser welding. Particularly, the high powered Nd: YAG laser provides high welding speeds, narrow and deep welds, excellent mechanical properties resulting from a small heat-affected zone and low distortion due to low heat input.

- The application of both the pre and post weld heat treatments greatly alters the microstructure and substructure.

- The laser welding process causes a substantial decrease in the mechanical properties of pre-weld heat treated samples however, the application of post-weld heat treatments regenerates the mechanical properties which were initially lost.

Furthermore the following important findings are also noted:

- There was no significant difference in the chemical composition of the weld metal and base metal after the welding process. Therefore, the contribution of chemical composition to the weld quality was negligible.

- The as-cast base metal composed of globular α-Al surrounded by the fine elongated Al-Si eutectic phase.

University of Cape Town

- Spheroidisation of eutectic Si in the base metal of the pre-weld T4 and T6 samples, and post-weld T4 and T6 samples had occurred during solution heat treatment process.

- The laser welded as-cast, pre-weld T4 and post-weld T4 heat treated samples showed a very narrow HAZ which was only observable under microstructural analysis and not in the microhardness profiles. The pre-weld T6 heat treated samples showed a wide HAZ which was clearly observed on the microhardness profiles which was due to overageing at this zone.

- The laser welded as-cast, pre-weld T4 and T6 heat treated samples showed a fine dendritic structure in the fusion zone. This was due to the solidification of liquid metal which occurred in this zone.

- The average secondary dendrite arm spacing (SDAS) was 5µm. The fine dendritic structure in the fusion zone accounts for the higher hardness at this zone. Secondly, the formation of supersaturated solid solution during rapid solidification at this zone which later naturally age over time also accounts for increased hardness.

- The fusion zone of the post-weld T4 and T6 samples showed spheroidised eutectic Si. For the post-weld T4 there was no significant increase in the hardness values due to post-weld heat treatments however, the post-weld T6 heat treated samples showed a substantial increase in the mechanical properties after post-weld T6 heat treatment.

- Microhardness profile for the laser welded as-cast samples showed a much harder fusion zone as compared to its base metal.

- The pre-weld T4 heat treated samples showed equal hardness for the fusion zone and base metal with a very narrow HAZ.

- In both the T4 and T6 heat treatment conditions, all the pre-weld heat treated conditions were able to recover by performing either a T4 or T6 post-weld heat treatment.

University of Cape Town

- In the pre-weld T6 heat treated samples, the base metal showed a higher hardness compared to both the HAZ and fusion zone. Basically in the base metal most probably there is complete coherency between the strengthening β"-Mg_2Si precipitates with the matrix. Similar hardness was observed for both the HAZ and fusion zone of the pre-weld T6 heat treated samples, which was due to the natural ageing of the supersaturated solid solution which had formed because of the heat conduction in the weld.

- For as-cast and pre-weld T4 heat treatment conditions, the mode of fracture was ductile fracture confined to the eutectic structure which led to the formation of dimples.

- The pre-weld T6 heat treated samples had mixed ductile fracture through the eutectic and α-Al crystals.

- Similar to the as-cast and pre-weld T4 heat treated conditions, the mode of fracture for both the post-weld T4 and T6 heat treated conditions was ductile fracture confined to the eutectic.

University of Cape Town

Chapter Six

Recommendations

The following recommendations are based on the laser welding process and the results of the heat treatments:

- The effect of chemical composition on the weld quality was negligible in the current study due to the fact that the chemical composition of major alloying elements was kept constant. It will be of paramount importance to investigate the effect of individual major alloying elements on the weld quality at fixed welding parameters.

- Perform the surface preparation optimisation process prior to welding. For example, carry out surface preparation study using different preparation methods such as no surface preparation compared to stainless steel brush with acetone washings or stainless steel brush without acetone washings, etc. This test will provide the most favourable surface preparation method to achieve excellent weld quality.

- Investigate the effect of time taken between the surface preparation process and the actual welding process on the weld quality and hence mechanical properties. The study will provide valuable information about the critical time that needs to be taken for surface preparation process prior to welding.

- Inspect the effects of welding parameters on the weld quality. This can be accomplished by varying one welding parameter while others are fixed. This will provide important information about laser welding parameters which to a large extent affect the weld quality and hence the mechanical properties.

- Perform a wide range of optimisation heat treatment tests. This test will provide valuable information about the times and temperatures that need to be applied to welded SSM castings to achieve the desired mechanical properties.

University of Cape Town

References

1. http://www.alcan.com/web/publishing.nsf/Attachments By Title/Investors-Presentations/ (2007/05/22).

2. J. Collot, Review of New Process Technologies in the Aluminium Die-Casting Industry, Materials and Manufacturing Processes, 16(5), 2001, pp 595-617.

3. M.L. Santella, T. Engstrom, D. Storjohann and T.Y. Pan, Effects of Friction Stir Processing on Mechanical Properties of the Cast Aluminium Alloys A319 and A356, Scripta Materialia, 53, 2005, pp 201-206.

4. R. Akther, L. Ivanchev and H.P. Burger, Effect of Pre-Heat Treatment on the Mechanical Properties of Laser Welded SSM Cast A356 Aluminium Alloy, Materials Science and Engineering, A447, 2007, pp 192-196.

5. J.R. Davies and Associates: Aluminium and Aluminium Alloys (ASM International, USA, 1993).

6. M.M. Haque and A.A. Khan, Influence of Magnesium on Structure and Properties of Al-Si Alloy, Advanced Materials Research, 23, 2007, pp 291-294.

7. Aluminium Federation of South Africa, Introduction to Aluminium, South Africa, 3rd Edition, 2007.

8. Aluminium Federation Ltd, The Properties of Aluminium and its Alloys, 9th Edition, UK, 1993, pp 6-14.

9. A.P. Mackwood and R.C. Crafter, Thermal Modelling of Laser Welding and Related Processes: A Literature Review, Optics and Laser Technology, 37, 2005, pp 99-115.

University of Cape Town

10. Y.C. Lee, A.K. Dahle, D.H. StJohn, and J.E.C. Hutt, The Effect of Grain Refinement and Silicon Content on Grain Formation in Hypo-eutectic Al-Si Alloys, Materials Science and Engineering, A259, 1999, pp 43-52.

11. E.N. Pan, H.S. Chiou, G.J. Liao, Effects of Modification and Solidification Conditions on the Feedig Behavior of A356 Al Alloy, AFS Transactions, 99, 1991, pp 605-621.

12. S.F. Malan and A.E. Paterson, Introduction to Aluminium, Aluminium Federation of South Africa, 2nd Edition, 1993, pp 1-112.

13. I.J. Polmear, Light Alloys: Metallurgy of the Light Metals, Edward Arnold Publishers Ltd, 2nd Edition, 2005.

14. D.L. Zhang and L. Zheng, The Quench Sensitivity of Cast Al-7wt PctSi-0.4wt PctMg Alloy, Metallurgical and Materials Transactions, A, 1996, pp 3983-3991.

15. H. Mőller, G. Govender and W.E. Stumpf, The T6 Heat Treatment of Semi-solid Metal Processed Alloy A356, The Open Materials Science Journal, 2, 2008, pp 6-10.

16. G. Kunene, G. Govender, L. Ivanchev, R. Knutsen and H. Burger, The Influence of Heat Treatments for Laser Welded Semi Solid Metal cast A356 Alloy on the Fracture Mode of Tensile Specimens, Solid State Phenomena, 141-143, 2008, pp 169-174.

17. E. Ogris, Development of Al-Si-Mg Alloys for Semi-Solid Processing and Silicon Spheriodization Treatment (SST) for Al-Si Cast Alloys, 2002, pp 1-119.

18. R.X. Li, R.D. Li, Y.H. Zhao, L.Z. He, C.X. Li, H.R. Guan and Z.Q. Hu, Age Hardening of Cast Al-Si base Alloy, Materials Letters, 58, 2004, pp 2096-2101.

19. J.R. Davis and G.M. Davidson, ASM Handbook: Heat Treating, Heat Treating of Aluminium Alloys, 4,

20. A.K. Gupta, D.J. Lloyd and S.A. Court, Precipitation Hardening in Al-Mg-Si Alloys With and Without Excess Si, Materials Science and Engineering, A316, 2001, pp 11-17.

University of Cape Town

21. M.M. Makhlouf and H.V. Guthy, The Aluminium-Silicon Eutectic Reaction: Mechanisms and Crystallography, Journal of Light Metals, 1, 2001, pp 199-218.

22. P.A. Rometsch and G.B. Schaffer, An age Hardening Model for Al-7Si-Mg Casting Alloys, Materials Science and Enginnering, A325, 2002, pp 424-434.

23. H.K. Jung, P.K. Seo and C.G. Kang, Microstructural Characterisation and Mechanical Properties of Hypo-eutectic and Hyper-eutectic Al-Si Alloys in the Semisolid Forming Process, Journal of Materials Processing Technology, 113, 2001, pp 568-573.

24. L.Y. Zhang, B.D. Zhou, Z.J. Zhan, Y.Z. Jia, S.F. Shan, B.Q. Zhang and W.K. Wang, Mechanical Properties of Cast A356 Alloy, Solidified at Cooling Rates Enhanced by Phase Transition of a Cooling Medium, Materials Science and Engineering, A448, 2007, pp 361-365.

25. A. Haboudou, P. Peyre, A.B. Vannes and G. Peix, Reduction of Porosity Content Generated During Nd:YAG Laser Welding of A356 and AA5083 Al Alloys, Materials Science and Engineering , A363, 2003, pp 40-52.

26. Y. Zhang, N. Ma, Y. Le, S. Li and H. Wang, Mechanical Properties and Damping Capacity After Grain Refinement in A356 Alloy, Materials Letters, 59, 2002, pp 2174-2177.

27. Y.C. Lee, A.K. Dahle, D.H. StJohn, and J.E.C. Hutt, The Effect of Grain Refinement and Silicon Content on Grain Formation in Hypo-eutectic Al-Si Alloys, Materials Science and Engineering, A259, 1999, pp 43-52.

28. S. Nafisi and R. Ghomashchi, Combined Grain Refining and Modification of Conventional and Rheo-cast A356 Al-Si alloy, Materials Characterization, 57, 2006, pp 371-385.

29. S. Nafisi, O. Lashkari, R. Ghomashchi, F. Ajersch and A. Charette, Microstructure and Rheological Behaviour of Grain Refined and Modified Semisolid A356 Al-Si Slurries, Acta Meterialia, 54, 2006, pp 3503-3511.

University of Cape Town

30. M.F. Horstemeyer, K. Gall, K.W. Dolan, A. Waters, J.J. Haskins, D.E. Perkins, A.M. Gokhale and M.D. Dighe, Numerical, Experimental, Non-destructive and Image Analysis of Damage Progression in Cast A356 Aluminium Notch Tensile Bars, Theoretical and Appliead Fracture Mechanics, 39, 2003, pp 23-45.

31. E.J. Zoqui, M.T. Shehata, M. Paes, V. Kao, E. Es-Sadiqi, Morphological Evolution of SSM A356 During Partial Remelting, Materials Science and Engineering, A325, 2002, pp 38-53.

32. Q.C. Wang, D. Apelian and D.A. Lados, Fatigue Behavior of A356/357 Aluminium Cast Alloys.Part II.Effect of Microstructural Constituents, Journal of Light Metals, 1, 2001, pp 85-97.

33. Y.X. Gao, J.Z. Yi, P.D. Lee and T.C. Lindley, A Mirco-cell Model of the Effect of Microstructure and Defects on the Fatigue Strength in Cast Aluminium Alloys, Acta Materialia, 52, 2004, pp 5435-5449.

34. Q.C. Wang, D. Apelian and D.A. Lados, Fatigue Behavior of A356-T6 Aluminium Cast Alloys.Part I.Effect of Casting Defects, Journal of Light Metals, 1, 2001, pp 73-84.

35. H. Mőller, G. Govender and W.E. Stumpf, Investigation of the T4 and T6 Heat Treatment Cycles of Semi-solid Processed Aluminium Alloy A356, The Open Materials Science Journal, 2, 2008, pp 11-18.

36. G. Govender, L. Ivanchev, N. Jahajeeah and R. Bëan, Application of CSIR Rheocasting Technology for the Production of an Automotive Component, Solid State Phenomena, 116-117, 2006, pp 501-504.

37. Z. Fan, Semisolid Metal Processing, International Materials Reviews, 47(2), 2002, pp 1-37.

38. T. Basner, Rheocasting of Semi-solid A357 Aluminium Alloy, SAE Technical Paper Series, 2000-01-0059, 2000, pp 1-5.

University of Cape Town

39. Z. Fan, X. Fang and S. Ji, Microstructure and Mechanical Properties of Rheo-diecasting (RDC) Aluminium Alloys, Materials Science and Engineering, A412, 2005, pp 298-306.

40. A Huntington and T.W. Eagar, Laser Welding of Aluminium and Aluminium Alloys, Welding Research Supplement, 1982, pp 105-107.

41. H. Fujii, H. Umakoshi, Y. Aoki, K. Nogi, Bubble Formation in Aluminium Alloy During Electron Beam Welding, Journal of Materials Processing Technology, 155-156, 2004, pp 1252-1255.

42. X. Cao, M. Jahazi, J.P. Immarigeon and W. Wallace, A Review of Laser Welding Techniques for Magnesium Alloys, Journal of Materials Processing Technology, 171, 2006, pp 188-204.

43. W.W. Duley, Laser Welding, John Wiley and Sons, USA, 1999.

44. Y. Peng, W. Chen, C. Wang, G. Bao and Z. Tian, Controlling the Plasma of Deep Penetration Laser Welding to Increase Power Efficiency, Journal of Physics D: Applied Physics, 34, 2001, pp 3145-3149.

45. X. Cao, W. Wallace and J.P. Immarigeon, Research and Progress in Laser Welding of Wrought Aluminium Alloys.I. Laser Welding Processes, Materials and Manufacturing Processes, 18, 2003, pp 1-22.

46. X. Jin and L. Li, An Experimental Study on the Keyhole Shapes in Laser Deep Penetration Welding, Optics and Lasers in Engineering, 41, 2004, pp 779-790.

47. H. Wang, Y. Shi and S. Gong, Effect of Pressure Gradient Driven Convection in the Molten Pool During the Deep Penetration Laser Welding, Journal of Materials Processing Technology, 184, 2007, pp 386-392.

48. R. Fabbro, S. Slimani, I. Doudet and F. Coste, Experimental Study of the Dynamical Coupling Between the Induced Vapour Plume and the Melt Pool for Nd:YAG CW Laser Welding, Institute of Physics Publishing, 39, 2006, pp 394-400.

University of Cape Town

49. http://www.twi.co.uk/j32k/unprotected/band_1/laser_fundamental.html, (2007/10/16).

50. E. Cicală, G. Duffet, H. Andrzejewski, D. Drevey and S. Ignat, Hot Cracking in Al-Mg-Si Alloy Laser Welding Operating Parameters and Their Effects, Materials Science and Engineering, A395, 2005, pp 1-9.

51. Z. Sun, A.S. Salminen, T.J.I. Moisio, Quality Improvement of Laser Beam Welds by Plasma Control, Journal of Materials Science Letter, 12, 1993, pp 1131-1133.

52. T. Sibillano, A. Ancona, V. Beradi, E. Schingaro, G. Basile and P.M. Lugarà, A Study of the Shielding Gas Influence on the laser Beam Welding of AA5083 Aluminium Alloys by in Process Spectroscopic Investigation, Optics and Lasers in Engineering, 2005, pp 1-13.

53. K. Easterling, Introduction to the Physical Metallurgy of Welding, Butterworth-Heinemann Ltd, Oxford, 2nd Edition, 1992.

54. M.S. Popa, C. Rus, D. Preja, R. Moldovan, Technological Approaches by Laser Beam Welding of Aluminium Alloys and Influence of Errors in Manufacturing Process, Eight International Symposium on Laser Metrology, 5776, 2005, pp 68-73.

55. E. Schubert, M. Klassen, I. Zerner, C.Walz and Sepold, Light-weight Structures Produced by laser beam joining for future applications in automotive and aerospace industry, Journal of Materials Processing Technology, 115, 2001, pp 2-8.

56. C Thomy and F. Vollertsen, Influence of Magnetic Fields on Dilution During Laser Welding of Aluminium, Advanced Materials Research, Vols 6-8, 2005, pp 179-186.

57. J. Rapp, C. Glumann, F. Dausinger and H. Hűgel, Laser Welding of Aluminium Light Weight Materials: Problems, Solutions, Readiness for Application, Optical and Quantum Electronics, 1995, pp 1203-1211.

58. M. Kern, P. Berger, and H. Hűgel, Magneto-Fluid Dynamic Control of Seam quality in CO_2 Laser Beam Welding, Welding Journal, 3, 2000, pp 72-78.

University of Cape Town

59. R.S. Xiao, G. Ambrosy and T.C. Zuo and H. Hűgel, New Approach to Improve the Laser Welding Process of Aluminium by Using an External Electrical Current, Journal of Materials Science Letters, 20, 2001, pp 2163-2165.

60. X. Cao, W. Wallace, J.P. Immarigeon and C Poon, Research and Progress in Laser Welding of Wrought Aluminium Alloys.II. Metallurgical Microstructures, Defects and Mechanical Properties, Materials and Manufacturing Processes, 18, 2003, pp 23-49.

61. C. Menzemer, P.C. Lam, T.S. Srivatsan and C.F. Wittel, An Investigation of Fusion Zone Microstructure of Welded Aluminium Alloy Joints, Materials Letters, 41, 1999, pp 192-197.

62. H. Wang, Y Shi and S. Gang, Effect of Pressure Gradient Driven Convection in the Molten Pool During the Deep Penetration Laser Welding, Journal of Materials Processing Technology, 184, 2007, pp 386-392.

63. Y.S. Yang, S.H. Lee, A Study on the Joining Strength of Laser Spot Welding for Welding Applications, Journal of Materials Processing Technology, 94, 1999, pp 151-156.

64. N. Pieron, P. Sallamand, S. Matteï, Study of Magnesium and Aluminium Alloys Absorption Coefficient During Nd:YAG Laser Interaction, Applied Surface Science, 253, 2007, pp 3208-3214.

65. B. Forbord, B. Andersson and F. Ingvaldsen, O. Austevik, J.A. Horst and I. Skauvik, The Formation of Surface Segregates During Twin Roll Casting of Al Alloys, Materials Science and Engineering, A415, 2006, pp 12-20.

66. E.A. Vieira and M. Ferrante, Prediction of Rheological Behaviour and Segregation Susceptibility of Semi-solid Aluminium-Silicon Alloys by a Simple Back Extrusion Test, Acta Materialia, 53, 2005, pp 5379-5386.

University of Cape Town

67. M.B. Djurdevic, J.H. Sokolowski, W.T. Kierkus and G. Byczynski, The Effect of Chemistry and Cooling Rate on the Latent Heat Released During the Solidification of the 3XX Series of Aluminium Alloys, Materials Science Forum, Vols 539-543, 2007, pp 299-304.

68. R. Akhter, L. Ivanchev, C. van Rooyen, P. Kazadi and H.P. Burger: Materials Science and Enginerring, A447, 2007, pp 192-197.

69. G. Govender, L. Ivanchev, H. Burger, R. Knutsen and G. Kunene, Weldability of SSM Rheo Processed Aluminium Alloy A356, Solid State Phenomena, 141-143, pp 773-778.

70. A.M. Gokhale and G.R. Patel, Analysis of Variability in Tensile Ductility of a Semi-solid Metal Cast A356 Al Alloy, Materials Science and Engineering, A392, 2005, pp 184-190.

71. M.M. Haque, N.I. Syahriah and A.F. Ismail, Effect of Silicon on Strength and Fracture Surfaces of Aluminium-Silicon Casting and Heat Treated Alloys, Key Engineering Materials, Vols 306-308, 2006, pp 893-898.

University of Cape Town